JPRS L/10072

26 October 1981

USSR Report

PHYSICS AND MATHEMATICS

(FOUO 9/81)

FBIS FOREIGN BROADCAST INFORMATION SERVICE

FOR OFFICIAL USE ONLY

APPROVED FOR RELEASE: 2007/02/09: CIA-RDP82-00850R000400060049-8

NOTE

JPRS publications contain information primarily from foreign newspapers, periodicals and books, but also from news agency transmissions and broadcasts. Materials from foreign-language sources are translated; those from English-language sources are transcribed or reprinted, with the original phrasing and other characteristics retained.

Headlines, editorial reports, and material enclosed in brackets [] are supplied by JPRS. Processing indicators such as [Text] or [Excerpt] in the first line of each item, or following the last line of a brief, indicate how the original information was processed. Where no processing indicator is given, the information was summarized or extracted.

Unfamiliar names rendered phonetically or transliterated are enclosed in parentheses. Words or names preceded by a question mark and enclosed in parentheses were not clear in the original but have been supplied as appropriate in context. Other unattributed parenthetical notes within the body of an item originate with the source. Times within items are as given by source.

The contents of this publication in no way represent the policies, views or attitudes of the U.S. Government.

APPROVED FOR RELEASE: 2007/02/09: CIA-RDP82-00850R000400060049-8

JPRS L/10072

26 October 1981

USSR REPORT

PHYSICS AND MATHEMATICS

(FOUO 9/81)

CONTENTS

ACOUSTICS

UDC 534.2:532

TWO-DIMENISONAL NONLINEAR WAVE PROCESSES IN PULSED LOCAL HEAT RELEASE IN A GAS FLOW

Moscow AKUSTICHESKIY ZHURNAL in Russian Vol 27, No 4, Jul-Aug 81 (manuscript received 13 May 80) pp 595-604

[Article by A. T. Fedorchenko, Moscow Physicotechnical Institute]

[Text] Development of nonlinear wave processes in a homogeneous gas flow near a stationary zone of pulsed heat release is numerically studied within the framework of a planar model. The study is done over a wide range of transonic and supersonic velocities of the unperturbed flow. Optimum conditions of generation to maximize pressure amplitudes are discussed.

A separate field of research [Ref. 1-7] involves the investigation of wave processes generated by a thermo-optical source moving in a gas (or equivalent processes in flow around a stationary beam along the normal to its axis). The phenomenon of amplification of sound waves as they are generated by continuous radiation in a transonic gas flow has been examined as a result of approximate analytical solutions (linear [Ref. 1-5] or with consideration of weak nonlinearity [Ref. 7]). An analogous effect has been experimentally detected [Ref. 8] at near sonic velocities of scanning of a laser beam over the surface of an absorbing liquid.

However, the approximate solutions have not enabled investigation of appreciably unsteady processes of pulsed excitation of acoustic waves of finite amplitude, much less under conditions of strong nonlinearity (i. e. at acoustic Mach numbers M_a of the order of unity or more). Obviously in solving nonlinear spatial problems of the given type under general conditions it is necessary to use a complete (two-dimensional as a minimum) system of gasdynamic equations. But solution of such problems as of now can be handled only on the basis of numerical methods with up-to-date computers. In doing this, both the construction of mathematical models and development of the appropriate numerical algorithms for solution constitute a separate class of problems, usually attended by considerable difficulties.

In this paper, numerical integration of complete two-dimensional equations of gas dynamics is used to solve some model problems where an investigation is made of appreciably nonlinear pulse processes of optical generation of intense waves in plane-parallel gas flows. In the given range of velocities of the undisturbed

flow (transonic and supersonic) and heat-release levels, pronounced two-dimensional effects of nonlinear interaction of the generated waves with the flow are observed. A detailed examination is made of the formational processes and subsequent evolution of shock waves; an analysis is made of some optimum conditions of wave generation to maximize pressure amplitudes. Notice is taken of the possibility of realization of resonant oscillatory phenomena in a supersonic flow by using a series of successive pulses.

Two-dimensional unsteady flows of perfect gas were studied in the rectangular region $G\{x\in(x_1; x_2),\ y\in(0; y_2),\ x_1<0,\ x_2>0\}$. The coordinate system that is used is fixed to the stationary axis of the beam (axis Oz) normal to the plane of the flow. The initial dimensionless system of gasdynamic equations had the form

$$
\begin{aligned}
&\frac{\partial\rho}{\partial t}+\frac{\partial\rho u}{\partial x}+\frac{\partial\rho v}{\partial y}=0,\\
&\frac{\partial\rho u}{\partial t}+\frac{\partial}{\partial x}(\rho u^2+p)+\frac{\partial\rho uv}{\partial y}=0,\\
&\frac{\partial\rho v}{\partial t}+\frac{\partial\rho uv}{\partial x}+\frac{\partial}{\partial y}(\rho v^2+p)=0,\\
&\frac{\partial\rho E}{\partial t}+\frac{\partial}{\partial x}[u(\rho E+p)]+\frac{\partial}{\partial y}[v(\rho E+p)]=Q\alpha I,\\
&p=\frac{\rho T}{\gamma},\quad E=e+\frac{u^2+v^2}{2},\quad e=c_vT=\frac{T}{\gamma(\gamma-1)},\quad \gamma=\frac{C_p}{C_v},\\
&Q=\frac{\alpha_0 r_0 I_0}{\rho_0 c_0^3}.
\end{aligned}
\tag{1}
$$

The dimenisonless values of coordinates x, y, velocity components u, v, time t, density ρ, pressure p, temperature T, internal energy e, volumetric absorption factor α, and radiation intensity I are respectively expressed in units r_0, c_0, r_0/c_0, ρ_0, $\rho_0 c_0^2$, T_0, c_0^2, α_0, I_0, where r_0 is characteristic radius of the beam, ρ_0, T_0 are parameters of the unperturbed gas flow, $c_0=\sqrt{\gamma RT_0}$ is the adiabatic speed of sound, α_0 is the average value of the coefficient of absorption on the investigated section of the length of the beam, I_0 is the characteristic (maximum) radiation intensity.

The principal dimensionless number Q can be represented as a product of two dimensionless parameters:

$$Q=\xi B,\ \text{where}\ \xi=\alpha_0 r_0,\ B=I_0/\rho_0 c_0^3.$$

Obviously formulation of the planar problem is correct only when $\xi\ll 1$.

It is assumed that the power of the sources of heat release is independent of a change in the local thermodynamic parameters of the gas in the zone of absorption, (i.e. $\alpha\cong\text{const}\cong 1$), and is completely determined by the unchanged spatial distribution (in the given case gaussian) of radiation intensity and the predetermined function $f(t)\geqslant 0$ (with norming condition $f_{max}=O(1)$) that characterizes the time modulation of the pulse:

$$
\begin{aligned}
&\alpha I=f(t)g(x, y),\quad g(x, y)=\exp(-x^2-y^2),\\
&t>0,\ x, y\in G.
\end{aligned}
$$

Pulses are considered with characteristic times of action $\tau_f \gtrsim 1$.

At the initial instant $t = 0$ throughout region G

$$u=M_\infty,\ v=0,\ T=\rho=1,\ p=p_*=1/\gamma. \tag{2}$$

On the lower boundary $G(x\in(x_1;\ x_2),\ y=0,\ t>0)$ symmetry conditions are used: $v = 0$, $\partial u/\partial y = \partial p/\partial y = \partial T/\partial y = 0$. The parameters of the unperturbed flow (2) are assigned on the left boundary $(x=x_1,\ y\in(0;\ y_2))$. The upper and lateral boundaries of G were sufficiently far away ($y_2 \gg 1$, $|x_1| \gg 1$, $x_2 \gg 1$) so that during the entire investigated time interval $(0;\ t_k)$ the influence of these boundaries did not reach as far as the investigated local zone close to the beam. In all calculations $\gamma = 1.4$.

For numerical integration of system (1), a difference scheme was used [Ref. 9] of the "predictor-corrector" class with second order of central spatial approximation. The presence of model viscosity (evaluated and adjusted in the computational process) enabled straight-through calculation of shock waves without appreciable manifestation of dissipating factors outside of the zone of discontinuity. Nonuniform grids were used with step $h_x = h_y = 0.1$ in the central zone of G (the total number of intersections of the grid over the region $N \gtrsim 3200$). The step with respect to time $h_t \cong 0.015$-0.02.

The main series of calculations was done with the use of the function $f_1(t)$:

$$f_1(t)=t\exp\left(-(t/\tau_1)^2\right),\ \tau_1=3,\ t\geqslant 0.$$

The maximum value of $(f_1)_{max} \cong 1.29$ is reached at $t \cong 2.12$. The quantity $J(f_1)$, which in the first approximation is proportional to the total pulse energy $\mathscr{E}_1$, we introduce in accordance with the formula

$$J(f_1)=\int_{t_1}^{t_2} f_1(t)\,dt,\quad t_2>t_1\geqslant 0,$$

where $[t_1;\ t_2]$ is the characteristic time range of action of pulse f_1. For $f_1(t)$ we get

$$J(f_1)=\int_0^\infty f_1(t)\,dt=\tau_1^2/2=4{,}5.$$

Setting $t_1 = 0$, $t_2 \cong 2\tau_1 \cong 6$, we find the similar value $J(f_1) \cong 4.4$.

A number of variants corresponding to fixed numbers $M_\infty = 0.8$, 1.0, 1.2, 1.6, 2.0 and 2.4 were calculated at a constant number $Q = 10$. Let us consider the main peculiarities of the investigated nonlinear wave processes based on the resultant series of numerical solutions at $0 < t \lesssim 6$-7.

An increase in heat release near the axis of the beam causes formation of a zone of compressed heated gas with initial (at $t \lesssim 1$) spatial distributions of ρ and T close to gaussian. Then intense wave radiation is observed to develop from the compression zone along with continuing heat release. At $M_\infty \ll 1$, this radiation could have been treated within the framework of the one-dimensional model of divergent cylindrical waves, but in the investigated range of M_∞ and Q, complicated nonlinear interaction shows up between waves and flow, leading to an appreciably

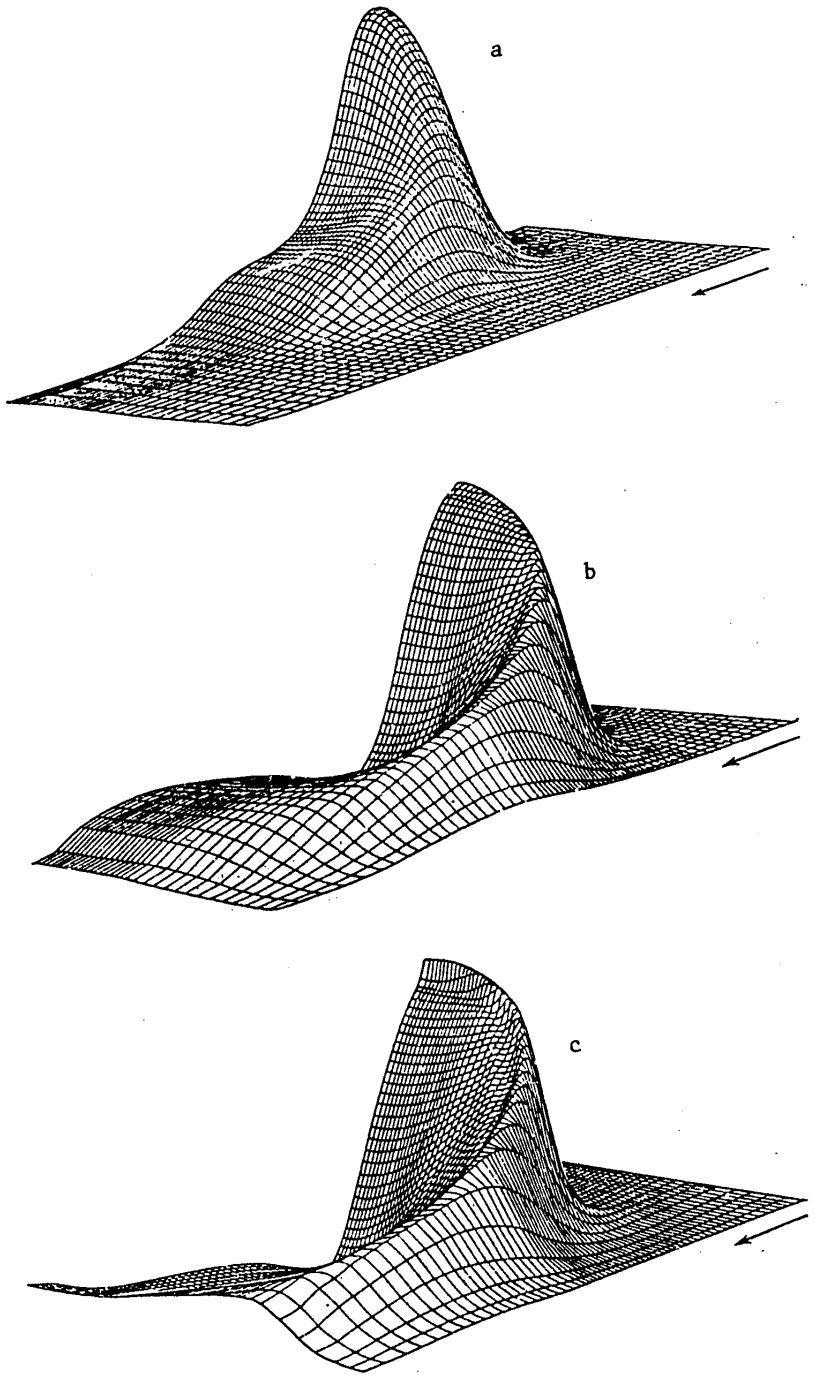

Fig. 1. Pressure distribution along the zone of absorption at different values of $t = 2$ (a), 4 (b), 6 (c) ($Q = 10$, $M_\infty = 1$)

two-dimensional pattern of the process. For example, in the direction opposite to the flow, characteristic nonlinear distortion of the compression wave profile was observed (fairly rapid at $Q = 10$), terminating in formation of a discontinuous shock wave front at $0.8 \leqslant M_\infty \leqslant 1.6$. At the same time, the wave radiation propagating in the direction of the flow (i. e. in the direction making angles $\theta^+ \in [0; \pi/2)$ to vector $\vec{u}_\infty$) leads to constant outflow of energy from the compression zone. In the entire series of calculations, formation of local zones of rarefaction (minimum pressures reaching $p(1.7; 0; 6.5)/p_a \cong 0.7$ in the variant with $M_\infty = 1.2$) was observed behind the compression wave downstream along axis $y = 0$ at $t \gtrsim 3$-4. This physical effect is typical of divergent waves that are close to cylindrical [Ref. 10].

Shown in Fig. 1a-c are pressure surfaces in the part of the computational region $\{x \in [-3; 8], y \in [0; 5]\}$ at $t = 2$, 4, 6 for the variant with $Q = 10$, $M_\infty = 1$. This series of graphs gives a clear representation of formation of the shock wave and the following rarefaction zone. The arrow indicates the direction of the velocity of the unperturbed gas flow.

It should be noted that in the variants with $M_\infty \leqslant 1.6$ during formation of the shock wave and its departure upstream, the heat release process still continues (at least until $t \cong 6$-7), and as a result, effects of shock wave interaction appear on the part of perturbations propagating from the paraxial zone of the beam through the region of locally subsonic flow behind the shock wave front.

Further contrary motion of the curved shock wave (with initial radius of curvature $r_w \cong 3$-4 at $t \cong 4$, $y \lesssim 2$, $M_\infty \leqslant 1.6$) is accompanied by a reduction in $p_w(t)$ ($p_w(t) = \max_{x \in (x_1, x_2)} p(x, 0, t) = p(x_w, 0, t)$ both due to wave radiation with respect to angles θ^+, and as a consequence of spatial divergence of the shock wave (with increasing r_w).

At $M_\infty \leqslant 1$ there is continuous motion of the forming shock wave against the flow with monotonic reduction in $p_w(t)$ ($p_w(t) \to p_*$, $x_w(t) \to -\infty$, $\partial x_w/\partial t \to M_* - 1$ as $t \to \infty$).

At $M_\infty > 1$ (more precisely at $1 < M_\infty \leqslant 1.6$ in the series of calculations with $Q = 10$), after p_w falls to some value $p_s(M_\infty) > p_a$, the shock wave stops, and then begins to move with the flow. The quantity $p_s(M_\infty)$ can be approximately evaluated from the known formula [Ref. 10] for a plane shock wave:

$$\frac{p_*}{p_a} = \frac{2\gamma}{\gamma+1} M_\infty^2 - \frac{\gamma-1}{\gamma+1}, \qquad M_\infty \geqslant 1. \tag{3}$$

In variants with $M_\infty \geqslant 2$, the pulse energy is no longer sufficient for reaching the initial degree of gas compression necessary for shock wave formation, much less for moving it against the stream. It should also be borne in mind that a reduction in maximum pressure amplitudes with increasing $M_\infty \gtrsim 2$ is due to a considerable extent to enhancement of "convective cooling" of the heat release zone, i. e. to an increase in the rate of heat transfer from the region of the beam along the flow ($\partial T_m/\partial M_\infty < 0$ on Fig. 4).

The described effects are partly reflected in Fig. 2a, b, c, showing graphs of instantaneous distributions of parameters along axis $y = 0$ (solid curves--$p(x, 0, t)/p_a$, dashed curves--$T(x, 0, t)$, dot-and-dash curves--local Mach numbers $M(x, 0, t)$) for variants with $M_\infty = 1.6$, 2.0 and 2.4 respectively ($Q = 10$).

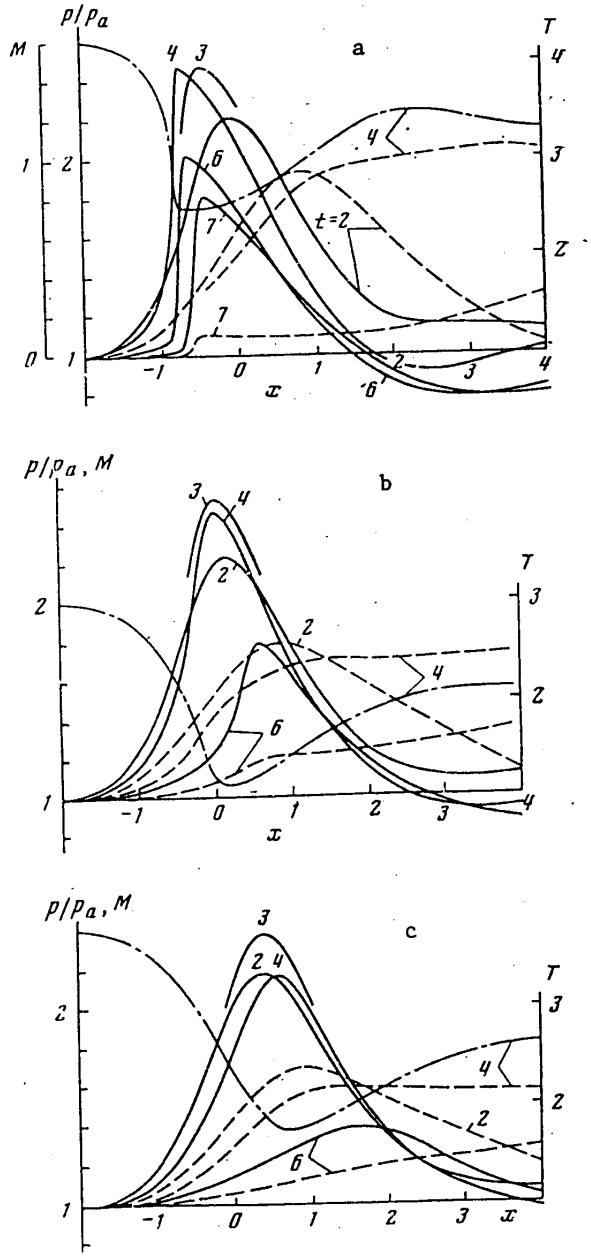

Fig. 2. Instantaneous distributions of parameters: $p(x, 0, t)/p_a$--solid curves, $T(x, 0, t)$--dashed curves, $M(x, 0, t)$--dot-and-dash curves; Figures a, b, c correspond to $M_\infty = 1.6$, 2.0 and 2.4 at $Q = 10$

Notice should be taken of the appreciably two-dimensional character of the flow around the absorption zone--the ratio $|u/v|$ close to the beam reached a value of the order of 0.5 in some cases. In this connection, it was practically only in variants with $M_\infty = 1.2$, 1.5 that formation of subsonic zones surrounded by supersonic flow was observed behind the shock wave. Behind the region of heat release, a heat trail propagating downstream is formed that is characterized by relatively weak dissipation of the temperature maximum.

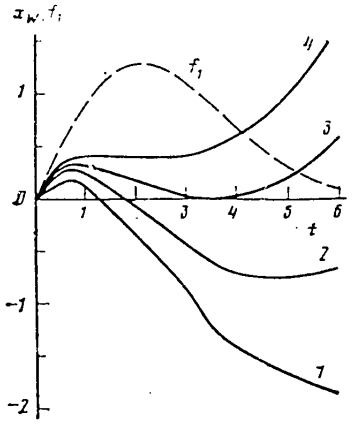

Fig. 3

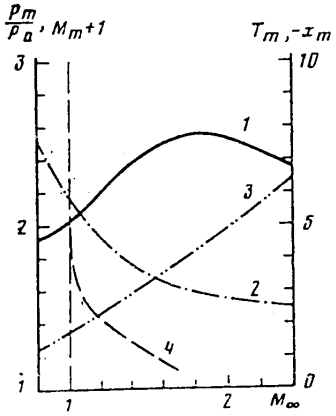

Fig. 4

Fig. 3. Longitudinal displacements $x_w(t)$ of the pressure maximum. Curves 1-4 correspond to $M_\infty = 1.2$, 1.6, 2.0, 2.4 at $Q = 10$

Fig. 4. Influence of number M_∞ (at $Q = 10$) on values of extremum parameters. Curves 1-4 correspond to p_{max}/p_a, T_{max}, M_{min}, $-x_m = -\min(x_w)$ at $Q = 10$

Fig. 3 shows the curve $f_1(t)$ the defines the given change in the level of heat release, and also a number of curves $x_w(t)$ that give an idea of the nature of displacement of maximum pressure p_w along the Ox axis in variants with $Q = 10$, $M = 1.2$, 1.6, 1.0, 2.4 (curves 1-4 respectively).

Naturally, the maximum advancement of the forming shock wave counter to the flow (until stopped) increases with a reduction in $M_\infty > 1$. For example, in the variant with $M_\infty = 1.2$ the shock wave stops at $t \cong 10$, $x_w \cong -2.1$. When this happens, $p_w(10)/p_a \cong 1.5$, which agrees well with the corresponding value of p_s/p_a from (3).

At $M_\infty = 2.4$, $u_w = \partial x_w/\partial t \geqslant 0$ for the duration of the whole pulse. Let us note that in variants with $M_\infty \geqslant 2$ at $t \gtrsim 5$ momentary maximum pressure amplitudes (throughout the region G) were observed on sloping sections of the compression wave (i. e. at $y > 0$). For example at $M_\infty = 2.4$ $P(4, 3, 6)/p_a \cong 1.74$, $p_w(6) \cong p(1.7, 0, 6) \cong 1.39$.

It can be seen from Fig. 2, 3 that the condition $|x_w(t)| \lesssim 0.5$ at $0 < t \leqslant 6$ when $M_\infty \cong 2$ is satisfied, resulting in near optimum conditions of continuous energetic additional pumping of the compression wave; these conditions lead to a value of $(p_w(t)/p_a)_{max} \cong 2.54$ that is maximum for all variants of the given series.

From the results of the entire series of calculations considered above with $Q = 10$, $f = f_1(t)$, graphs are plotted for the maximum pressures $p_m(M_\infty)/p_a$ and temperatures $T_m(M_\infty)$, minimum local Mach numbers $M_m(M_\infty)$ and quantities $x_m = \min_{t>0}(x_*(t))\,(x_m < 0)$ -- curves 1-4 respectively on Fig. 4. The extremum values p_m, T_m, M_m in each variant were determined from the set $x, y \in G, t \in (0; 6)$.

Thus from Fig. 4 we can graphically determine the "optimum" Mach number $M_\infty^* \cong 1.9$ at which the absolute maximum $(p_m/p_a)_{max} = p_w^*/p_a \cong 2.56$ is reached.

An analogous series of experiments was also done for $Q = 1$ ($f = f_1(t)$). In this case we found $M_\infty^* \cong 1.3$ ($p_w/p_a \cong 1.18$). For the variant with $M_\infty = 1.2$ (i. e. in the near optimum mode of generation), graphs of the instantaneous distributions of parameters along $y = 0$ are shown in Fig. 5 (notation analogous to Fig. 2). In the given case, a shock wave was not observed to form (analogously to $M_\infty = 2$ at $Q = 10$) and for the entire heat release process $|x_*(t)| \leq 0{,}15$ ($t \in (0; 6)$).

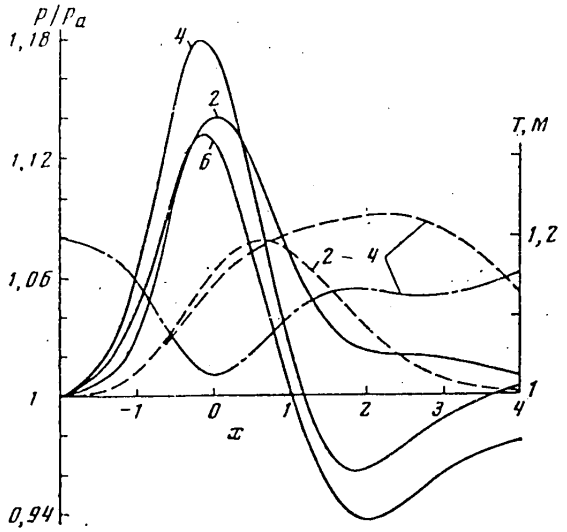

Fig. 5. Instantaneous distributions of parameters: $p(x, 0, t)/p_a$ --solid curves; $T(x, 0, t)$--dashed curves; $M(x, 0, t)$--dot-and-dash curves at $Q = 1$, $M = 1.2$. Numbers near the curves denote the values of dimensionless time t

It is characteristic that in the two series of calculations with $Q = 1$ and $Q = 10$ the quantity $\eta^* = (M_\infty^* - 1)/\sqrt{Q} \cong \text{const} \cong 0.3$ (the parameter $\eta = (M_\infty - 1)/Q$ is proportional to the dimensionless number δ introduced in Ref. 7 for the model of one-dimensional wave processes with weak nonlinearity). General similarity of solutions with respect to the parameter η was not observed, which is natural in light of the considerable differences of the given problem (strong nonlinearity, two-dimensionality, the pulse nature of heat release, etc.) from the conditions of the one-dimensional model of Ref. 7.

In a series of corresponding one-dimensional calculations ($v \equiv 0$, $g = \exp(-x^2)$), the maximum pressure amplitudes were considerably higher, which was to be expected

since no consideration was taken of wave propagation in the transverse direction. For example in the one-dimensional problem with $f = f_1(t)$, $Q = 10$, $M_\infty = 2$ the result was $p_w(4)/p_a \cong 4.4$; $T_m \cong 2.9$.

It is natural to assume that at $\partial g/\partial t = 0$ for any fixed number $M_\infty > 1$ and given time interval $\tau_f = \alpha(t_2 - t_1) \gtrsim 1$ that determines the characteristic duration of the heat release pulse there is some set of pulses $\{Qf\}$ (similar with respect to norm $\|Qf\| \cong QJ(f)/(t_2 - t_1)$) for which the compression wave is generated with attainment of maximum pressure amplitudes p_w^* on line $y = 0$ at $t \in (t_1; t_2)$. This optimum mode of generation, apparently, is realized simultaneously with satisfaction of the condition

$$|x_w(t)| < \varepsilon, \quad t \in (t_1; t_2), \tag{4}$$

where $\varepsilon < 1$ is a rather small quantity that may depend in turn on Qf, τ_f, g,...

In the general case, p_w^* can be determined either as the absolute maximum of $p(x, y, t)$ $(x, y \in G, t \in (t_1, t_2))$, or as the maximum average $\overline{p}_w^*$ (for the required time interval $(t_a; t_b)$ evaluated with respect to a set of points x, y belonging to some subregion $L \subset G$.

In the inverse problem being considered here (finding the "optimum" number M_∞^* for a given pulse shape Qf(t)), the optimality of the selected set $\{M_\infty, Qf\}$ is determined to a considerable extent by the smallness of the quantity ε found in the process of solution. Taking as the initial field the solution of variant $\{Q = 10, M_\infty = 1.6\}$ at $t = 7$ (i. e. after practical cessation of the action of pulse f_1 and at $x_w(7) \cong -0.4$), a solution was found for the problem of the effect of the second pulse $f_2(t)$ $(Q = 10, M_\infty = 1.6, t > 7, t_m = 8, \tau_2 = 1)$, where

$$f_2(t) = \begin{cases} \cos^4(\pi(t - t_m)/2\tau_2) \text{ when } t \in [t_m - \tau_2; t_m + \tau_2], \\ 0 \text{ when } t > t_m + \tau_2, \end{cases} \tag{5}$$

$$(f_2)_{max} = f_2(8) = 1; \quad J(f_2) = 0{,}75.$$

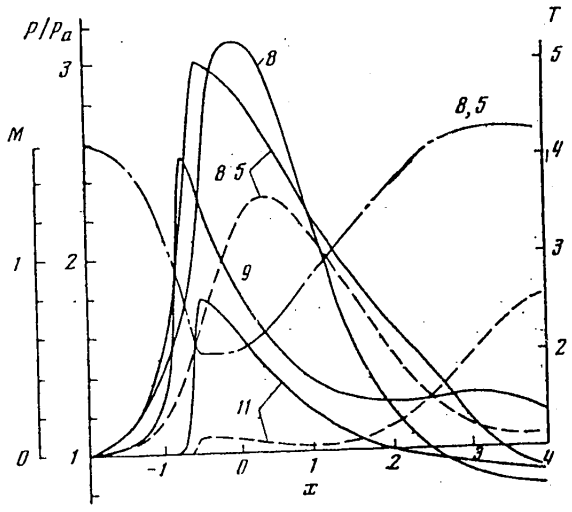

Fig. 6. Distributions of $p(x, 0, t)/p_a$, $T(x, 0, t)$, $M(x, 0, t)$ in the variant with $Q = 10$, $M_\infty = 1.6$, $f = f_2(t)$, $(t > 7)$. Numbers near the curves correspond to different t.

Graphs of instantaneous distributions of parameters along the Ox axis at $7 < t \leqslant 11$ are shown in Fig. 6 (notation analogous to Fig. 2). In the investigated process at total pulse energy $\mathscr{E}(f_2) \approx \mathscr{E}(f_1)/6$ not only higher amplitudes p_w are reached than in Fig. 2a ($p_w(8)/p_a \cong 3.1$), but also greater average values p_w: $\bar{p}_w(7; 11) \cong 2.4 > \bar{p}_w(0; 7) \cong 2.1$, where

$$\bar{p}_w(t_a; t_b) = \frac{1}{p_a(t_b - t_a)} \int_{t_a}^{t_b} p_w(t)\,dt, \quad t_b > t_a \geqslant 0.$$

It is characteristic that at $t = 11$, the field of parameters close to the beam takes on qualitative and quantitative similarities to the initial field (at $t = 7$), so that repeated application of a pulse of type f_2 (with $t_m \cong 12$, $\tau_2 \cong 1$) will give a presumably analogous effect in the range $t \in (11; 15)$.

For the sake of comparison, calculation was done where a pulse of type $f_2(t)$ was given as the original pulse ($Q = 10$, $M_\infty = 1.6$, $t > 0$, $t_m = 1$, $\tau_2 = 1$). In this case, a maximum pressure was attained of $p_m/p_a \cong p_w(1)/p_a \cong 2.5$ ($x_m \cong -0.6$).

Obviously the examined phenomenon of "summing" of the actions of sequential pulses can show up most effectively only in the case of relatively small time intervals between pulses, and also upon satisfaction of condition (4) (at least with $\varepsilon = O(1)$) throughout the time of action of pulses f_1, f_2,...

Thus in the case of a stationary beam position, the conditions that are optimum (in the sense of attainment of maximum pressure amplitudes) for a sufficiently long process of generation of intense waves in a flow with $M_\infty > 1$ can be realized by different methods: either by ensuring continuous energy release by means of an isolated pulse Qf at $M_\infty = M_\infty^*$ (and accordingly under condition (4)), or by using a series of successive short pulses $(Qf)_i$ ($i = 1, 2, 3,...$) synchronized with times t_i^* corresponding to return of the shock wave to $x = 0$ (each pulse in the series being obliged to advance the compression wave against the flow by a certain amount). In the second case by special selection of the sequence of pulses (Qf) it is possible to generate a resonant oscillatory process.

At $x_w \gtrsim 1$, $u_w > 0$, or at $M_\infty \leqslant 1$, effective additional energetic pumping of the primary wave is possible only by shifting the beam along the Ox axis behind point $x_w(t)$, i. e. it is necessary that $\partial g/\partial t \neq 0$. This motion of the beam under certain conditions may be equivalent to transition to a new value of relative velocity of the flow $M_\infty' \neq M_\infty$.

The problem of determining the optimum conditions of generation brings forward the general problem of controlling the gasdynamic system to be modeled by by means of distributed sources of volumetric heat release. The obvious advantages of modeling are associated with the capability of a rather arbitrary change in the "controlling functions" α, I (or f, g) directly in the process of calculation with continuous analysis of some set of parameters from the solution of the problem on the preceding time interval. The given approach is actually realized in variant (5), where selection of the algorithm of the controlling action (i. e. selection of $f_2(t)$ for the second pulse) is determined by solution of the problem on the preceding time interval (0; 7).

Naturally the process of operational "external" control of heat release sources (especially within the limits of quite short time intervals) is not always feasible under the conditions of an actual experiment. However, in some cases internal physical mechanisms of regulating local levels of heat release are possible. There are real situations where the coefficient of volumetric absorption α increases strongly in some region with increasing ρ or p (for example the mass coefficient of absorption $\alpha_m = \alpha/\rho = \text{const}$). Then under certain conditions the forming shock wave may make periodic advances against the flow with $M_\infty > 1$, receiving energetic additional pumping in the zone of the undisturbed beam with practically constant level of radiation intensity I.

In the case where α depends mainly on temperature (for example $\partial\alpha/\partial T > 0$), the problem of optimum energy pumping of the compression wave is complicated in view of displacement of the hot spot along the flow (at any $M_\infty > 0$).

In studying processes of generation of intense compression waves, an important question is the form of the function g(x, y) that defines the spatial distribution of radiation intensity. For example when $g(x, y) = F[(x/r_1)^2 + (y/r_2)^2]$, where $r_2 > r_1$, the zone of energy release extends in the transverse direction over the wave front, improving the optimality of wave amplification. Obviously a technique of this kind can be used in some cases to increase maximum pressure amplitudes without changing the overall pulse energy.

The question of possible effects of thermal self-stress of the beam (change in function g along axis Oz) at considerable levels of heat release remains open since an answer would require solution of an appreciably three-dimensional non-linear problem (in contrast to the linearized problems of Ref. 3, 11).

The author thanks K. I. Artamonov, S. A. Akhmanov and O. V. Rudenko for discussing the results and for constructive remarks.

REFERENCES

1. Hayes, J. N., "Thermal Blooming of Rapidly Slued Laser Beams", APPL. OPTICS, Vol 13, No 9, 1974, pp 2072-2074.

2. Ellinwood, J. W., Mirels, H., "Density Perturbations in Transonic Sluing Laser Beams", APPL. OPTICS, Vol 14, No 9, 1975, pp 2238-2242.

3. Wallace, J., Pasciak, J., "Thermal Blooming of a Rapidly Moving Laser Beam", APPL. OPTICS, Vol 15, No 1, 1976, pp 218-222.

4. Belokon', V. A., Rudenko, O. V., Khokhlov, R. V., "Aerodynamic Phenomena in Supersonic Flow Around a Laser Beam", AKUSTICHESKIY ZHURNAL, Vol 23, No 4, 1977, pp 632-634.

5. Kogan, M. N., Kucherov, A. N., Mikhaylov, A. S., Fonarev, A. S., "Planar Gas Flows in the Case of Weak Energy Supply", IZVESTIYA AKADEMII NAUK SSSR: MEKHANIKA ZHIDKOSTI I GAZA, No 5, 1978, pp 95-102.

6. Akhmanov, S. A., Rudenko, O. V., Fedorchenko, A. T., "Optical Generation of Intense Waves in Transonic Gas Flows", PIS'MA V ZHURNAL TEKHNICHESKOY FIZIKI, Vol 5, No 15, 1979, pp 934-936.

7. Karabutov, A. A., Rudenko, O. V., "Nonlinear Plane Waves Excited by Volumetric Sources in a Medium Moving at Transonic Velocity", AKUSTICHESKIY ZHURNAL, Vol 25, No 4, 1979, pp 536-541.

8. Bunkin, F. V., Malyarovskiy, A. P., Mikhalevich, V. G., Shipulo, G. P., "Experimental Study of the Sound Field of a Moving Optical-Acoustic Antenna", KVANTOVAYA ELEKTRONIKA, Vol 5, No 2, 1978, pp 457-459.

9. Fedorchenko, A. T., "On a Method of Calculating Two-Dimensional Unsteady Flows of Viscous Gas in Nozzles", DOKLADY AKADEMII NAUK SSSR, Vol 251, No 3, 1980, pp 578-582.

10. Landau, L. D., Lifshits, Ye. M., "Mekhanika sploshnykh sred" [Mechanics of Continuous Media], Moscow, Gostekhizdat, 1953.

11. Kogan, M. N., Kucherov, A. N., "Self-Focusing of a Gaussian Beam in a Supersonic Gas Flow", DOKLADY AKADEMII NAUK SSSR, Vol 241, No 1, 1978, pp 48-51.

6610
CSO: 8144/1798-B

CRYSTALS AND SEMICONDUCTORS

UDC 621.378.9:535

REGISTRATION OF PARAMETERS OF PULSED RADIATION USING THE SEMICONDUCTOR-METAL PHASE TRANSITION IN VANADIUM DIOXIDE

Moscow KVANTOVAYA ELEKTRONIKA in Russian Vol 8, No 6(108), Jun 81 pp 1363-1366

[Article by L. P. Ageykina, V. N. Gavrilov, V. V. Kapayev, V. G. Mokerov, I. V. Ryabinin and A. A. Chastov]

[Text] An investigation is made of the feasibility of measuring the cross sectional area of beams S and the energy E of pulsed radiation by utilizing the photoinduced stepwise change in the electrical resistance $\Delta\rho$ and coefficient of light transmission Δt associated with the semiconductor-metal phase transition in VO_2. Based on measurement of the amplitude and duration of the photoresponse pulses $\Delta\rho$ and Δt as functions of E and S, an analysis is made of the shape of these two pulse responses. It is shown that measurements of amplitudes and decay times of pulses $\Delta\rho$ and Δt can be used for simultaneous determination of S and E of pulsed radiation.

The strong change in coefficients of reflection R and light transmission t, and in the electrical resistance ρ accompanying the semiconductor-metal phase transition in vanadium dioxide [Ref. 1], and the feasibility of optically inducing this phase transition [Ref. 2] enable the use of VO_2 for determining the parameters of optical radiation [Ref. 3, 4]. However, although higher sensitivity was attained in Ref. 3 than for conventional pyroelectric sensors, the principle of controlling a "string" of metal phase that was used in that research is inconvenient because of the smallness of the effective sensing area. The method used in Ref. 2 to record laser intensity from measurement of the change in R during the phase transition is limited to the case of short pulses (10^{-6} s or less) during which the relaxation of heat in the substrate can be disregarded. The pulse energies E measured in Ref. 2 were of the order of the latent heat of the phase transition in thin VO_2 layers.

In this paper we will investigate for the first time the feasibility of simultaneous determination of two parameters of laser radiation--energy E and cross sectional area of the beam S--by recording either the amplitudes of responses with respect to electrical resistance $\Delta\rho$ and light transmission Δt, or their decay times τ_ρ and τ_t accompanying an optically induced phase transition. In doing this, the requirements for focusing of radiation are less severe than in Ref. 3, and the range of measurable energies is shifted toward higher values than in Ref. 2. The relaxation of heat into the substrate in our case enables registration of laser pulses with

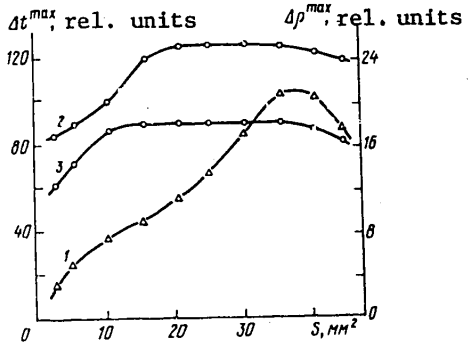

Fig. 1. Maximum values of response with respect to electrical resistance $\Delta\rho^{max}$ (1) and with respect to light transmission Δt^{max} (2, 3) as dependent on the area of irradiation S on a wavelength $\lambda = 1.06$ μm for pulse energy E = 660 (1, 2) and 470 mJ (3)

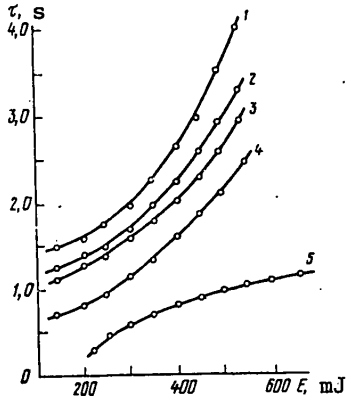

Fig. 2. Transmission signal decay time τ_t (1-4) and electrical resistance decay time τ_ρ (5) as dependent on pulse energy E for area S = 2.43 (1), 10.6 (2), 18.5 (3), 45.0 (4) and 10-50 mm² (5)

duration of 10^{-3}-10^{-2} s, which gives the capability of working with cw radiation sources as well when the appropriate modulators are used.

The VO_2 specimens were thin epitaxial layers (0.2-0.5 μm) produced by precipitation from a vapor-gas mixture of $VOCl_3$-CO_2-H_2-Ar on single-crystal sapphire substrates. Specimen diameter was 30 mm, substrate thickness 0.3-0.4 mm. The jump in ρ(T) at the phase transition was by a factor of 10^4, the zone of "smearing" of the phase transition $\Delta T_t = 3$ K, and the width of temperature hysteresis $\Delta T_H = 0.5$ K. For measurements of ρ and Δρ, point metallic electrodes were sputtered on diametrically opposed edges of the specimens. The wavelengths λ of the pulsed radiation were 0.69 and 1.06 μm. We point out that the given method is suitable for any $\lambda \leqslant 1.2$ μm (in the vicinity of strong absorption in VO_2). The duration of laser pulses τ_p was 10^{-3} s, E = 40-700 mJ, S = 2-50 mm². In the measurements, the VO_2 specimens were thermostatically held at 3 K (±0.1 K) lower than the temperature of "onset" of the phase transition. Heat exchange conditions were such that the initial state of the specimen after completion of a laser pulse was restored by heat exchange with the ambient medium in a time of ~100 s. An AL-107A light-emitting diode with radiation maximum close to $\lambda = 0.85$ μm was used to record the response with respect to Δt. There was at least a five-fold jump in t during the phase transition on this wavelength. The diameter of the readout beam in the plane of the specimen was ~0.8 mm. Radiation with any λ in the range of 0.7 μm $\leqslant \lambda \leqslant$ 6 μm can be used for "readout", where the jump in t during the phase transition exceeds a factor of 2, and the substrate is transparent. The angles of incidence of the recording and "readout" beam on the specimen were ~10° and 0° respectively. The measured pulse and the pulse responses Δρ(τ) and Δt(τ) were recorded on an oscilloscope with a relative error of amplitude measurements of ±5%.

It was found as a result of the measurements that there is a considerable difference in the shape of pulse responses with respect to resistance $\Delta\rho(\tau)$ and with respect to transmission $\Delta t(\tau)$: $\Delta\rho = \Delta\rho^{max}$ was reached in time $\tau \approx 10^{-3}$-10^{-2} s (depending on E and S), and the fall time τ_ρ was 0.1-1 s; $\Delta t = \Delta t^{max}$ was reached in $\tau \approx 10^{-2}$-10^{-1} second, and fall time τ_t was 1-5 s. We point out that since there was a noticeable change in ρ with T not only during the phase transition, but also within the limits of the semiconductor phase, τ_ρ was defined as the time of fall-off of $\Delta\rho$ to a specified level of 25 kΩ (for $\Delta\rho^{max} = 250$-300 kΩ) with relative error of ±10-12%. On the other hand, since the change in t(T) took place only in the zone of "smearing" of the phase transition, τ_t was taken as the time for Δt to a certain fraction of Δt^{max} ($^1/_{20}$), the relative error for τ_t being ±5-7%. Curves for $\Delta\rho^{max}$, Δt^{max} and τ_ρ, τ_t as functions of E and S are shown in Fig. 1 and 2.

Now let us turn to discussion of the principal results. Since the substrate is transparent for the wavelengths that we have chosen, the radiation energy is initially absorbed in the VO_2 film, and then transmitted to the substrate after a characteristic time $\tau_D = h^2/\kappa \approx 10^{-2}$ s (κ is the coefficient of thermal diffusivity of the substrate, and h is its thickness). Since this time is commensurate with τ_p and the size of the irradiated region was always greater than h, the temperature of the film and substrate becomes equal during the action of the pulse, and when $\tau > \tau_p$ the response pulse shape should be determined by the diffusion of heat along the substrate (since the thickness of the VO_2 film is much less than h, the role of the pulse shape at $\tau > \tau_p$ reduces to indication of the substrate temperature).

The actual dependences $\rho(T)$ and t(T) [Ref. 1] of the investigated VO_2 films in the vicinity of the phase transition can be approximated by piecewise-linear functions, i. e. at $T_1 < T < T_2$ $\rho, t \sim \gamma T$ (γ is a coefficient that is different for ρ and t; T_1 and T_2 are the temperatures of "onset" and "completion" of the phase transition) and ρ, t = const at $T > T_2$ and $T < T_1$. In view of the narrowness of ΔT_H, the temperature hysteresis can be disregarded here. Let us denote the changes in ρ and t during the phase transition by δ_ρ and δ_t. Let us arbitrarily break down the irradiated film area into three regions S_1, S_2 and S_3 in which $T > T_2$, $T_1 < T < T_2$ and $T < T_1$ respectively. Then the change in transmission during irradiation can be written as

$$\Delta t = \delta_t S_1 + \delta'_t S_2/k_2. \tag{1}$$

where $\delta'_t = \delta_t (T_{S2}^{max} - T_1)/(T_2 - T_1)$. Here T_{S2}^{max} is the maximum temperature of the film at the given instant in region S_2, the coefficient $k_2 > 1$ is introduced to account for the way that temperature in region S_2 depends on the x coordinate in the plane of the film (the quantity $k_2 = 2$ for a linear function T(x)).

Since the temperature T_0 of thermostatic control of the specimen is close to T_1, we can assume (disregarding heat transfer to the ambient space) that all the energy E is concentrated in regions 1 and 2. In this case

$$E = c\left[\left(T_2 - T_1 + \frac{T_{S1}^{max} - T_2}{k_1}\right) S_1 + \frac{T_{S2}^{max} - T_1}{k_2} S_2\right], \tag{2}$$

where c is the heat capacity of the substrate; k_1 plays the same role as k_2 in (1); T_{S1}^{max} is the maximum temperature in region S_1. Expressing S_2 from (2) and

substituting in (1), we readily see that the quantity Δt increases with decreasing S_1. At $S_1 = 0$, $\Delta t = \Delta t^{max} \sim E\delta_t/[c(T_2 - T_1)]$ is determined only by the energy in the pulse, and is independent of the irradiated area and T^{max}. This explains the wide interval of S over which the quantity Δt^{max} does not depend on S (see Fig. 1). The reduction in Δt (from Δt^{max}) at large S is due to drainage of heat from S_2 to S_3.

For the response with respect to resistance we can write

$$\Delta\rho \sim \delta_\rho l_1 + \delta_\rho' l_2/k_2, \tag{3}$$

where l_1, l_2 are the linear dimensions of regions S_1 and S_2 ($l_1 \sim \sqrt{S_1}$, $l_2 \sim \sqrt{S_1 + S_2} - \sqrt{S_1}$). Substituting S_2 from (2) in (3) we can see that $\Delta\rho$ in contrast to Δt decreases with a reduction in S_1 (at least at small S_1). This shows that the maximum value of $\Delta\rho$ is reached at $S_1 \neq 0$ ($T^{max} > T_2$), i. e. prior to Δt^{max}. For this reason, $\tau_\rho < \tau_t$. The maximum $\Delta\rho$ depends on the value of T^{max}, and hence on the initial area of irradiation. Thus the given simple arguments enable us to understand not only the difference in the shape of responses $\Delta t(\tau)$ and $\Delta\rho(\tau)$, but also to explain the behavior of the curves shown in Fig. 1 and 2.

Taking consideration of the fact that there is a segment of $\Delta t^{max}(S)$ on Fig. 1 that is independent of S, measurements of the dependences of Δt^{max} and $\Delta\rho^{max}$ on E and S can be used for simultaneous determination of the E and S of light beams. Vaporization of the VO_2 film is observed at high radiation density. This shows up as a steep drop in Δt^{max} and $\Delta\rho^{max}$ as S decreases for $S < 10$ mm^2 on Fig. 1. As a result of measurements of the dependences of τ_ρ on E and S it was established that like the case of $\Delta t^{max}(S)$ in the interval $S = 10$-45 mm^2, τ_ρ was independent of S, and was determined only by E, which shows up as coincidence of curves $\tau_\rho(E)$ for different S (see Fig. 2). On the other hand, τ_t depends on both E and S. This difference in the behavior of τ_ρ and τ_t may be due both to the different definition of τ_ρ and τ_t in our experiment, and to the above-mentioned differences in the nature of the description of responses with respect to ρ and t. These data are certainly of practical interest since measurements of τ_ρ and τ_t can be used as well as measurements of Δt^{max} and $\Delta\rho^{max}$ for simultaneous determination of E and S. The former method is preferable in view of the great simplicity and accuracy of determining time intervals. Here the value of E is first determined from τ_ρ (for the response with respect to $\Delta\rho$), and then S is determined from this E from family of curves (1-4) on Fig. 2. It has been established that threshold sensitivity with respect to E is 0.14 J/cm^2 for registration with respect to $\Delta\rho$, and 0.21 J/cm^2 for registration with respect to Δt, and the maximum permissible energy of the registered energy is 34 J/cm^2 (at $E \geq 34$ J/cm^2 the material vaporizes). The error of determining E within these limits is no greater than ±10%. Our measurements of S ranged from 10 to 50 mm^2.

REFERENCES

1. Mokerov, V. G., Rakov, A. V., FIZIKA TVERDOGO TELA, Vol 10, 1968, p 1556; Verleur, H. W., Barker, A. S., Berglund, C. N., PHYS. REV., Vol 172, 1968, p 788.

2. Roach, W. R., Balberg, J., SOLID STATE COMMS, Vol 9, 1971, p 551.

3. Jelks, E. S., Walser, R. M., Neal, W. H., APPL. PHYS. LETTS, Vol 26, 1975, p 355.

4. Semskov, K. I., Kazaryan, M. A., Mokerov, V. G., Petrash, G. G., Petrova, A. G., KVANTOVAYA ELEKTRONIKA, Vol 5, 1977, p 425.

6610
CSO: 1862/242

UDC 621.373.826.038.825.4

LASER SCREENS MADE OF SINGLE-CRYSTAL ZnSe AND ZnTe FILMS GROWN ON SAPPHIRE

Moscow KVANTOVAYA ELEKTRONIKA in Russian Vol 8, No 6(108), Jun 81 pp 1380-1382

[Article by A. V. Dudenkova, A. S. Nasibov, E. A. Senokosov, S. D. Skorbun, Yu. M. Popov, A. N. Usatyy and V. M. Tsaran, Physics Institute imeni P. N. Lebedev, USSR Academy of Sciences]

[Text] Lasing is realized on single-crystal ZnSe and ZnTe films grown on sapphire with longitudinal electron-beam excitation.

At the present time, the process of making semiconductor laser screens for cathode ray tubes consists of a number of technological operations: growing single crystals, making disks from these crystals up to 50 mm in diameter with subsequent chemical and mechanical polishing, application of reflecting coatings and cementing to a transparent backing [Ref. 1]. Of considerable interest is the possibility of simplifying the technology of making laser screens by growing a single-crystal semiconductor film directly on a transparent substrate such as sapphire. In this case, the reflective coatings that form the optical cavity are applied to the surface of the semiconductor film on the side where the electron beam is incident on the backing.

A promising semiconductor material for laser screens that radiate in the blue region of the spectrum ($\lambda = 450$ nm at $T = 80$ K) is ZnTe. At present there are a number of reports on production of single-crystal layers of ZnSe on sapphire backings (e. g. Ref. 2-4). These reports note a high degree of perfection of the epitaxial layers, effective radiative recombination in the region of 445-450 nm, and also laser emission with transverse electron-beam excitation [Ref. 4]. Material of much higher quality is required to get lasing with longitudinal electron-beam excitation.

This article is the first to report attainment of lasing with longitudinal electron-beam excitation of a laser screen in which the active element was epitaxial layers of ZnSe and ZnTe grown on thin sapphire backings (300 and 500 μm thick).

The single-crystal layers of ZnSe and ZnTe were grown by a quasi-closed volume technique [Ref. 5]. The substrates were sapphire crystal plates of various orientation. The grown layers of ZnSe 20-50 μm thick and 20-50 mm in diameter had quasi-parallel orientation relative to the substrate with retention of the following epitaxial relations: (111) ZnSe parallel to (0001) Al_2O_3 and (111) ZnSe parallel to $(\bar{2}110)$ Al_2O_3.

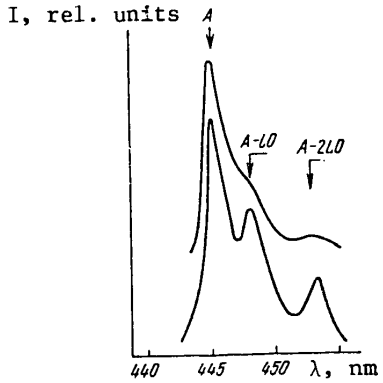

Fig. 1. Cathodoluminescence spectra of single-crystal ZnSe films grown on sapphire

The surface morphology of the ZnSe layers depended to a great extent on the orientation of the substrates. Layers grown on substrates (0001) had a smooth surface showing growth figures in the shape of triangles or hexgons formed as a result of superposition of several triangles. For ZnSe layers on substrates $(\bar{2}110)$ Al_2O_3 a typical feature is growth in steps with dimensions that reach 0.1-0.5 mm.

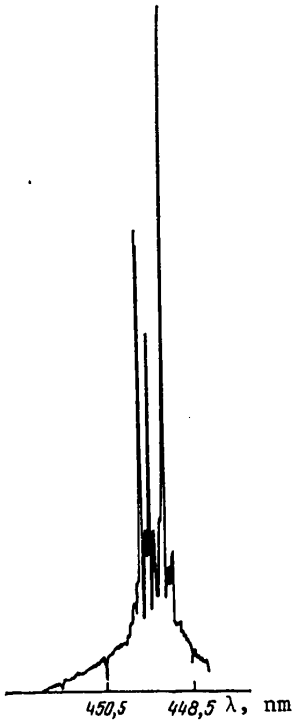

Fig. 2. Spectrum of stimulated emission of a laser screen based on a film of ZnSe on sapphire; $E_0 = 75$ keV, $j = 100$ A/cm^2, $T = 80$ K. Thicknesses of the film and sapphire plate 40 and 300 μm respectively

X-ray and electron-radiographic studies and investigation of the spectra of photo and cathodoluminescence showed that the grown layers have a high degree of crystallinity, with a quantum radiation yield approaching that of massive single crystals [Ref. 6]. The cathodoluminescence spectra of such layers (Fig. 1) at low excitation levels (energy of excitation electrons $E_0 = 20$ keV, pumping current density $j < 1$ A/cm^2, $T = 80$ K) show lines of emission of a free exciton (A) and its phonon repetitions (A - *LO*, A - 2*LO*).

In making the laser screen the surface of the film was mechanically polished to get a mirror surface, and then the resultant destroyed layer was etched away by a polishing etchant. The finished thickness of the investigated ZnSe films was 18 and 40 μm. A silver reflective coating ($R_1 = 92\%$) was applied to the semiconductor film, and a multilayered dielectric mirror ($R_2 = 80\%$) was applied to the sapphire. Excitation was realized in the television mode by an electron beam with $E_0 = 75$ keV and diameter on the target of 10 μm. The laser screen was attached to the sapphire window of a nitrogen cryostat.

Lasing was observed at a current density of about 90 A/cm^2. Removal of the reflective coating applied to the sapphire increased the threshold to 200 A/cm^2. Fig. 2

shows the spectrum of stimulated emission of the laser screen. The distance between modes corresponds to a compound cavity, and maximum intensity is shown by the modes that are simultaneously the fundamental of the epitaxial layer and the cavity formed by the mirrors. The compound mode makeup and the considerable increase in the threshold upon removal of the reflective coating from the sapphire show that lasing took place in the cavity with external mirror.

Similar results were found on laser screens made from single-crystal ZnSe films grown on sapphire ($j_{th} \cong 90$ A/cm^2), $\lambda = 531$ nm; width of the spectrum at half-amplitude $\Delta\lambda = 0.96$ nm. Emission power on the lasing threshold ~50 mW).

A reduction in the thickness of the sapphire to 50-100 μm or an increase in the diameter of the electron beam to 100 μm should reduce the lasing threshold several times. Practical use of such a technique for making laser screens necessitates an increase in active element diameter to 50 mm, improvement of semiconductor layer homogeneity, and a higher quantum yield.

REFERENCES

1. Basov, N. G., Bogdankevich, O. V., Kamenev, V. M., Papusha, V. P., Pochernyayev, I. M., Nasibov, A. S., Pechenov, A. N., DOKLADY AKADEMII NAUK SSSR, Vol 205, 1972, p 72.

2. Ratcheva, T. M., Dragieva, PHYS. STAT. SOL., Vol A 29, 1975, p 579.

3. Stutius, W., APPL. PHYS. LETTS, Vol 33, 1978, p 656.

4. Dudenkova, A. V., Popov, Yu. M., Senokosov, E. A., Skorbun, S. D., Usatyy, A. N., Tsaran, V. M., KRATKIYE SOOBSHCHENIYA PO FIZIKE, FIAN, Vol 4, 1978, p 3.

5. Senokosov, E. A., Usatyy, A. N., Tsaran, V. M., Tsirulik, L. D., in: "Fizicheskiye protsessy v geterostrukturakh i nekotorykh soyedineniyakh A^2B^6" [Physical Processes in Heterostructures and Some A^2B^6 Compounds], Kishinev, Shtiintsa, 1974, p 85.

6. Dudenkova, A. V., Popov, Yu. M., Senokosov, E. A., Skorbun, S. D., Tsaran, V. M., "Tezisy dokladov XXVII soveshchaniya po lyuminestsentsii (kristallofosfory)" [Abstracts of Reports to the Twenty-Seventh Conference on Luminescence (Crystal Phosphors)], Ezerniyeki, Latvian SSR, 13-16 May, 1980, p 203.

6610
CSO: 1862/242

FLUID DYNAMICS

UDC 532.135;532.526

BOUNDARY LAYER OF A BODY OF REVOLUTION IN A DRAG-REDUCING POLYMER SOLUTION

Moscow IZVESTIYA AKADEMII NAUK SSSR: MEKHANIKA ZHIDKOSTI I GAZA in Russian No 3, May-Jun 81 (manuscript received 8 Aug 79) pp 40-48

[Paper by V.B. Amfilokhiyev, V.V. Droblenkov, G.I. Kanevskiy and N.P. Mazayeva, Leningrad]

[Text] The reduction of the viscous resistance of solids moving in a drop liquid by means of dissolving certain long molecular chain polymers in it must be recognized as one of the most promising methods of decreasing resistance at the present time [1]. Since the major effect of the introduction of polymers is a sharp reduction in turbulent friction, it is natural to make use of a semi-empirical turbulence theory for the calculation of flows of weak polymer solutions. One of these theories [2] was successfully applied to the calculation of the boundary layer at a flat plate [3] and a current with a pressure gradient near the flat contour [4].

A possible method of calculating an axially symmetric boundary layer is presented in this paper for the case of the motion of a solid in weak polymer solutions with a constant concentration. The method is based on the utilization of the velocity profile and a system of integral equations which most completely take into account the effects of the transverse curvature of the streamlined surface. The computational scheme makes it possible to account for a change in flow conditions in the boundary layer.

1. One of the major features of the calculation of an axially symmetric boundary layer is the necessity of taking into account the transverse curvature of the streamlined surface, and related to this, the finite thickness of the layer as compared to the local cross-sectional radius of the solid of revolution, It is insufficient to calculate the axially symmetric boundary layer as a thin layer, i.e., with the assumption that $\delta << R_w$, where δ is the boundary layer thickness and R_w is the cross-sectional radius of the solid, especially in the case where a polymer solution flows around the solid, and where the calculation errors which follow from the assumption that $\delta << R_w$ can substantially distort the gain predicted through the use of polymers. For this reason, it is expedient to handle the calculation of the boundary layer of a solid of revolution as a "thick" one, for which one can use either partial

differential equations for the boundary layer, or integral relationships. From a practical viewpoint, the integral equations are more attractive, first of all because of their economy, and secondly, because of the fact that in their application, no data is needed on the fine turbulent mechanisms, and only a successful approximation is needed for the profiles of the longitudinal components of the averaged velocity. At the same time, it has been demonstrated for a plane boundary layer [5, 6], that if the family of these profiles is specified as a multiparameter family, the results are not inferior in terms of precision to those obtained by means of differential techniques, while accounting for the introduction of polymer additives into the flow causes no fundamental difficulties [3, 4].

The integral method of [7] is adopted in the following for the calculation of the boundary layer on a body of revolution around which the polymer solution flows, where this method is based on a three parameter family of profiles for the longitudinal component of the averaged velocity, which has the form:

$$U/v^* = \varkappa^{-1} \ln (v^* Y/\nu) + B + \varkappa^{-1} \Pi(X) W(Y/\delta) + f(Y/R_\omega) \tag{1.1}$$

Here, U is the longitudinal averaged velocity, $v^* = \sqrt{\tau_w/\rho}$ is the dynamic velocity, $\tau_w = \tau_w(X)$ is tangential stress at the streamlined surface, X is the longitudinal coordinate which coincides with the meridian line circling the solid, ρ is the fluid density, $\kappa = 0.4$ is the first constant of turbulence, Y is the transverse coordinate normal to the meridian line circling the solid, B is the second constant of turbulence or the parameter which takes into account the influence of the polymers, W is the Coles function, f is a function which takes into account the influence of the transverse curvature of the streamlined surface and ν is the kinematic fluid viscosity coefficient.

It can be seen from formula (1.1) that the first two terms take the form of the usual logarithmic law, justified in the region near the wall for practically any turbulent boundary layer, while the third term reflects the special features of turbulent intermixing in the outer region, where the Coles parameter $\Pi(X)$ makes it possible to take into account the influence of the longitudinal curvature of the solid and the external pressure gradient. To facilitate the calculations, the form of the function $W(Y/\delta)$ was simplified as compared to the usually employed cosine curve [8]:

$$W(Y/\delta) = 6(Y/\delta)^2 - 4(Y/\delta)^3 \tag{1.2}$$

The approximation (1.2) used here satisfies the boundary conditions $W(0) = W'(0) = W'(1) = 0$, $W(1) = 2$ and is in sufficiently good agreement with experimental data. The form of the fourth term of the right side of (1.1) was determined from various considerations in [8, 9]; the proposed functions were different in form, but yielded close results numerically. Since the form of both functions is rather complex [8], a simple parabolic approximation is used instead of them:

$$f(Y/R_\omega) = A\varkappa^{-1}(Y/R_\omega)^{1/4} \tag{1.3}$$

which when $A = -0.46$ practically coincides with the curves of [8, 9]. The match of this approximation to the experimental data for gradient-free, axially symmetric flow was confirmed in [7] by means of comparing the results of experiments on longitudinally streamlined cylinders [10].

By substituting expression (1.2) and (1.3) in formula (1.1), and converting to dimensionless quantities, we obtain:

$$u\omega^{-1}=\varkappa^{-1}\ln(\omega u_\delta \mathrm{Re}\, y)+B+\Pi\varkappa^{-1}[6(y/\delta_1)^2-4(y/\delta)^3]+ \\ +A\varkappa^{-1}(y/r_w)^{1/2} \\ \delta_1=\delta/L,\quad y=Y/L,\quad x=X/L,\quad r_w=R_w/L \\ \omega=v^*/U_\delta,\quad u=U/U_\delta,\quad u_\delta=U_\delta/v_\infty,\quad \mathrm{Re}=v_\infty L/\nu \tag{1.4}$$

Here, L is the length of the solid, v_∞ is the unperturbed flow velocity, $U_\delta = U_\delta(X)$ is the velocity at the outer boundary of the boundary layer.

Expression (1.4) defines the dimensionless family of profiles of the longitudinal averaged velocity in a boundary layer containing three dimensionless parameters: $\delta_1(x)$, $\Pi(x)$ and $\omega(x)$.

The following are integrated to determine these parameters: the momentum equation, the mass capture equation and the law governing the resistance, which follows from expression (1.4). The integral momentum relationship is used in a form which contains integral areas and is suitable for a thick, axially symmetric boundary layer:

$$\frac{d\theta_1^{**}}{dx}+\frac{1}{u_\delta}\frac{du_\delta}{dx}(\theta_1^*+2\theta_1^{**})=r_w\omega^2 \\ \theta^*=\int_0^\delta (1-u)R\,dY,\quad \theta^{**}=\int_0^\delta u(1-u)R\,dY \\ \theta_1^*=\theta^*/L^2,\quad \theta_1^{**}=\theta^{**}/L^2,\quad R=R_w+Y\cos\beta \tag{1.5}$$

Here, θ^* is the displacement area (per radian of the angular cylindrical coordinate), θ^{**} is the area of loss of momentum, R is the radial cylindrical coordinate, β is the angle between the axis of the solid of revolution and the tangent to the line circling it at the meridian.

The integration of the differential continuity equation over the thickness of the boundary layer, or the utilization of the equality of the fluid mass entering and leaving a section of the boundary layer of length dX, gives a mass capture equation which has the following form for an axially symmetric flow:

$$\frac{1}{U_\delta R_\delta}\frac{d}{dX}[U_\delta(\theta-\theta^*)]=\frac{d\delta}{dX}-\frac{V_\delta}{U_\delta} \\ \theta=\int_0^\delta R\,dY=R_w\delta+0{,}5\delta^2\cos\beta,\quad R_\delta=R_w+\delta\cos\beta \tag{1.6}$$

Here, θ is the boundary layer area, R_δ is its outer boundary radius and V_δ is the transverse averaged component of the velocity at the boundary of the layer.

The processing of the experimental data of [11] made it possible to establish the fact that the right side of equation (1.6) can be replaced by a mass capture function in form found in [8], proposed for a plane boundary layer, if the argument of this function is computed not in terms of the thicknesses, but rather in terms of the areas of the boundary layer:

(1.7) $$d\delta/dX - V_\delta/U_\delta = F(H_1) = 0{,}0306\,(H_1-3)^{-0{,}653}$$
$$H_1 = (\theta_1 - \theta_1^*)/\theta_1^{**}, \quad \theta_1 = \theta/L^2$$

Taking (1.7) into account, equation (1.6) can be written in the form:

(1.8) $$d[u_\delta(\theta_1 - \theta_1^*)]/dx = Eu_\delta r_\delta$$

The law governing the resistance is derived from the velocity profile (1.4) and can be written in differential form as follows:

(1.9) $$\left(\frac{1}{\delta_1} + \frac{A}{2\delta_1^{1/2} r_w^{1/2}}\right)\frac{d\delta_1}{dx} + 2\frac{d\Pi}{dx} + \left(\frac{1}{\omega} + \frac{\varkappa}{\omega^2}\right)\frac{d\omega}{dx} =$$
$$= -\frac{1}{u_\delta}\frac{du_\delta}{dx} + \frac{A\delta_1^{1/2}}{2r_w^{1/2}}\frac{dr_w}{dx} - \varkappa\frac{dB}{dx}$$

In the absence of polymers, the last term disappears, since in this case, B = const.= = 4.9.

The Runge-Kutta method was used to integrate the system of three ordinary differential equations (1.5), (1.8) and (1.9). The calculations were performed on a BESM-6 digital computer programmed in ALGOL-60 and a YeS-1022 computer programmed in FORTRAN. The initial conditions for the system of differential equations were derived using one of three procedures:

1. If the boundary layer was assumed to be turbulent, starting with the critical bow point, then at a distance along the axis of Z = 0 to 0.2, its characteristics were determined just as for a flat plate with the corresponding Reynolds number.

2. If the boundary layer was calculated assuming that the change of flow modes occurs at a conditional laminar--turbulent transition point, then the momentum continuity condition $\theta_L^{**} = \theta_T^{**}$ was used at this point, where the subscripts L and T correspond to the laminar and turbulent portions. The laminar section was computed by the conventional single parameter technique, while the transition cross-section was defined either as the cross section where an agitator is located, or on the basis of the empirical formula of [7]:

(1.10) $$\mathrm{Re}_{LT}^{**} = \exp(44{,}9 - 14{,}7H), \quad \mathrm{Re}^{**} = U_\delta\delta^{**}/\nu, \quad H = \delta^*/\delta^{**}$$
$$\delta^* = \int_0^\delta (1-u)\,dY, \quad \delta^{**} = \int_0^\delta u(1-u)\,dY$$

Here, the double subscript LT indicates the transition cross-section, δ^* is the displacement thickness and δ^{**} is the momentum loss thickness. Formula (1.10) is justified for a degree of free turbulence of ε = 0.3 - 0.7%. The system of the following transcendental equations was solved to determine the initial values of δ_{LT}, Π_{LT} and ω_{LT}: $\theta_1^{**} = \theta_1^{**}(\delta_1)$, $H = \delta^*/\delta^{**}$ and (1.4) for the case where $y = \delta_1$ and $u = u_\delta$.

3. If the boundary layer was calculated taking into account the laminar, transition and turbulent flow regions, then the characteristics of the laminar layer were determined using the method of L.G. Loytsyanskiy, while the parameters of the transition region were determined on the basis of the distribution of the intermixing

coefficient using the procedure proposed in [12]; following after the center of the transition region, where the intermixing coefficient was taken as 0.5, a cross-section was chosen in which the momentum loss area of the laminar boundary layer calculated from the critical bow point matched that of the turbulent boundary layer which was calculated from the transition onset point.

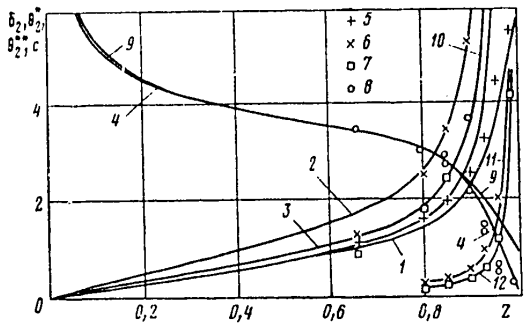

Figure 1.

It must be noted that for all three variants of the determination of the initial conditions, the characteristics of the turbulent portion of the boundary layer differ slightly from one another if the laminar--turbulent transition occurs far away from the bow extremity of the solid, something which almost always occurs at Reynolds numbers of practical interest.

The results of calculating the boundary layer of the solid of revolution described in [11], in the case where an ordinary viscous liquid flows around it, were compared with the experimental data of [11] for Re = $1.262 \cdot 10^6$ in Figure 1. Curves 1, 2 and 3 correspond to the dimensionless characteristics of the boundary layer, $\delta_2 = 10^2\delta_1$, $\theta_2^* = 10^3\theta_1^*/r_w$ and $\theta_2^{**} = 10^3\theta_1^{**}/r_w$. Curves 11 and 12 take the form of extensions of curves 2 and 3, drawn to a scale of 1:10. Curve 4 corresponds to the distribution of the local coefficient of friction $C_j = 2\tau_k/\rho U_\delta^2 = 2\omega^2$, where $C = 10^3 C_f$. Experimental points 5, 6, 7 and 8, which are given in the data of paper [11], correspond to these same characteristics. As can be seen from the comparison made above, the results of the calculations are in good agreement with the measurement data, practically right out to the very tail end extremity of the body.

If the boundary layer is calculated as a thin one, i.e., the assumption that $\delta << R_w$ is used, then $\delta^* R_w$ must be substituted for θ^*, $\delta^{**} R_w$ for θ^{**} and δR_w for θ in equations (1.5) and (1.8), while one must set $f(Y/R_w) = 0$ in expressions (1.1), (1.4) and (1.9) (this can be done by formally setting A = 0). The results of the calculation of the local coefficient of friction and the boundary layer thickness, performed with these assumptions for the same body of revolution, are shown in Figure 1 (curves 9 and 10). The use of such simplifications leads to the fact that the agreement with the experimental data in the region of the tail extremity of the body becomes worse. The cited results confirm the expediency of taking into account the finite thickness of the axially symmetric boundary layer.

2. When calculating the boundary layer of a solid of revolution in a polymer solution, equations (1.5) and (1.8), which essentially take the form of the laws of momentum and mass conservation, do not change. In equation (1.9), the last term $\varkappa dB/dx \neq 0$, since the parameter B, included in the velocity profile (1.4), is not a constant in a polymer solution.

Several semi-empirical theories exist at the present time, in which relationships are proposed for B as a function of the properties of the polymer and the characteristics of the polymer-solvent system. In the simplest of them, and apparently, the first one to appear, it is proposed that B be treated as a sum [13]:

$$B=B_0+\Delta B, \quad (B_0=\text{const})$$
$$v^*\leqslant v_0^*: \quad \Delta B=0, \quad v^*\geqslant v_0^*: \quad \Delta B=\alpha \ln (v^*/v_0^*) \tag{2.1}$$

Here, $B_0 = 4.9$ (for a tube, 5.5), ΔB is the "polymer increment", the coefficient α depends on the kind and concentration of the polymer, while v_0^* is the threshold dynamic velocity, starting at which the presence of polymers in the solution becomes effective. We obtain from formula (2.1):

$$dB/dx=\alpha(\omega u_\delta)^{-1}d(\omega u_\delta)/dx \tag{2.2}$$

Expression (2.2) should be substituted in (1.9), and relationships (2.1) substituted in (1.4). The values of α and v_0^* should be determined experimentally. For example, for a solution of WSR-301 polyethylene oxide with a mass concentration of $c = 10^{-5}$ they are equal to $v_0^* \approx 0.023$ m/sec and $\alpha = \alpha(c, M) = 4.2 - 4.5$ (it was assumed in the calculations that $\alpha = 4.343$; M is the molecular weight of the polymer).

A more sophisticated theory to account for the polymer increments was developed in [1 - 4]. In this case, one of the possible and simplest approximations of the parameter B has the form [14]:

$$B=8{,}8F^{-0{,}6}-3{,}9, \quad F=1-b\operatorname{arctg}[1{,}7(v^*/v_0^*-1)],$$
$$b=0{,}37\operatorname{arctg}(1{,}2\,cM^{0{,}89}) \tag{2.3}$$

As can be seen from the formulas cited here, it is not necessary with this theory to determine the two parameters from experiments, since the first of them, b = b(c, M), similar to α in Meyer's correlation of (2.1), is computed from the universal function (2.3), while:

$$v_0^* = DM^{-0.89} \tag{2.4}$$

where D depends only on the type of polymer. The application of (2.4) to WSR-301 polyethylene oxide ($D = 1.37 \cdot 10^4$ m/sec) yields $v_0^* = 0.0246$ m/sec, which is almost no different than the experimental value given above. The use of (2.3) yields a value of b = 0.49.

It should be noted that the structure of expressions (2.3) is more reasonable than that of relationships (2.1). Using formulas (2.1), it turns out that at high rates of motion ($v^* \to \infty$), the polymer effect increases without bound ($B \to \infty$). The use of formulas (2.3) when $v^* \to \infty$ leads to a value of $F = F_\infty = 0.235$, i.e., there is no increase in the velocity that can lead to a reduction in the resistance of more than that corresponding to B = 17.3.

Differentiating expression (2.3) with respect to x, taking into account the fact that $v^* = \omega u_\delta v_\infty$, yields:

$$\frac{dB}{dx} = \frac{8{,}976bF^{-1{,}6}(v_\infty/v_0^*)}{1+[1{,}7(\omega u_\delta(v_\infty/v_0^*)-1)]^2}\frac{d}{dx}(\omega u_\delta) \tag{2.5}$$

Attention is drawn to the fact that using Meyer's correlation, the increment added to differential equation (1.9), besides the variables ω and u_δ, contained only the constant parameter α, while in accordance with the theory of [1 - 4], the added increment contained the additional ratio v_∞/v_0^* related to the rate of travel. The influence of this added component is rather complex, but when $v_\infty \to \infty$, it turns out that $dB/dx \to 0$, i.e., the impact of polymers present in the flow in the case of the transition to a resistance law in differential form for very high velocities, is primarily taken into account solely through the initial conditions, in which the undifferentiated resistance function plays a part. It is not precluded that such a result is obtained only by virtue of the form of the proposed approximation (2.3). In order to avoid the "disappearance" of dB/dx at large values of v_∞, in the denominator of expression (2.5), there should be a linear function of v_∞/v_0^*, rather than a square law. One can arrive at the desired result if the arctangent in the second of the formulas of (2.3) is replaced by the logarithm:

$$\operatorname{arctg}[1{,}7(v^*/v_0^*-1)] \approx a \ln (v^*/v_0^*) \tag{2.6}$$

For a range of variation of the argument $v^*/v_0^* = 1$ to 10, good agreement is obtained between the left and right sides of expression (2.6) when a = 0.945. In this case, strict equality occurs when $v^*/v_0^* = 4.4$. Using this value, one can choose the coefficients of the linear expression with which it is desireable to replace the square law in the denominator of formula (2.5). As a result, one can derive:

$$\frac{dB}{dx} = \frac{8{,}976bF^{-1{,}6}(v_\infty/v_0^*)}{1.+9{,}826[\omega u_\delta(v_\infty/v_0^*)-1]}\frac{d}{dx}(\omega u_\delta) \tag{2.7}$$

It can be seen that when $v_\infty \to \infty$ ($v^* \to \infty$), expression (2.7) automatically changes over to a form analogous to (2.2). This is responsible for the possibility in the case of using Meyer's correlation of not seeking out α each time experimentally, but rather determining its value analytically by means of the parameters of the theory of [1 - 4]:

$$\alpha = 0.913\, b\, F_\infty^{-1.6} = 9.2\, b \tag{2.8}$$

For the example considered here, formula (2.8) yields $\alpha \approx 4.48$. The threshold value of the dynamic velocity for both theories can likewise be calculated from formula (2.4).

The calculations of the boundary layer of the solid of revolution described in [11] were carried out for the case of streamline flow around it by a solution of WSR-301 polyethylene oxide with a molecular weight of $M \approx 3 \cdot 10^6$ at a concentration of $c = 10^{-5}$ in two variants: using Meyer's correlation and based on the theory of [1 - 4]. All of the calculations were performed for two variants of the specification of the initial data:

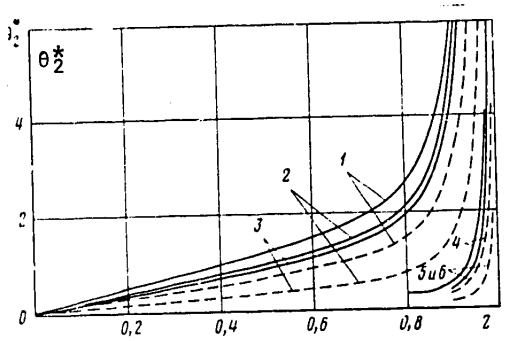

Figure 2.

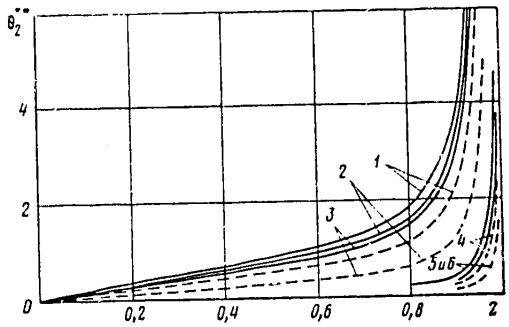

Figure 3.

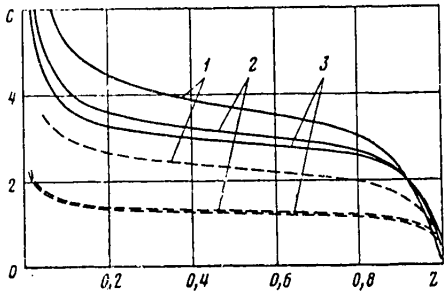

Figure 4.

1. L = 1.578 m, v_∞ = 0.913 m/sec, Re = $1.262 \cdot 10^6$
2. L = 3.2 m, v_∞ = 15.0 m/sec, Re = $3.057 \cdot 10^7$

The results of calculations of the dimensionless integral areas of the boundary layer and the coefficient of local friction are given in Figures 2 - 4, where the designations are analogous to those of Figure 1. In these figures, curves 1 correspond to streamline flow around the solid by an ordinary viscous liquid,

curves 2 are for calculations using Meyer's correlation and curves 3 are calculations based on the theory of [1 - 4]. The solid curves apply to a Reynolds number of $1.262 \cdot 10^6$, while the dashed curves are for $Re = 3.057 \cdot 10^7$; curves 4, 5 and 6 take the form of extensions of curves 1, 2 and 3 on a scale of 1:10.

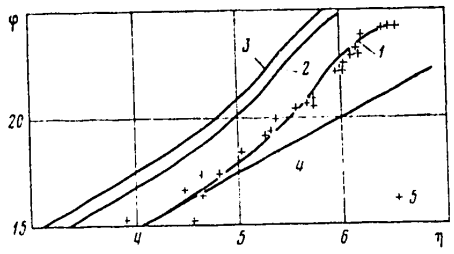

Figure 5.

The cited results show that when using any of the theories considered here, the advantage gained in the frictional resistance increases with an increase in the velocity of the body. Thus, the overall coefficient of frictional resistance falls off by approximately 20% when the solid is subjected to streamline flow by a polymer solution, as compared to streamline flow of the solvent when $Re = 1.262 \cdot 10^6$, and when $Re = 3.057 \cdot 10^7$, the decrease is 50%. The nature of the distribution curves for the coefficient of local friction as a function of the Reynolds number, the length of the solid and the rate of motion are in qualitative agreement with the results obtained for a flat plate [3]. In the case of a smaller Reynolds number, somewhat of a divergence is observed between the results of calculations using various correlation formulas, which take into account the influence of polymer additives on the flow characteristics. When $Re = 3.057 \cdot 10^7$, the calculations based on both theories yield very close results. Because of the definite divergence of the calculation results based on different functions for relatively small Reynolds numbers, i.e. in the region of the onset of the manifestation of the polymer effect, an answer can be given to the question of the preferability of any one of the theories only on the basis of a comparison of the numerical results with the data of a carefully performed experiment.

The profiles of the longitudinal component of the averaged velocity determined from the calculation results are shown in Figure 5. The profiles were plotted for a cross-section with a dimensionless abscissa of $z = 0.662$ in coordinates of $\phi = U/v^*$ and $\eta = \ln(v^*Y/\nu)$ for a Reynolds number of $1.262 \cdot 10^6$. In the case of streamline flow around the solid without polymer additives (curve 1), completely satisfactory agreement is observed between the computed profile and the measurement data of [11] (points 5). Lines 2 and 3 in Figure 5 correspond to the velocity profile determined from the results of boundary layer calculations using Meyer's correlation and the functions proposed in [1 - 4]; curve 4 is the usual logarithmic law. All of the data demonstrates the extremely strong influence of polymer additives on the velocity profile.

BIBLIOGRAPHY

1. Sedov L.I., Vasetskaya N.G., Ioselevich V.A., "O raschetakh turbulentnykh pogranichnykh sloyev s malymi dobavkami polimerov" ["On Calculations of Turbulent Boundary Layers with Small Amounts of Polymers Added"], in the book, "Turbulentnyye techeniya" ["Turbulent Flows"], Moscow, Nauka Publishers, 1974, p 205.

2. Vasetskaya N.G., Ioselevich V.A., "O postroyenii poluempiricheskoy teorii turbulentnosti slabykh rastvorov polimerov" ["On the Construction of a Semi-empirical Theory for the Turbulence of Weak Polymer Solutions"], IZV. AN SSSR, MZhG [PROCEEDINGS OF THE USSR ACADEMY OF SCIENCES, FLUID AND GAS MECHANICS], 1970, No 2, p 136.

3. Vasetskaya N.G., Ioselevich V.A., "Polimernyye dobavki v pogranichnom sloye ploskoy plastiny" ["Polymer Additives in the Boundary Layer of a Flat Plate"], NAUCH. TRUDY INSTITUTA MEKH. MGU [SCIENTIFIC PROCEEDINGS OF THE INSTITUTE OF MECHANICS OF MOSCOW STATE UNIVERSITY], 1974, No 32, p 178.

4. Ioselevich V.A., Pilipenko V.N., "O turbulentnom techenii zhidkosti s polimernymi dobavkami v pogranizhnom sloye s prodol'nym gradiyentom davleniya" ["On the Turbulent Flow of a Fluid with Polymer Additives in a Boundary Layer with an Arbitrary Pressure Gradient"], DOKL. AN SSSR [REPORTS OF THE USSR ACADEMY OF SCIENCES] 1973, Vol 213, No 4, p 808.

5. "Computation of Turbulent Boundary Layer", 1968, Proc. AFOSR-IFR Stanford Conference, Ed. Kline S.J., Morkovin M.V., Sovran G., Cockrell D.J., 1969, Vol 1.

6. Levkovich, Khodli, Khorlok, Perkins, "Semeystvo integral'nykh metodov dlya rascheta turbulentnogo pogranichnogo sloya" ["A Family of Integral Methods for the Calculation of a Turbulent Boundary Layer"], RAKETNAYA TEKHNIKA I KOSMONAVTIKA [ROCKET ENGINEERING AND ASTRONAUTICS], 1970, Vol 8, No 1, p 51.

7. Amfilokhiyev V.B., Droblenkov V.V., Mazayeva N.P., Shklyarevich A.I., "Raschet eksperimental'noye issledovaniye tolstogo osesimmetrichnogo turbulentnogo pogranichnogo sloya" ["The Calculation and Experimental Investigation of a Thick Axially Symmetric Turbulent Boundary Layer"], in the book, "Abstracts of Reports to the All-Union Scientific and Engineering Symposium on Questions of Improving the Propulsion Qualities and Operational Characteristics of Domestically Produced Ships of the Future", Leningrad, Sudostroyeniye Publishers, 1978, p 5.

8. Fedyaevskiy K.K., Ginevskiy A.S., Kolesnikov A.V., "Raschet turbulentnogo pogranichnogo sloya neszhimayemoy zhidkosti" ["The Calculation of the Turbulent Boundary Layer of an Incompressible Fluid"], Leningrad, Sudostroyenie Publishers, 1973, 256 pp.

9. Rao G.N.V., "The Law of the Wall in a Thick Axisymmetric Turbulent Boundary Layer", TRANS. ASME, SERIES E., JOURNAL APPL. MECH., 1967, No 1. p 237.

10. Willmarth W.W., Winkel R.E., Sharma L.K., Bogar T.J., "Axially symmetric Turbulent Boundary Layers on Cylinders: Mean Velocity Profiles and Wall Pressure Fluctuations", J. FLUID. MECH., 1976, Vol 76, Pt. 1, p 35.

11. Patel V.C., Nakayama A., Damian R., "Measurements in the Thick Axisymmetric Turbulent Boundary Layer Near the Tail of a Body of Revolution", J. FLUID MECH., 1974, Vol 63, Pt. 2, p 345.

12. Droblenkov V.V., Kanevskiy G.I., "O postroyenii metoda rascheta ploskogo pogranichnogo sloya v slabykh rastvorakh polimerov s laminarnoy, perekhodnoy i turbulentnoy zonami techeniya" ["On the Formulation of a Computational Technique for a Plane Boundary Layer in Weak Polymer Solutions with Laminar, Transition and Turbulent Flow Regions"], IZV. AN SSSR. MZhG, 1977, No 3, p 42.

13. Meyer W.A., "A Correlation of Frictional Characteristics for Turbulent Flow of Dilute Viscoelastic Non-Newtonian Fluids in Pipes", AIChE JOURNAL, 1966, Vol 12, No 3, p 522.

14. Vasetskaya N.G., Ioselevich V.A., Pilipenko V.N., "Mekhanicheskaya destruktsiya polimernykh molekul v turbulentnom potoke" ["The Mechanical Destruction of Polymer Molecules in a Turbulent Flow"], in the book, "Nekotoryye voprosy mekhaniki sploshnykh sred" ["Some Questions of the Mechanics of Continuous Media"] Moscow, Moscow State University Publishers, 1978, p 55.

8225
CSO: 8144/1532

LASERS AND MASERS

UDC 621.371:538.566:551.511.6

PROPAGATION OF LASER BEAM IN TURBULENT ATMOSPHERE

Novosibirsk RASPROSTRANENIYE LAZERNOGO PUCHKA V TURBULENTNOY ATMOSFERE in Russian 1981 (signed to press 18 Feb 81) pp 2-8

[Annotation, preface and table of contents from book "Propagation of a Laser Beam in a Turbulent Atmosphere", by V. L. Mironov, Institute of Physics of the Atmosphere, Siberian Department, USSR Academy of Sciences, Izdatel'stvo "Nauka"]

[Text] This book examines the physical principles of the influence that spatial localization of a field of wave beams has on processes of fluctuations of laser emission during propagation in a turbulent atmosphere. Methods are given for approximating the solution of the wave equation for the statistical moments of the beam field based on spectral expansions.

A theoretical and experimental investigation is made of the influence that spatial localization of the wave field has on the patterns of turbulent broadening of the angular dimension, distortions of spatial coherence of the field, fluctuations of intensity and phase, and random refraction of laser beams. An examination is made of methods of determining parameters of atmospheric turbulence by transillumination of the atmosphere with a narrow laser beam. Results are systematized for the first time on fluctuations of laser emission accompanying lidar location in a turbulent atmosphere.

The book is addressed to specialists in the field of wave propagation, and also to developmental engineers specializing in atmospheric optical laser systems.

Preface

The atmosphere has a considerable influence on propagation of optical waves. Atmospheric gases and aerosols are chiefly responsible for energy attenuation of optical radiation, whereas fluctuations of the index of rrfraction of atmospheric air that arise with turbulent intermixing of layers with different temperatures lead to considerable random distortions of the field of coherent optical waves.

The timeliness of research on processes of fluctuations of laser emission in the turbulent atmosphere is dictated by the start that has been made on using laser optical systems intended for operation under terrestrial atmospheric conditions. In fact, the information capacity of optical communication lines, spatial and

temporal resolution of lidars, the accuracy of geodetic laser instruments and other technical characteristics of laser optical systems can be evaluated only with consideration of fluctuations of a field of optical beams. On the one hand, the results of investigations of the field of a laser beam are used for calculating the limiting possible technical characteristics of laser instruments with operation in the atmosphere. On the other hand, they are necessary in the process of utilization of laser equipment under a variety of weather conditions. The latter circumstance is due to the considerable variations in technical characteristics of laser optical systems as a result of changes in meteorological conditions, so that in some cases the very feasibility of using them is determined on the basis of operative forecasting of the fluctuations in the field of the laser beam.

Questions of fluctuations of laser emission in a turbulent atmosphere have been studied especially intensely over the last decade. This problem is a component part of the broader scientific field of radio physics--propagation of electromagnetic waves in randomly inhomogeneous media--whose fundamentals have been formulated in papers by eminent Soviet scientists A. M. Obukhov, S. M. Rytov, V. I. Tatarskiy and L. A. Chernov. Results of investigations of fluctuations of optical waves in a turbulent atmosphere have been generalized on certain stages in several surveys and monographs. Early surveys and a monograph by V. I. Tatarskiy give mainly the results of theoretical and experimental studies of weak fluctuations in the field of optical waves in a turbulent atmosphere, where the relative dispersion of intensity fluctuations is small compared with unity. All major conclusions on the principles governing field fluctuations are formulated here for the simplest types of waves--planar and spherical. The method of geometric optics and S. M. Rytov's method of smooth perturbations were the principal working methods in theoretical studies of weak fluctuations of the field of optical waves.

The development of lasers has brought up fundamentally new problems in the area of propagation of optical waves in a turbulent atmosphere. The small angular divergence of laser emission has enabled transmitting the energy of optical waves over great distances in the terrestrial atmosphere with ease. At the same time, the high spatial coherence of laser radiation has made it possible to produce collimated and focused spatially bounded wave beams at a considerable distance from the source without difficulty. In studying the process of propagation of laser emission, a problem has arisen on the one hand of so-called strong fluctuations of the intensity of the optical wave (relative dispersion of fluctuations exceeds unity) that are caused by multiple scattering on inhomogeneities of the medium. On the other hand, it has become necessary to study the influence that the diffraction parameters of wave beams responsible for their original angular divergence have on processes of fluctuations of laser emission in a turbulent atmosphere. The solution of these problems is reflected in more recent surveys and monographs.

The tasks that have been formulated have required first and foremost the development of fundamentally new methods of the theory of wave propagation in randomly inhomogeneous media with simultaneous consideration of multiple scattering of waves by inhomogeneities in the medium, and diffraction of the wave beam by the radiating aperture. The next stage in solving the problem of fluctuations of laser emission in the turbulent atmosphere was solution of specific physical problems and theoretical investigation of the patterns of field fluctuations under different conditions of propagation in the atmosphere and beam diffraction parameters.

As a consequence of using different kinds of hypotheses and assumptions made in constructing the theory of multiple scattering and in describing the statistical properties of the field of the index of refraction in the turbulent atmosphere, the solution of physical problems of this kind are always only an approximate description of real processes of fluctuations of the field of the laser beam in the atmosphere. Therefore, experimental verification of the major conclusions of approximate theories is an absolutely essential research stage. Of course, the part played by experimental studies is not limited to checking the main relations of a theory. In particular, it was experiments that first revealed the fundamentally new phenomena of saturation of relative dispersion of strong fluctuations of intensity, and saturation of focusing of laser radiation, that were later theoretically substantiated.

The results of theory and experiment cannot be compared without access to means of on-the-spot measurement of atmospheric turbulence. On long transmission paths (from a few hundred meters to tens of kilometers) the determination of parameters by meteorological sensors that measure characteristics at isolated points become either less informative when a limited number of sensors is used, or else too expensive and inconvenient for practical use if the sensors are to be placed along the laser beam. In this connection it becomes necessary to develop methods of determining the turbulence parameters by using the laser beam itself through measurements of the distortion of the light field. One of the advantages of these methods is that they give the integral characteristics of turbulence along the transmission path. At the same time, they permit reconstruction of the spatial distribution of these characteristics by methods of solution of inverse problems of optics of atmospheric turbulence. We can conclude from this that development of laser methods of determining turbulence parameters is an essential component part of studying fluctuations of the field of a laser beam in a turbulent atmosphere.

Methods of the theory of laser beam propagation, results of theoretical and experimental studies of the patterns of optical wave field fluctuations, laser methods of determining optical parameters of atmospheric turbulence, systematized information on the statistical characteristics of fluctuations in the index of refraction in the aggregate make up the physical foundations of engineering prediction of fluctuations of the field of a laser beam in a turbulent atmosphere, which for practical purposes is the most important result of physical studies.

This monograph presents the results of theoretical and experimental investigations that encompass the above-mentioned components, and that are devoted to the study of the influence that the diffraction parameters of wave beams have on processes of fluctuations of laser radiation in a turbulent atmosphere. This problem has been only partly studied in one previous monograph.

The first chapter contains background required for the presentation on turbulent fluctuations of the index of refraction in the atmosphere, and methods of the theory of propagation of electromagnetic waves in the optical band in a turbulent medium. The second chapter is devoted to exposition of methods of approximate solution of the stochastic wave equation in a turbulent medium. Chapters three through seven contain the results of investigations of angular broadening (chapter 3), coherence distortions and phase fluctuations (chapter 4), weak fluctuations of the logarithm of amplitude (chapter 5), intensity fluctuations (chapter 6) and random refraction (chapter 7) of laser beams in a turbulent atmosphere. The eighth chapter examines laser methods of determining parameters of the process of turbulent micropulsations of the index of refraction.

Section numbers in the book are made up of the ordinal number of the chapter and of the given section. For example §1.2 is the second section of the first chapter. The formulas have their own ordinal numbering in each section, which is retained within the confines of that section. In cross references, the number of the formula is made up of the number of the section and of the formula. For example the notation (2.1.3) indicates the third formula of section one of chapter 2. To facilitate reading of the text, the section number is placed at the top of each page.

The monograph has been written from results of the author's research done at the Institute of Optics of the Atmosphere, Tomsk Affiliate, Siberian Department of the USSR Academy of Sciences, including work done jointly with colleagues of the Institute of Physics of the Atmosphere, USSR Academy of Sciences, and the Buryat Institute of Natural Sciences, Buryat Affiliate, Siberian Department of the USSR Academy of Sciences. The book also contains a detailed analysis of the results of research prior to the author's investigations and predetermining their formulation. In addition, wherever possible a comparison has been made between the results given and published research on the pertinent problem.

I am deeply grateful to all my coauthors, without whose cooperation it would have been impossible to study the complex problem of fluctuations of the field of a laser beam in the turbulent atmosphere. The author also thanks K. S. Gochelashvili, V. Ye. Zuyev, A. S. Gurvich, M. V. Kabanov, S. M. Rytov, V. I. Tatarskiy, V. I. Shishov and I. G. Yakushkin whose advice and constructive criticism to a great extent determined the direction and results of the author's research.

Contents page

6610
CSO: 1862/231

UDC 621.375.8

HIGH-POWER PULSE LASER

Moscow IZVESTIYA AKADEMII NAUK SSSR: SERIYA FIZICHESKAYA in Russian Vol 45, No 6, Jun 81 pp 989-994

[Paper delivered to the Tenth All-Union Conference on Coherent and Nonlinear Optics, Kiev, 14-17 October, 1980, by V. V. Apollonov, F. V. Bunkin, Yu. I. Bychkov, I. N. Konovalov, V. F. Losev, G. A. Mesyats, A. M. Prokhorov, V. F. Tarasenko, K. N. Firsov and S. M. Chesnokov, Physics Institute imeni P. N. Lebedev, USSR Academy of Sciences, Institute of High-Current Electronics, Siberian Department, USSR Academy of Sciences]

[Text] The development of powerful lasers with active volume of tens and hundreds of liters is a timely problem as such lasers are widely used for studying the interaction of radiation with matter. There are reports in the literature on excimer lasers and CO_2 lasers with energy of 10^2-10^4 J [Ref. 1-6]. Usually laser radiation in the UV and IR bands of the spectrum is produced on different facilities since considerably different conditions of excitation are required.

This paper describes a powerful universal laser facility that can produce emission in both the IR and UV regions of the spectrum, and results are given on studies of stimulated emission on molecules of CO_2 ($\lambda = 10.6$ μm), XeF* ($\lambda \sim 0.35$ μm), XeBr* ($\lambda \sim 0.28$ μm) and XeCl* ($\lambda \sim 0.308$ μm).

The laser facility consists of a pulse voltage generator supplying an accelerator, a laser chamber, pulse voltage generators supplying the laser gap, main and remote control panels, a synchronization system, a system for evacuation and mixture preparation. The mixture could be excited by an electron beam with density up to 8 A/cm^2 or by an electron-beam stabilized discharge. The laser chamber was designed for a pressure of up to 2.5 atm, and the active volume could be varied over a wide range. We did experiments with an active volume of 50 (20 x 20 x 125 cm), 28 (20 x 10 x 140 cm), 12 (12 x 8 x 125 cm) and 7 (10 x 5 x 140 cm) liters. The accelerator was supplied by an 8-stage pulse voltage generator with LC correction, and the gas chamber was supplied by three 5-stage pulse voltage generators with LC correction connected in parallel. All pulse voltage generators used IK-100/0.4 capacitors, and the LC correction circuit used IMN-100/0.1 capacitors. The impact capacitance of the pulse voltage generator of the accelerator was 0.08 μF, and of the pulse voltage generators of the laser gap--0.24 μF; wave impedance and pulse duration could be varied by changing the total inductance of the pulse voltage generators, and the inductance of the LC correction.

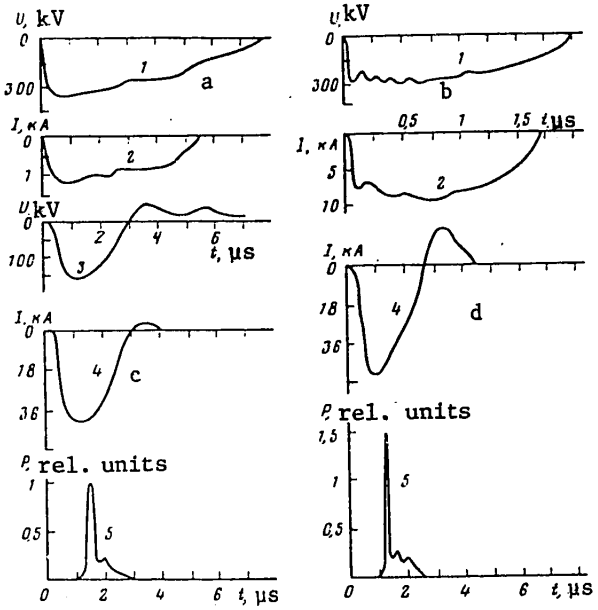

Fig. 1. Oscillograms of voltage (1) and current (2) of the accelerator, the voltage pulses across the gap (3) and the current through the laser chamber (4) and voltage pulses (5). Mixture CO_2:N_2:He = 1:2:2, pressure p = 2 atm, charging voltage of the accelerator pulse voltage generator U_1 = 50 kV, other parameters as follows: a) correction inductance L_1 = 32 μH, inductance of the pulse voltage generator L_2 = 101 μH; b) L_2 = 5.1 μH, L_1 = 1.64 μH; c) L_2 = 101 μH, L_1 = 32 μH, charging voltage of pulse voltage generators feeding the gap, U_2 = 58 kV, V_a = 50 liters; d) L_2 = 101 μH, L_1 = 32 μH, U_2 = 52 kV, V_a = 12 liters

Fig. 1 shows oscillograms of the electron beam current behind the grid, and the voltage across the vacuum diode for two modes of operation of the accelerator. The use of LC correction gave close to square-wave beam current pulses. Screens were used for focusing the electron beam. The vacuum in the accelerator was no worse than 10^{-4} mm Hg. The electron beam was coupled out through aluminum foil or Mylar film. All pulse voltage generators used dischargers with dry air blasting, enabling attainment of high firing stability, ±20 ns, as well as synchronization of the discharge current pulse in the gas chamber relative to the beam current. The voltage pulse was fed to the laser chamber with delay relative to the beam current of 0.3 μs, and as a result the discharge took place at constant beam current density and electron energy; the latter is important for increasing discharge stability since it gets rid of the low-energy part of the electrons formed on the rising and falling sections of the accelerating voltage.

In the most powerful CO_2 lasers known in the literature [Ref. 3-5] that are excited by a non-self-maintained discharge with duration of 10^{-6} s, controlled by an electron

beam, pumping has been done under unmatched conditions, the energy reserve in the accumulator being much greater than the energy introduced into the discharge. As a result, when the excitation pulse has been completed a residual voltage remains across the electrodes of the laser chamber, and because of the possibility of discharge contraction this limits the attainment of high field strength in the gas gap and precludes high energy inputs. The use of matched conditions in pumping a CO_2 amplifier with characteristic excitation time of ~10^{-6} [s] was first reported in Ref. 6. However, no data were given on the output energy characteristics of the radiation, and the specific energy inputs did not exceed 0.2 J·cm^{-3}.

The use of pulse voltage generators with LC correction in the proposed laser provides effective transfer of energy from the accumulator to the discharge in the matched mode. Realization of matching of the excitation system and discharge gap does not require exact satisfaction of the equality $R_l = \rho$ (R_l is the load resistance, ρ is the wave impedance of the supply system) since the reduction in the power of the energy input does not exceed 10% for $0.75\rho \leqslant R_l \leqslant 2\rho$. The important thing is that as R_l changes from 0.75ρ to 2ρ, the voltage across the plasma changes from $0.47U_0$ to $0.74U_0$, i. e. by changing the plasma resistance, for example by varying the beam current density, we can get an electric field strength in the plasma that corresponds to maximum laser efficiency. When a laser with active volume of 50 liters is used, the plasma resistance is $R_l = 3.8\ \Omega$ for mixture $CO_2:N_2He = 1:2:2$ at a pressure of 2 atm.

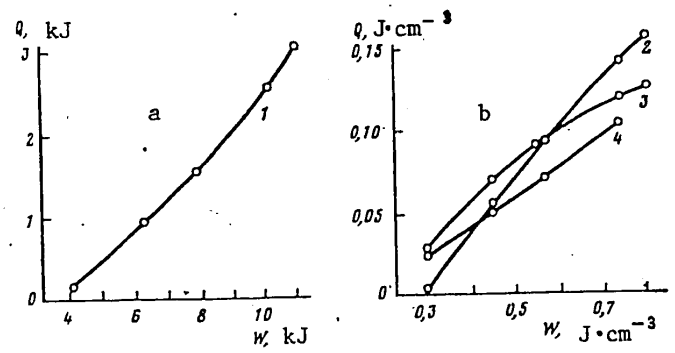

Fig. 2. Dependence of total radiation energy on input energy for active volume $V_a = 50$ liters (a) and dependence of specific radiation energy on specific input energy for $V_a = 12$ liters (b). Mixture $CO_2:N_2:He = 1:2:2$, pressure $p = 2$ atm (1, 2, 3) and 1.2 atm (4). Output window KRS (1, 3, 4) and NaCl (2).

Oscillograms of the voltage pulses across the plasma, the discharge current and the radiation pulse at a charging voltage of $U_2 = 58$ kV are shown in Fig. 1c, and the dependence of the total radiation energy on the energy stored in the pulse voltage generators that feed the discharge gap is shown in Fig. 2a. Maximum radiation energy was 3 kJ, efficiency ~27%. In the central part of the output window the energy density reached 15 J·cm^{-3}.

To study the feasibility of high energy inputs under matched conditions, the volume of the laser was reduced to 12 liters (8 x 12 x 125 cm). Plasma resistance in this

case was 2.5 Ω. Oscillograms of the discharge current and radiation pulse are shown on Fig. 1d. Since the input energy in the second half-period does not exceed 10%, pumping conditions can be taken as matched. The amplitude value of the voltage across the plasma was 136 kV, accordingly $E/p = 8.5$ kV·(cm·atm)$^{-1}$, and the energy inputs were up to 0.6 J·(cm·atm)$^{-1}$. Dependences of radiation energy on energy input for mixture pressure of 1.2 and 2 atm are shown in Fig. 2b.

Optical cavities with output windows of NaCl and KRS were used. Maximum radiation energy from a volume of 12 liters was obtained on a mixture of $CO_2:N_2:He = 1:1:2$ and amounted to 1.8 kJ. The radiation energy on mixtures $CO_2:N_2:He = 1:3:2$ and 1:1:1 was lower by a factor of 1½. In operation on a mixture without helium $CO_2N_2 = 1:2$ the radiation energy decreased in comparison with the radiation energy on a mixture of $CO_2:N_2:He = 1:2:2$ at the same working pressures. Diluting the $CO_2:N_2$ mixture with helium without changing other conditions also increased the radiation energy. Let us note that as the energy inputs increased, the duration of the first peak of the radiation pulse decreased, and its power increased (Fig. 1). At output energy density ⩾15 J/cm^2 the output window of the cavity was damaged.

This facility was also used to study lasing on molecules of XeF*, XeBe* and XeCl*. In these experiments the working pressure of the mixture was 2 atm, active volume V_a was 28 liters for the XeF and XeBr lasers and 7 liters for the XeCl laser. The active volume for lasing on XeCl* molecules was reduced to attain higher pumping powers. The interelectrode gap was reduced to improve the homogeneity of ionization of the gas mixture in the discharge gap since mixtures for lasing on excimer molecules use gases with higher specific weight at higher pressures than in the CO_2 laser. The working mixture consisted of argon, xenon and one of the halide carriers: NF_3, $C_2F_4Br_2$ or CCl_4. The optical cavity was formed by a flat aluminum mirror with protective coating, and a plane-parallel quartz plate. A low-inductance capacitor C, usually equal to 3 μF, was connected to the anode. The inductance of the discharge circuit was 155 nH.

Fig. 3 and 4 show curves for specific radiation energy Q and specific energy W transferred to the gas by the beam and discharge as dependent on the initial electric field for mixtures of $Ar:Xe:NF_3$, $Ar:Xe:C_2F_4Br_2$ and $Ar:Xe:CCl_4$ at different beam current densities. The maximum specific radiation energy on molecules of XeF* was 0.9 J/liter (total energy 25 J), on XeBr*--0.32 J/liter (total energy 9 J), and on XeCl*--0.4 J/liter (total energy 3 J). A distinguishing feature of the given mode of excitation of excimer molecules is intense processes of gas

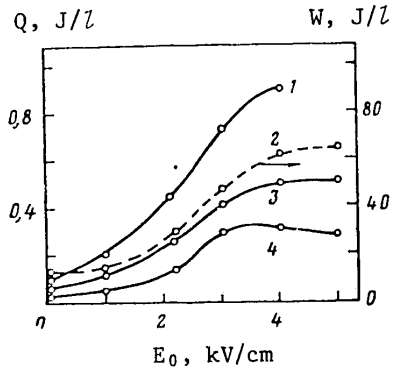

Fig. 3. Radiation energy (1, 3, 4) and energy input to the gas (2) as dependent on electric field strength for XeF* molecules: 1--in mixture $Ar:Xe:NF_3 = 1000:10:1$; 2-4--in mixture $Ar:Xe:NF_3 = 2000:10:1$. Parameters: 1--beam current density $j = 3$ A/cm^2, beam duration $\tau = 1.2$ μs, $C = 6$ μF; 2, 4--$j = 1.2$ A/cm^2, $\tau = 1$ μs; 3--$j = 3$ A/cm^2, $\tau = 1.2$ μs

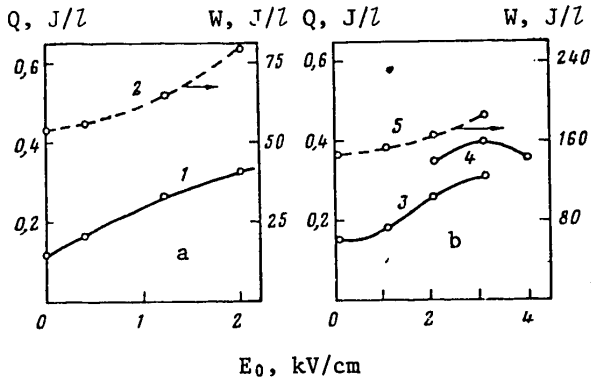

Fig. 4. Radiation energy (1, 3, 4) and energy input to the gas (2, 5) as dependent on electric field strength for molecules of XeBr* (a) and XeCl* (b): curves 1, 2--mixture $Ar:Xe:C_2F_4Br_2$ = 6000:40:1, $j = 3$ A/cm^2, $\tau = 1.2$ μs; curves 3-5--$Ar:Xe:CCl_4$ = 2000: 50:1, $j = 6$ (3, 5) and 8 (4) A/cm^2, $\tau = 1$ μs

amplification, enabling attainment of a ratio of five for the discharge-to-beam energy input to the gas for mixture $Ar:Xe:NF_3$ = 2000:10:1.

Let us note the peculiarities of excitation with gas amplification. In the case of a non-self-maintained discharge, the discharge current pulse copies the electron beam current, and the energy input to the gas from the discharge under these conditions is commensurate with the energy input to the gas from the electron beam. The radiation pulse in this case is a bell curve, and its delay from the onset of the current pulse may exceed 150 ns. With an increase in the charge voltage, and accordingly in the voltage across the discharge plasma, the discharge current is determined not only by the intensity of the electron beam, but also by the extent of gas amplification processes. Under these conditions, the discharge is volumetric for a time, and then contraction sets in. The duration of the volumetric stage may exceed the duration of the electron beam pulse.

Efficient energy transfer from the storage element to the volumetric discharge requires satisfaction of two conditions: first, pulse supply to the gas vessel must be such that voltage is removed before the instant of discharge contraction, and second, the impedance of the storage element must be matched to the resistance of the plasma. The resistance of the plasma in the case of excitation by a discharge with ionization multiplication decreases during pumping, and therefore complete matching can be realized only by using a stripline with variable wave impedance. Let us note that contraction in mixtures of inert gases with halides is much different from that in mixtures typical of CO_2 lasers. The channels that are formed in excimer mixtures have comparatively high resistance, and may exist simultaneously with the volumetric discharge for a considerable time (~10^{-7} s or longer).

We made an attempt to get the maximum duration of the radiation pulse on the XeF* molecule on the described facility. At a beam current duration of 5.4 μs and current density $j = 0.4$ A·cm^{-2} in a mixture of $Ar:Xe:NF_3$ = 1100:5:1 we attained a radiation

pulse duration of 5.5 μs. However, a reduction in pumping power led to a considerable reduction in radiation energy because the gain was unsaturated. Maximum radiation energy at a pulse duration of 5.5 μs in these experiments was ~1 J.

Thus a universal laser system has been developed that enables variation of excitation conditions over a wide range, and that can use different gas mixtures to get powerful emission pulses in the IR and UV regions of the spectrum.

The authors thank B. M. Koval'chuk and V. I. Manylov for assistance in making the pulse voltage generators, and V. A. Yamshchikov for helping with the experiments.

REFERENCES

1. Hoffman, J. M., Hays, A. H., Tisons, G. C., APPL. PHYS. LETTS., Vol 28, 1976, p 538.

2. Rokni, M., Mangano, J. A., Jacob, J. H., Hsia, J. C., IEEE J. QUANT. ELECTRON., Vol QE-14, 1978, p 464.

3. Orishich, A. M., Ponomarenko, A. G., Posukh, V. G., Soloukhin, R. I., Shalamov, S. P., PIS'MA V ZHURNAL TEKHNICHESKOY FIZIKI, Vol 3, 1977, p 39.

4. Bychkov, Yu. I., Karlova, Ye. K., Karlov, N. V., Koval'chuk, B. M., Kuz'min, G. P., Kurbatov, Yu. A., Manylov, V. I., Mesyats, G. A., Orlovskiy, V. M., Prokhorov, A. M., Rybalov, A. M., PIS'MA V ZHURNAL TEKHNICHESKOY FIZIKI, Vol 2, 1976, p 212.

5. Adamovich, V. A., Baranov, V. Yu., Bevov, R. K., Samkovskiy, Yu. B., Strel'tsov, A. P., PIS'MA V ZHURNAL TEKHNICHESKOY FIZIKI, Vol 4, 1978, p 988.

6. "Status Report on Laser Program at LASL (u)" LA-5251-PR, 1972.

6610
CSO: 1862/244

UDC 621.375.826

INVESTIGATION OF GASDYNAMIC LASER USING ACETYLENE COMBUSTION PRODUCTS

Moscow KVANTOVAYA ELEKTRONIKA in Russian Vol 8, No 6(108), Jun 81 pp 1202-1207

[Article by Yu. N. Bulkin, B. A. Vyskubenko, G. A. Kirillov, S. B. Kormer, V. M. Linnik, Yu. V. Savin and V. D. Urlin]

[Text] The paper describes a gasdynamic laser based on combustion of a mixture of C_2H_2-O_2-N_2. Experiments and calculations give the temperature and pressure dependences of the gain as well as the total and specific powers of radiation in a combustion chamber at pressures up to 70 atmospheres. Mathematical modeling of the experimental facility gives the losses associated with vibrational relaxation, heating of the cavity mirrors and entrainment of stored energy by the gas flow.

1. Introduction

Active research is now in progress to develop different kinds of gasdynamic lasers. Of particular interest among such lasers are those based on combustion of hydrocarbon fuel [Ref. 1-5]. The use of acetylene or benzene gives optimum compositions of working mixtures at fairly high combustion temperatures. Ref. 4 gives the result of measurements of the gain in cw gasdynamic lasers based on products of combustion of a benzene-air mixture at combustion temperatures up to 1700 K and pressure $p_0 \approx 30$ atmospheres. Experiments with acetylene-air mixtures at $p_0 \lesssim 20$ atmospheres are described in Ref. 3. The authors of this work established that at the amplification-optimum stagnation parameters ($p_0 = 5$-10 atm, $T_0 = 1.4$-1.7 kK) the gain was $8 \cdot 10^{-3}$ cm^{-1}. Maximum specific lasing energy output was 7.8 J/g at $p_0 = 6.3$ atmospheres. The power and specific energy output of lasing obtained in this work are limited to the region of low stagnation pressures. Considering the necessity of optimizing gasdynamic lasers not only with respect to specific energy output, but also with respect to radiation power, as well as the fact that the used gas may be exhausted into the atmosphere, it is of interest to study the operation of a gasdynamic laser based on combustion of acetylene at higher stagnation pressures.

Our paper is a report on optimization of a laser using products of combustion of a mixture of C_2H_2-O_2-N_2 in the region of stagnation pressures up to 70 atmospheres. The gain, power and specific lasing energy output were measured as functions of the composition and stagnation parameters of the working medium in a quasi-cw

gasdynamic laser. Two-dimensional profiled nozzles were used in the experiment with different heights of the critical cross section and Mach numbers. The investigated gasdynamic laser was optimized with respect to finding the region of stagnation parameters with near maximum specific energy output and lasing power.

The gain and the power of stimulated emission of the gasdynamic laser were calculated in a one dimensional model in the geometric optics approximation for a plane-parallel optical cavity. The mathematical model was analogous to that used in Ref. 6-9.

2. Description of the Experimental Facility

The experimental facility is described in general outline in Ref. 9. The pulsed combustion chamber was a steel cylindrical vessel with volume V = 45,500 cc and length of 1.6 m. The fuel mixture admitted to the chamber was ignited by an electric discharge. The resultant pressure pulse was recorded by an inductive pressure sensor. The gas temperature T(t) in the combustion chamber and the flowrate G(t) of gas through the nozzle were calculated by a method described in Ref. 9. Both the composition and pressure of the initial fuel mixture were varied in the experiments. The concentration of acetylene and oxygen in all experiments was chosen on the basis of the stoichiometric ratio 1:2.5. The acetylene concentration in the mixture was varied from 3.6 to 6.0%. The nozzles used with critical cross section height $h^* = 0.04$ and 0.08 cm had geometric degree of expansion $A/A^* = 35.8$; a nozzle with $h^* = 0.025$ had $A/A^* = 75.6$. The width of all nozzles was 17 cm. The profile of the supersonic part of the nozzle was found from the method of characteristics for a gas with constant adiabatic exponent without consideration of viscosity.

The gain was measured by a conventional arrangement using a single-mode electric-discharge CO_2 laser (transition P(20) of band 00°1-10°0) with stabilized power supply. The reference and amplified signals of the emission were registered by photoresistors.

Lasing experiments were done using hemispherical resonant cavities arranged in series along the gas flow, the axes of these cavities being 4.5, 8.5 and 12.5 cm away from the critical cross section of the nozzle. The opaque mirrors (copper-coated glass) had a rectangular cross section of 40 x 40 mm and radius of curvature of 10 m. The flat output mirror measuring 40 x 120 mm made of BaF_2 with dielectric coating was common to all three cavities, and had reflectivity $r \approx 93\%$ at $\lambda \approx 10.6$ μm. The leading edge of the first hemispherical cavity for all nozzles was 2.5 cm away from the critical cross section. The mirrors were located close against the gas flow. The pulse energy and instantaneous radiation power were measured by calorimeters and photoresistors. The optical measurement system was designed for measuring the energy and shape of the radiation pulse separately in regions $\lambda \sim 9.5$ and 10.6 μm corresponding to P-transitions of bands 00°1-02°0 and 00°1-10°0 of CO_2 molecules.

3. Results of the Experiment and Calculation, and Discussion

The results of measurements of the power and specific energy output of radiation as a function of pressure and temperature in the combustion chamber are shown in

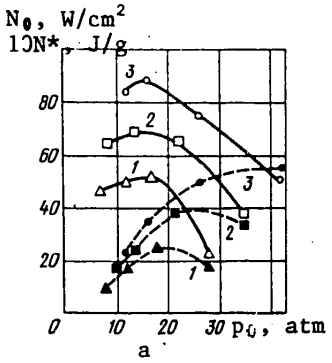

Curves for normalized radiation power N_0 (broken lines) and specific energy output N* (solid lines) as a function of stagnation pressure p_0 for a mixture of 4.5% C_2H_2 and nozzles with h* = 0.08 (a), 0.04 (b) and 0.025 cm (c) (compositon of combustion products $CO_2:H_2O:N_2$ = 9.2: 4.6:86.2% at T_0 = 1.5 (1), 1.7 (2), 1.9 (3) and 2.1 kK (4)

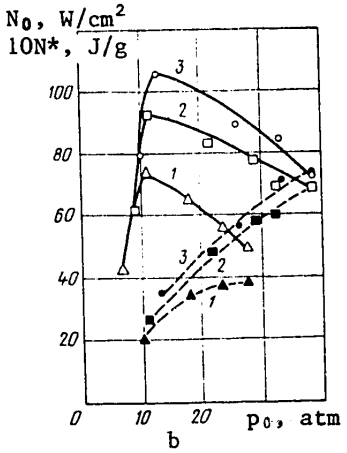

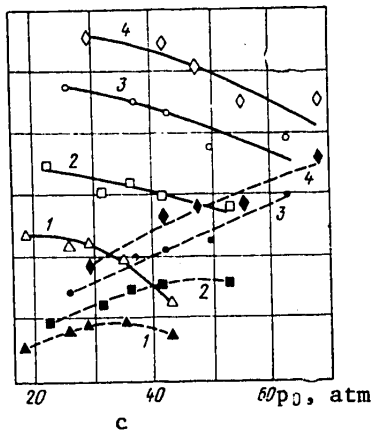

TABLE 1

Mixture	h*, см	A/A*	p_0, атм	T_0, кК	N*, J/g	N_0, W/cm²
3,6 % C_2H_2	0,08	35,8	24,0 30,0 37,5	1,5 1,5 1,5	5,9 4,5 3,0	40,0 40,0 32,6
	0,04	35,8	25,0 33,5 42,0	1,5 1,5 1,5	5,5 7,9 4,7	37,5 75,5 57,9
6,0 % C_2H_2	0,08	35,8	22,0 30,0	2,3 2,3	7,2 3,6	34,0 21,9
	0,04	35,8	22,0 30,0	2,3 2,3	6,2 3,8	26,0 25,4
5,0 % C_2H_2 [3]	0,04	25	6,3 14,5	1,42 1,6	7,9 5,9	20,8 34,0
$CO--O_2—N_2$ [11]	0,08	14	17,0	1,4	4,3	66,7

the figure and Table 1. The characteristic of radiation power of the gasdynamic laser was the normalized emission power $N_0 = N/S_{out}$, defined as the ratio of the generated radiation power to the area of the output cross section of the nozzle (or nozzle cascade). The introduction of such a specific characteristic enables comparison of different gasdynamic laser facilities with respect to their attainable emission power level. For a gasdynamic laser of a specific type with known emission power, this characteristic enables evaluation of the necessary overall dimensions of the nozzle unit. Of course such an estimate requires correction of the emission power with respect to possible variation of the cavity efficiency (in connection with a change in length of the active part and the type of cavity) and losses of stored vibrational energy in the wakes of the gas flow (with a change from a mono-nozzle to a nozzle cascade).

As can be seen from the figure, despite the short length of the active part of the cavities (17 cm), a mixture containing 4.5% acetylene gave maximum specific energy outputs exceeding those obtained in Ref. 3. Curves for $N^*(p_0)$ for nozzles with $h^* = 0.04$ and 0.08 cm have characteristic optima due to two factors. At low gas pressures in the combustion chamber there is a small concentration of active particles in the cavity region, which reduces the efficiency of the cavity that is used. With an increase in pressure there is a rise in the relaxational losses of vibrational energy stored in the mixture as the gas expands in the nozzle, i. e. there is a reduction in both nozzle and cavity efficiencies. As the gas temperature increases in the combustion chamber at constant pressure, all the investigated nozzles show an increase in both the specific energy output and the radiation power. This is due to the fact that in the investigated temperature region with increasing T_0 the increase in vibrational energy stored in the gas at the nozzle intake predominates over the increase in the vibrational relaxation rate as the gas expands in the nozzle. Comparing the specific energy outputs for nozzles with a similar profile of the supersonic part (see the figure, a, b), we can see that in the region of $p_0 \approx 40$ atm, as was anticipated [Ref. 10], it is preferable to use nozzles with a lower height of the critical cross section. The use of a nozzle with large aperture $A/A^* = 75.6$ and $h^* = 0.025$ cm, as can be seen from Fig. c, gave a fairly high energy output (~8 J/g) at $p_0 \approx 70$ atm and $T_0 = 2.1$ kK. In this connection, no noticeable increase was observed in N^* in the region of low stagnation pressures, which is apparently due to low cavity efficiency. It can also be seen from the figure that the optima of specific energy output and normalized power lie in different regions of p_0. Nevertheless, in the region of stagnation parameters $p_0 = 40$ atm, $T_0 = 1.9$ kK for the nozzle with $h^* = 0.04$ cm, and $p_0 \approx 70$ atm, $T_0 = 2.1$ kK for the nozzle with $h^* = 0.025$ cm one can get fairly large normalized radiation power at specific energy outputs of ~70% of the optimum values.

When mixtures were used that contain 3.6 and 6.0% acetylene in the initial state, the maximum specific energy output and normalized radiation power were lower than for the mixture with 4.5% acetylene (see Table 1). For the first mixture this is due to the low combustion point of the fuel mixture; for the second, it is due to the the less than optimum copmposition of the working mixture after combustion. For comparison, Table 1 gives the energy characteristics of gasdynamic lasers described in other research. It can be seen that the maximum specific energy outputs obtained in our work are greater than the known values observed with ignition of acetylene [Ref. 3] and carbon monoxide [Ref. 11]. The maximum normalized radiation

TABLE 2

$p_{нсх}$, атм	r (λ~9,5 μm), %	r (λ~10,6μm), %	E (λ~9,5 μm), J	E (λ~10,6 μm), J	Nozzle parameters
5,2	91,5	94,5	0	391	
	92,0	93,0	1,0	402	$h^* = 0,04$ см $A/A^* = 35,8$
			6,0	470	
			39,0	507	
6,0			45,0	544	$h^* = 0,025$ см $A/A^* = 75,6$
6,8	88,5		0,7	680	

Note. Composition of initial mixture 4.5% C_2H_2; $p_{нсх}$ is the pressure of the initial mixture in the combustion chamber.

TABLE 3

p_0, атм	T_0, кК	η_c, %	E, J/g	N^*, J/g	$N_{рел}$, J/g	$N_э$, J/g	$N_п$, J/g	$k_т$, 10^3 см$^{-1}$	$k_э$, 10^3 см$^{-1}$
10	1,7	58,0	35,0	7,5	2,6	2,9	22,0	7,4	
	1,9	58,8	45,7	7,6	3,4	3,0	31,7		
20	1,7	47,0	28,6	8,3	3,6	3,2	13,5	7,8	8,5
	1,9	48,4	37,6	9,2	4,8	3,6	20,0		
30	1,7	39,0	23,6	6,4	3,7	2,5	11,0	6,5	7,2
	1,9	40,0	31,0	6,8	5,8	2,6	15,8		
40	1,7	33,0	20,0	4,5	3,8	1,7	10,0	5,4	5,5
	1,9	33,6	26,0	4,6	4,6	1,8	15,0		

Note. E is the stored vibrational energy at the inlet to the cavity; $N_{рел}$ are the losses of stored energy due to relaxation in the cavity; $N_э$ are losses of energy in the cavity mirrors; $N_п$ is the vibrational energy remaining in the gas flow; $k_т$ is the calculated gain at a distance of 4.5 cm from the critical corss section of the nozzle; $k_э$ are the experimental values of the gain.

powers found in our research are about double the values obtained in Ref. 3, and coincide with the data of Ref. 11.

Investigation of the spectral composition of the radiation gave some interesting results. Considerable instability of the emission pulse shape was seen in the first lasing experiments with identical initial conditions. Since the sensitivity

of the Ge-Au photosensors that were used was not the same in the 9-11 μm band, this suggested a complex nature of the spectral composition of the radiation. Table 2 shows the results of some typical experiments. It can be seen that the percentage of lasing energy on $\lambda \sim 9.5$ μm increases if the reflectivities of the output mirror on $\lambda \sim 9.5$ and 10.6 μm are close, and if a nozzle with large aperture is used. In the former case, this is a consequence of the fact that the storage factor of the cavity $Q \sim 1/\lambda$. In the latter case, the observed behavior can be attributed to a reduction in the competition of band transitions 00°1-10°0, 00°1-02°0, since the density of radiation with $\lambda \sim 10.6$ μm inside the cavity is low, and besides, level 02°0 is effectively deactivated as a consequence of the high concentration of water in the mixture.

Results of mathematical modeling of the investigated gasdynamic laser are reflected in Table 3. The calculation was done for a nozzle with $h^* = 0.04$ cm and composition of working mixture $CO_2:H_2O:N_2 = 9.2:4.6:86.2\%$ which corresponds to an initial fuel mixture with 4.5% acetylene, assuming complete combustion. Our paper compares the results of calculation and experiment with respect to gain and the specific energy output of emission. As we can see from Table 3 and figure c, the results of calculation and experiment are in satisfactory agreement. For some stagnation parameters, Table 3 enables evaluation of the principal losses of stored vibrational energy in the gas as it moves through the cavity. For example for stagnation parameters $p_0 = 30$ atm, $T_0 = 1.9$ kK the efficiency of the nozzle $\eta_c = 40\%$, cavity efficiency $\eta_p = 21.9\%$, losses in the mirrors 8.6%, losses to relaxation of vibrational energy inside the cavity $\eta_{рел} = 18.5\%$, and 51% of the vibrational energy was carried off by the gas flow. The resultant data imply that a further increase in the spedific energy of the radiation requires primarily an increase in cavity efficiency, e. g. by increasing the active part of the cavity.

REFERENCES

1. Tulip, J., Seguin, H., APPL. PHYS. LETTS, Vol 19, 1971, p 263.

2. Kozlov, G. I., Ivanov, V. N., Korablev, A. S., ZHURNAL EKSPERIMENTAL'NOY I TEORETICHESKOY FIZIKI, Vol 65, 1973, p 82.

3. KOZLOV, G. I., IVANOV, V. N., KORABLEV, A. S., SELEZNEVA, I. K., ZHURNAL EKSPERIMENTAL'NOY I TEORETICHESKOY FIZIKI, Vol 68, 1975, p 1647

4. Ktalkherman, M. G., Mal'kov, V. M., Petukhov, A. V., Kharitonova, Ya. I., FIZIKA GORENIYA I VZRYVA, Vol 12, 1976, p 578.

5. Shmelev, V. M., Vasilik, N. Ya., Margolin, A. D., KVANTOVAYA ELEKTRONIKA, Vol 1, 1974, p 1711.

6. Losev, S. A., MAKAROV, V. I., KVANTOVAYA ELEKTRONIKA, Vol 1, 1974, p 1633.

7. Losev, S. A., Makarov, V. I., ZHURNAL PRIKLADNOY MEKHANIKI I TEKHNICHESKOY FIZIKI, No 8, 1975, p 3.

8. Losev, S. A., Makarov, V. I., KVANTOVAYA ELEKTRONIKA, Vol 3, 1976, p 960.

9. Vyskubenko, B. A., Demenyuk, Ye. T., Yeremin, A. D., Kirillov, G. A., Kolobyanin, Yu. V., Kormer, S. B., Ladagin, V. K., Linnik, V. M., Nitochkin, N. A., Urlin, V. D., KVANTOVAYA ELEKTRONIKA, Vol 5, 1978, p 10.

10. Losev, S. A., "Gazodinamicheskiye lazery" [Gasdynamic Lasers], Moscow, Nauka, 1977.

11. Gerry, E. T., LASER FOCUS, No 6, 1970, p 27.

6610
CSO: 1862/242

UDC 621.378.33

CHEMICAL DF LASER WITH DIFFRACTION RADIATION DIVERGENCE

Moscow KVANTOVAYA ELEKTRONIKA in Russian Vol 8, No 6(108), Jun 81 pp 1208-1213

[Article by V. P. Borisov, S. D. Velikanov, V. D. Kvachev, S. B. Kormer, M. V. Sinitsyn, G. V. Tachayev and Yu. N. Frolov]

[Text] An investigation was made of the feasibility of achieving diffraction diverence of the radiation of a pulsed chemical DF laser with flashlamp pumping when the planar cavity was replaced by an unstable cavity of telescopic type. Under optimum working conditions of the laser with unstable cavity, radiation divergence of $\theta_{0.5E} = 70$ μrad, practically at the diffraction limit, was obtained at fairly high energy efficiency (~60%) as compared with the similar laser using a planar cavity. It is experimentally shown that by appropriate "misalignment" of the unstable cavity, the radiation energy distribution in the far zone can be measured without using auxiliary focusing elements.

1. Introduction

One of the interesting peculiarities of chemical lasers is the capability for bringing about conditions under which inhomogeneities of the working medium will be comparatively small, which creates certain prerequisites for getting the diffraction divergence of emission [Ref. 1].

One of the most promising and widely used methods of getting small divergence of laser radiation is to use an unstable cavity of telescopic type [Ref. 2, 3].

In this paper we study the problem of effectiveness of using an unstable cavity in a pulsed DF chemical laser with optical initiation to get the diffraction divergence of radiation.

2. Formulation of the Experiment

The experiments were done on a pulsed DF laser with working mixture of $F_2:D_2:SF_6:O_2 = 22:7:22:7$ mm Hg. The radiation of such a chemical laser occupies the spectral range of 3.6-4.2 μm.

The chemical laser cell was a quartz tube with inside diameter of 7.2 cm and length of 70 cm with windows of CaF_2. Diaphragms on the ends of the cell with inside

diameter of 7 cm reduced the influence that bright reflections from the walls of the cell have on laser radiation.

Optical initiation of the chemical reaction was by a xenon flash lamp with design analogous to that described in Ref. 4. Power supply to the lamp was from a capacitor bank with capacitance C = 3 μF at voltage V = 20 kV.

An experimental study was done on the influence that the magnification M of the unstable cavity ($M = f_1/f_2$, where f_1, f_2 are the focal lengths of the concave and convex mirrors of the unstable cavity) has on the parameters of stimulated emission, and a comparison was also made with the parameters of a laser with planar cavity.

The planar cavity consisted of a flat copper mirror and a flat CaF_2 plate separated by a distance of $l_p = 180$ cm. The unstable cavity of telescopic type consisted of spherical concave and convex copper mirrors.

The optical arrangement of the experiments is shown in Fig. 1. Emission energy was recorded by TPI calorimeter 1. The time parameters of the lasing pulse were registered by gold-doped germanium FSG-22-3A photoresistor 2, the signal being sent to an S8-2 oscilloscope.

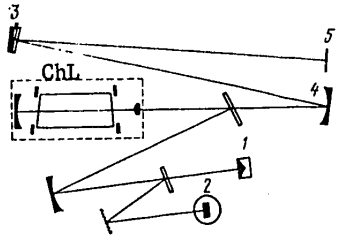

Fig. 1. Optical arrangement of experiments

The radiation divergence of the chemical laser ChL was measured by Ragul'skiy's wedge 3, using a method described in Ref. 5. To do this, the radiation of the chemical laser was focused by spherical mirror 4 with focus f = 11 m on screen 5 made of black photographic paper. Placed in the path of the convergent beam was mirror-reflecting Ragul'skiy's wedge 3 with semitransparent mirror having transmission T = 50%. In the experiments with the unstable cavity, the dynamic range of recordable intensities in the far zone was about 2000.

When the planar cavity was used, the focusing mirror with f = 11 m was replaced by a mirror with f = 1.5 m, and the range of recordable intensities was ~1000.

3. Results of the Experiments, and Discussion

The main purpose of our experiments was to study the feasibility of getting diffraction divergence of chemical laser radiation.

Let us estimate the value of M of the unstable cavity necessary for attaining this goal. The radiation of a laser with ideal unstable cavity and homogeneous working medium should have diffraction divergence [Ref. 2, 3]. In the presence of inhomogeneities of the active medium, the divergence of radiation of a laser with unstable cavity will be greater than the diffraction level $\theta_{dif} \approx 2.4 \cdot \lambda/d_1$ (where λ is the wavelength of laser emission, d_1 is the diameter of the working part of the concave mirror) by the amount [Ref. 3]

$$\theta_u \approx 2l_a \nabla n/(1 - 1/M), \quad (1)$$

where l_a, ∇n are the length of the active medium and the gradient of its index of refraction.

Based on the defined value of inhomogeneities, we can estimate the maximum value of M at which the radiation divergence will differ but little from the diffraction value:

$$\theta_{dif} > 10\theta_u. \tag{2}$$

From (1) and (2) we get

$$M > (1 - 8.3 l_a \nabla n d_1/\lambda)^{-1}. \tag{3}$$

On the other hand, it is known that the diffraction divergence of radiation is formed mainly by the rays that make the maximum number of passes m_{max} inside the unstable cavity before leaving it [Ref. 6]:

$$m_{max} = 1 + \frac{\ln\left[d_1^2/(2\lambda f_1)\right]}{\ln M}. \tag{4}$$

There is no distortion of diffraction divergence when saturation of the gain of the active medium is attained after a number of passes $m \geqslant m_{max}$.

It follows from Ref. 1 that in this case it is necessary that

$$m_{max} \leqslant \frac{\ln\left(4\pi f_1^2/d_1^2\right)}{2\alpha l_a}, \tag{5}$$

where α is the gain of the active medium.

From formulas (4) and (5) we can determine the possible values of M for getting the diffraction divergence:

$$M \geqslant \exp \frac{2\alpha l_a \ln\left[d_1^2/(2\lambda f_1)\right]}{\ln\left(4\pi f_1^2/d_1^2\right) - 2\alpha l_a}. \tag{6}$$

Thus to get the diffraction divergence we should use an unstable cavity with magnification M that satisfies the stronger of conditions (3) or (6).

In the experiments, the concave mirror of the unstable cavity had a focus $f_1 = 200$ cm. To estimate ∇n we can use the results of Ref. 1 since that research also used a system of initiation of the chemical reaction, composition of the working mixture and other conditions of experiments similar to ours. Therefore we will assume that during lasing $\nabla n < 5 \cdot 10^{-8}$ cm^{-1}.

According to our measurements, the gain of the active medium $\alpha \approx 0.015$ cm^{-1}. At values of $d_1 = 7$ cm, $\lambda = 3.9$ μm, $f_1 = 200$ cm and $l_a = 70$ cm, we get $M > 2$ from formula (3), and $M \geqslant 5.5$ from formula (6).

Thus under the conditions of the experiments the condition $M \geqslant 5.5$ must be met to attain the diffraction divergence of emission of the investigated laser.

TABLE 1

Conditions and averaged results of investigation of chemical lasers

cavity type	M	N_{eq}	E_{las}, J	$\frac{E_{unst}}{E_{pl}}$, %	$\theta_{0,5E}$, mrad	τ_{dur}, μs	τ_{del}, μs
planar	—	—	6,7	—	1,2	9,4	6,6
unstable	2,5	21	5,7	85	0,16	8,5	6,0
unstable	4,0	16	4,7	70	0,09	8,1	6,6
unstable	8,0	10	4,0	60	0,07	7,5	7,0

Note. τ_{dur}, τ_{del} are the duration and delay of the lasing pulse.

TABLE 2

Theoretical (th) and experimental (ex) dimensions of diffraction rings in the far zone of the laser, and distribution of radiation intensities and energies with respect to these rings

M	Ring №	θ_{th}, mrad	θ_{ex}, mrad	I_{th}^{max}, rel. units	I_{ex}^{max}, rel. units	E_{th}, %	E_{ex}, %
2,5	1	0,117	0,12	1	1	65	40
	2	0,266	0,27	0,07	0,22	30	49
	3	0,369	0,39	0,032	0,023	2	6
	4	0,452	0,50	0,001	0,005	0,2	1
4	1	0,126	0,13	1	1	75	60
	2	0,266	0,28	0,038	0,1	15	32
	3	0,340	0,39	0,011	0,01	2	3
	4	0,480	0,52	0,0036	0,005	6	3
8	1	0,134	0,14	1	1	83	80
	2	0,256	0,27	0,022	0,04	10	15
	3	0,352	0,38	0,0027	0,005	2	2
	4	0,490	0,50	0,0027	0,005	4	3

For experimental verification of the conclusions drawn above, unstable cavities were used with magnifications M = 2.5, 4 and 8 and equivalent Fresnel numbers N_{eq} = 10-20.

Table 1 gives the averaged results of experiments with planar and unstable cavities.

In the entire investigated range of magnifications of the unstable cavity M = 2.5-8, the intensity distribution in the far zone had the form of concentric rings typical of Fraunhofer diffraction.

Fig. 2 shows the distribution of lasing energy with respect to angle for lasers with unstable cavities (M = 2.5-8) and with a planar cavity. The radiation divergence of the laser with an unstable cavity is less than that of a similar laser with planar cavity by about an order of magnitude. With increasing M, the divergence decreases from $\theta_{0.5E}$ = 0.16 mrad at M = 2.5 to 0.07 mrad at M = 8. The results of measurement of the divergence of a laser with planar cavity enable us to estimate Δn in the investigated mixture in the lasing process [Ref. 8]:

$$\Delta n \approx \theta_{pl}^2 l_p / 8 l_a \approx 5 \cdot 10^{-7}, \qquad (7)$$

Which agrees with the results of Ref. 1.

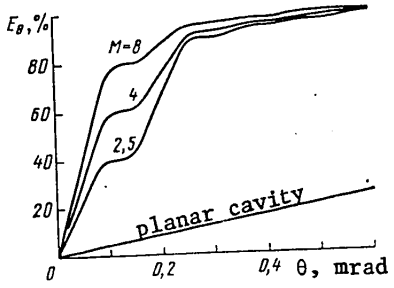

Fig. 2. Lasing energy distribution with respect to angle for lasers with unstable and planar cavities

The studies showed that the use of an unstable cavity in a chemical laser as compared with a planar cavity results in a reduction of total lasing energy. Although energy losses increase with increasing M from 15% for M = 2.5 to 40% for M = 8, the axial luminance of the emission B increases, reaching 45, 125 and 180 times the B_{pl} for M = 2.5, 4 and 8 respectively.

The method of calculation of Fraunhofer diffraction on an annular aperture [Ref. 9] was used to interpret the resultant distributions of radiation intensity of the laser with unstable cavity in the far zone.

Table 2 gives experimental and theoretical results of determination of minima of the intensity in the diffraction pattern in the far zone, and also the distribution of intensities and energies with respect to the rings.

Comparison shows coincidence of the calculated and experimentally determined positions of minima of the diffraction pattern for all investigated values of M. As we can see from Table 2, with increasing M there is an improvement in the correspondence of energy distribution with respect to diffraction rings as determined from the experiments and calculated for an empty ideal unstable cavity. At M = 8, this agreement is quite good, which confirms the conclusions.

To verify whether there are appreciable wings in the radiation distribution with respect to angle, a number of experiments were done in which the radiation energy was measured simultaneously in angles of θ_1 = 1 and θ_2 = 10 mrad by using

TABLE 3

Parameters of chemical laser with "misaligned" unstable cavity ($M = 8$, $f_1 = 200$ cm, $f_2 = 25$ cm)

Δ, см	R, м	E_{las}, J	τ_{dur}, μs	τ_{del}, μs
0	∞	4,0	7,5	7,0
5	80,8	4,0	7,4	7,0
10	41,4	3,8	7,3	6,9
30	15,12	3,9	7,4	6,9
60	8,56	3,8	7,4	7,0

calorimeters. It was established in these experiments that the radiation energy in the given angles is the same, proving the absence of wings with appreciable energy in the radiation pattern of the investigated chemical laser with unstable cavity beyond the limits of an angle of 1 mrad. This is further evidence that the energy distributions with respect to angle that are shown in Fig. 2 completely characterize radiation divergence.

Analysis of measurements of the time parameters of the lasing pulse showed that pulse duration τ_{dur} decreases by about 1 μs with a change from planar to unstable cavity. With increasing M, pulse duration decreases somewhat (see Table 1).

Lasing pulse delay τ_{del} relative to the beginning of initiation of the reaction showed almost no change in any of the experiments.

In a series of experiments with a high-speed streak camera an investigation was made of the time behavior of divergence of a chemical laser with unstable cavity. Black photographic paper was used as the radiation recorder. It was found by this technique that the radiation pulse of a laser with unstable cavity (at $M = 4$ and 8) consists of regular intensity spikes with period coinciding with the round-trip time of a light quantum through the cavity $\tau_{rt} = 2l_p/c$ (the photoresistor-oscillograph technique does not resolve these spikes). This was also confirmed by experiments in which the distance between mirrors of the unstable cavity was changed. This same spike behavior of lasing was observed in Ref. 10, where an investigation was made of an HF laser with unstable cavity.

An interesting feature of the unstable cavity is the capability of measuring small radiation divergences with good precision without additional focusing elements by "misalignment" of the unstable cavity. When this is done, the radius of curvature of the convergent wave is defined by the expression [Ref. 5]

$$R = f_1 + (f_1^2 - f_2^2)/\Delta + \delta, \tag{8}$$

where Δ is the amount of mismatch of the cavity, δ is a corrective term that is very small ($\delta \ll R$) at $M < 10$.

By using this cavity detuning technique in several experiments, a lasing far zone was found that is no different in energy distribution from that found conventionally by focusing mirrors (see Fig. 2).

As we can see from Table 3, with a change in radius of curvature of the surface of the radiating front from 8 to 80 m, the energy and time parameters of the radiation did not change within the limits of measurement error. Thus when the unstable cavity is intentionally detuned the major parameters of the laser remain practically unchanged, and the far zone of the radiation can be obtained on a screen located at a given distance R (see (8)) from the output mirror of the cavity.

4. Conclusion

An investigation is made of the feasibility of getting diffraction divergence of the radiation of a DF chemical laser with flashlamp pumping by using an unstable cavity of telescopic type.

The theoretical estimates showed that an unstable cavity with magnification $M \geqslant 5.5$ must be used in this laser to get emission with divergence close to the diffraction limit.

Unstable cavities with M= 2.5-8 were studied. It was experimentally shown that as M increases, the radiation divergence decreases, reaching a value of $\theta_{0.5E}$ = 70 μrad, which is almost the diffraction limit. Although in this case the energy losses are 40% as compared with a chemical laser with planar cavity, the axial luminance of the radiation increases by a factor of 180.

It was discovered as a result of the experiments that the lasing pulse with an unstable cavity at M= 4 and 8 consists of individual spikes with recurrence rate $\tau \approx 2l_p/c$.

It was shown that laser radiation can be focused at a given distance by appropriate detuning of the unstable cavity. This causes no noticeable distortion of the diffraction distribution of energy in the far zone; when this is done there are no appreciable changes in the radiation energy or time parameters of the pulse.

REFERENCES

1. Zykov, L. I., Kirillov, G. A., Kormer, S. B., Nikolayev, V. D., Sukharev, S. A., KVANTOVAYA ELEKTRONIKA, Vol 4, 1977, p 1336.

2. Siegman, A. E., PROC. IEEE, Vol 53, 1965, p 277

3. Anan'yev, Yu. A., KVANTOVAYA ELEKTRONIKA, No 6, 1971, p 3; USPEKHI FIZICHESKIKH NAUK, Vol 103, 1971, p 705.

4. Batovskiy, O. M., PRIBORY I TEKHNIKA EKSPERIMENTA, No 2, 1973, p 171.

5. Ragul'skiy, V. V., Fayzullov, F. S., OPTIKA I SPEKTROSKOPIYA, Vol 27, 1969, p 707.

6. Zemskov, K. I., Isayev, A. A., Kazaryan, M. A., Petrash, G. G., Rautian, S. G., KVANTOVAYA ELEKTRONIKA, Vol 1, 1974, p 863.

7. Isayev, A. A., Kazaryan, M. A., Petrash, G. G., Rautian, S. G., Shalagin, A. M., KVANTOVAYA ELEKTRONIKA, Vol 4, 1977, p 1325.

8. Kirillov, G. A., Kormer, S. B., Kochemasov, G. G., Kulikov, S. M., Nikolayev, V. D., Sukharev, S. A., Urlin, V. D., KVANTOVAYA ELEKTRONIKA, Vol 2, 1975, p 666.

9. Born, M., Wolf, E., "Osnovy optiki" [Principles of Optics], Moscow, Nauka, 1970, pp 449-453.

10. Simonis, G. J., APPL. PHYS. LETTS, Vol 29, 1976, p 42.

6610
CSO: 1862/242

UDC 621.375.826

STIMULATED EMISSION ON 18.4 μm IN CO_2 GASDYNAMIC LASER WITH ELECTRIC-ARC HEATING

Moscow KVANTOVAYA ELEKTRONIKA in Russian Vol 8, No 6(108), Jun 81 pp 1312-1315

[Article by D. G. Bakanov, A. A. Vedeneyev, S. Yu. Volkov, A. I. Demin, A. A. Infimovskaya, Ye. M. Kudryavtsev, A. I. Odintsov and A. I. Fedoseyev]

[Text] A report on activation and investigation of a CO_2-Ar gasdynamic laser ($\lambda = 18.4$ μm) with pulsed electric-arc heating of the working mixture. It is proved by measurement of the wavelength (18.38 ± 0.04 μm) that lasing occurs on the Q-branch of transition $03^10\text{-}10^00$. The maximum energy in a pulse with duration of about 20 ns was ~0.04 J at stagnation parameters in the prechamber of $T_0 = 1000$ K, $p_0 = 10$ atm for mixture CO_2:Ar = 1:2. In accordance with the theoretical data, the energy in a pulse decreased smoothly with change in CO_2 concentration. According to estimates, the power density inside the cavity was ~3 kW/cm^2, and the specific energy output from the flow was ~10 J/g.

The suggestion of development of a thermal gasdynamic laser on transitions between levels of paired modes of CO_2 was formulated in Ref. 1, 2. Ref. 1 was the first report on attainment of stimulated emission on the transition ($03^10\text{-}10^00$) with wavelength of 18.4 μm in a CO_2-Ar gasdynamic laser implemented by shock tube. This same paper proposed a mathematical model of such a laser in which the process of vibrational relaxation is described in terms of the total energy of paired modes ν_1, ν_2. In subsequent theoretical and experimental research an investigation was made of the way that initial pressures and temperatures and the composition of the working mixture influence the extent of inversion and the gain [Ref. 3, 4], and the anticipated lasing power was calculated [Ref. 4, 5]. It was shown that the CO_2-Ar gasdynamic laser on $\lambda = 18.4$ μm has advantages over the CO_2-N_2 gasdynamic laser on $\lambda = 10.6$ μm in higher efficiency (2%) and the possibility of a reduction in the temperature of gas heating. However, until recently the experimental study of the 18-micron CO_2 gasdynamic laser has been based on a facility using a shock tube and having a comparatively short active region (9 cm). Therefore we have had no clear idea of the outlook for realization of such a gasdynamic laser with more convenient methods of thermal excitation than heating in a shock tube. This paper is a report on attainment of quasi-cw lasing on a transition with $\lambda = 18.4$ μm in a gasdynamic laser with electric-arc heating of the gas mixture. Preliminary results are given on the investigation of characteristics of such a gasdynamic laser.

The experiments were done on a facility [Ref. 6] used previously for studying a CO_2 gasdynamic laser with emission wavelength of 10.6 μm. The facility was altered only in the parameters of the nozzle and optical cavity. A diagram of the setup is shown in Fig. 1. The gas was heated by a powerful pulsed electric discharge from capacitor bank 1; the discharge with duration of ~0.1 ms was initiated by electric explosion of a fine wire. Immediately before energizing the discharge, prechamber 2 of the gasdynamic laser was filled with the working mixture of gases by high-speed solenoid valve 3. The pressure in the prechamber was registered by piezoelectric sensor 4. A specially shaped single nozzle was used with critical cross section 0.1 mm in height and degree of expansion of 150. The nozzle terminated in a channel of fixed cross section connected to a vacuum chamber. Cavity 5 was placed immediately beyond the nozzle outlet at a distance of 3.5 cm from the critical cross section; the length of the active medium was about 40 cm. The cavity was formed by two mirrors with f = 100 cm (6, 7) with gold reflective coating. In the center of the mirrors were 0.5 mm holes for coupling out the emission.

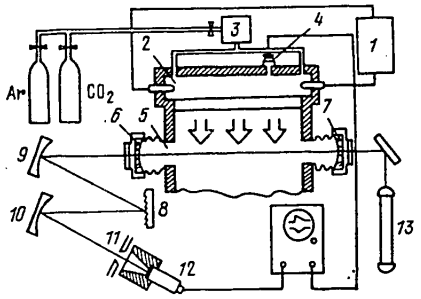

Fig. 1. Diagram of the experimental facility

The lasing wavelength was measured by a monochromator in the Ebert arrangement consisting of a diffraction grating of 50 lines/mm (8) and spherical mirrors with f = 50 cm (9, 10). The first collimated the radiation leaving the optical cavity, and the second focused the beam reflected from the grating on output slit 11 with a width of 0.5 mm. The radiation was registered by a variety of receivers. In the investigation of the lasing spectrum, inertial semiconductor bolometer 12 was used, which had an identical fairly high sensitivity over a wide spectral region. The bolometer signal was sent to an oscilloscope. A copper cone polished on the inside was placed in front of the bolometer for purposes of collimation. The system was calibrated with respect to high-order diffraction maxima of the radiation from helium-neon laser 13 ($\lambda = 0.6328$ μm). Linear dispersion in the plane of the output slit of the monochromator was 0.04 μm/mm. The emission wavelength of the gasdynamic laser as measured by this system was 18.38 ± 0.04 μm, enabling us to assign it with confidence to lines of the Q-branch of the vibrational transition (03^10-10^00) of the CO_2 molecule.

The radiation energy in the lasing pulse was determined by an IMO-2 laboratory meter. A rapid-response photosensor based on Ge-Zn cooled by liquid nitrogen was used to study the pulse shape. Fig. 2 shows oscillograms of the gas pressure in the prechamber, and of the lasing pulse; the latter was obtained by a Ge-Zn sensor. The total lasing pulse duration was about 20 ns. The maximum lasing power is displaced relative to the maximum of the pressure pulse. This shows that optimum conditions for stimulated emission correspond to pressures and temperatures of the gas in the prechamber that are lower than those at the beginning of the working cycle. The maximum output energy of the lasing pulse of 0.04 J was obtained for a mixture of CO_2:Ar = 1:2 at initial values of the pressure and temperature of the gas in the prechamber of $p_0 = 10$ atm, $T_0 = 1000$ K. In this case, the power at the maximum of the lasing pulse was about 3 W.

On Fig. 3, the experimental dependences of lasing pulse energy on relative CO_2 content in the mixture are compared with theoretical curves for the gain. The calculations were done by simultaneous solution of one-dimensional equations of gas dynamics and the relaxation equation for the total energy of modes ν_1, ν_2, in accordance with a method given in Ref. 1, 3 with consideration of the nozzle profile used in the given facility. The experimental and theoretical results agree fairly well, which confirms the correctness of the mathematical model. The reduction in gain and lasing power at high CO_2 concentrations in the mixture can be attributed on the one hand to reduced cooling of the gas in the nozzle due to a lowered adiabatic exponent, and on the other hand to a relative increase in the role of processes of VT-relaxation of paired modes of CO_2 [Ref. 3].

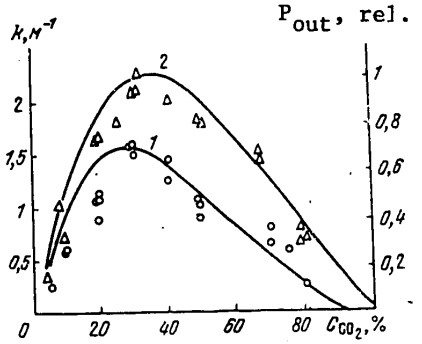

Fig. 3. Gain (calculated curves) and lasing power (experimental points) as a function of the relative content of CO_2 in the mixture for the following initial conditions: 1--p_0 = 20 atm, T_0 = 2000 K; 2--p_0 = 15 atm, T_0 = 1500 K

Let us note that the attained output power (~3 W) does not in the least characterize the energy capabilities of the given laser since the parameters of the optical cavity were not optimized. Overly small dimensions of the beam holes in the mirrors precluded efficient coupling of the radiation out of the cavity. Actually, in experiments done with a mixture of CO_2-N_2-He at flow parameters near optimum the measurements of lasing output power in the 10.6 μm region were even somewhat less than 3 W. This is indirect evidence that the two types of gasdynamic lasers are comparable in power. An estimate of the power density inside the cavity with consideration of the output beam hole of the mirror gives $I \sim 3$ kW/cm^2. If we take a reasonable value for the beam cross section inside the cavity ($S \sim 1$ cm^2) and assume that the cavity losses per pass lie in a range of 0.02-0.05, we can get a rough lower estimate of the lasing power taken from the flow of P_{las} = 60-150 W. An estimate made with consideration of the gas flowrate (~10 g/s) shows that the specific energy output from the flow under the given conditions is ~10 J/G.

In conclusion, we note that this research marks the first realization of an 18-micron gasdynamic laser with pulsed electric-arc heating of the working mixture. This facility is closer to a model of a cw gasdynamic laser than that based on a shock tube [Ref. 1]. Products of dissociation of CO_2 and other contaminants formed in the electric discharge initiated by an exploding wire have no decisive detrimental effect on the operation of the laser. The results show that a cw gasdynamic laser with steady-state electric-arc heating is suitable for producing radiation with wavelength of 18 μm.

The next step in research should be optimization of the profile and dimensions of the nozzle, the composition and parameters of the working mixture, and also improvement of the optical cavity. To do this, we are planning diagnosis of supersonic flow parameters and gain measurement. The comparatively long optical path of

this facility gives us hope that lasing might be attained on some other transitions of the CO_2 molecule as well [Ref. 1, 3], and also on transitions of other molecules [Ref. 7].

Just as important is the fact that the comparatively small overall dimensions, the relative simplicity of the construction and utilization of the facility enable its use for studying the capabilities for utilizing coherent emission with wavelength of 18 μm in science and engineering.

The authors thank A. M. Prokhorov for support in the work.

REFERENCES

1. Vedeneyev, A. A., Volkov, A. Yu., Demin, A. I., Logunov, Ye. M., Kudryavtsev, Ye. M., Sobolev, N. N., PIS'MA V ZHURNAL TEKHNICHESKOY FIZIKI, Vol 41, 1978, p 681; Preprint of Lebedev Physics Institute, USSR Academy of Sciences, Moscow, 1978, No 68.

2. Konyukhov, V. K., Fayzulayev, V. N., KVANTOVAYA ELEKTRONIKA, Vol 5, 1978, p 2586.

3. Vedeneyev, A. A., Volkov, A. Yu., Gomenyuk, Yu. V., Demin, A. I., Kudryavtsev, Ye. M., Poluyan, V. P., Preprint of Lebedev Physics Institute, USSR Academy of Sciences, Moscow, 1979, No 20.

4. Brunne, M., Zielinski, A., Milewski, J., Volkov, A. Yu., Demin, A. I., Kudryavtsev, Ye. M., in: "Proc. Int. Conf. on Lasers", Ed. by V. J. Corcoran, McLean, VA, USA, STS Press, 1980, pp 554-561

5. Volkov, A. Yu., Demin, A. I., Kudryavtsev, Ye. M., Brunne, M., in "Gas-Flow and Chemical Lasers", Ed. by J. Wendt, Rhode-Saint-Genese, Hemisphere Publ. Corp., 1979, pp 249-252.

6. Odintsov, A. I., Fedoseyev, A. I., Bakanov, D. G., PIS'MA V ZHURNAL TEKHNICHESKOY FIZIKI, Vol 2, 1976, p 145.

7. Volkov, A. Yu., Demin, A. I., Gomenyuk, Yu. V., Kudryavtsev, Ye. M., Poluyan, V. P., Preprint of Lebedev Physics Institute, USSR Academy of Sciences, Moscow, 1980, No 40.

6610
CSO: 1862/242

UDC 535.853.31

FEASIBILITY OF USING LIQUID METAL HEAT-TRANSFER AGENTS FOR COOLING THE ELEMENTS OF HIGH-POWER OPTICAL SYSTEMS BASED ON POROUS STRUCTURES

Moscow KVANTOVAYA ELEKTRONIKA in Russian Vol 8, No 6(108), Jun 81 pp 1328-1331

[Article by V. V. Apollonov, P. I. Bystrov, Yu. A. Broval'skiy, V. F. Goncharov and A. M. Prokhorov]

[Text] A theoretical investigation is made of the heat and thermodeformational characteristics of laser mirrors based on metal fiber structures cooled by liquid alkali metals (Na-K coolant of eutectic composition). The given estimates confirm the outlook for using liquid metal heat transfer agents to cool the heat-stressed elements of high-power optical systems with minimal heat distortions of the mirror surface.

It was pointed out for the first time in Ref. 1 that the threshold of optical destruction of mirror surfaces based on porous structures can be further increased by using liquid alkali metals and their alloys as coolants. The outlook for using liquid metal heat-transfer agents to cool the elements of high-power optical systems is dependent on the feasibility of attaining a high coefficient of heat exchange in the porous layer by a favorable combination of thermophysical properties of liquid metals. This relaxes the requirements for heat conduction of the material of the porous structure, which opens up the possibility for using new structural materials in the reflectors with a low coefficient of thermal expansion and poor heat conduction.

Of particular interest for purposes of cooling laser mirrors is the use of eutectic alloys of liquid metals that have a low melting point (for example Na-K alloy with melting point of -11°C). The use of liquid metal coolants will enable convective cooling of reflectors at temperatures close to the that of final adjustment of the mirror surface.

Ref. 2 generalizes processes of heat and mass transfer in porous structures with a decisive effect on the temperature fields and hydraulic characteristics of the reflector cooling system. On this basis a method was developed for predicting the heat and thermodeformational characteristics of laser reflectors enabling determination of the optimum type and parameters of the structure to ensure removal of the required heat flows for permissible distortions of the mirror surface.

Taking our lead from Ref. 2, let us consider some results of theoretical estimates of the heat and thermodeformational characteristics of laser reflectors cooled by eutectic alloy Na-K.

Within the framework of the assumptions made in Ref. 2, the equation of heat exchange that describes temperature distribution with respect to thickness of a porous layer can be written as

$$\frac{d^2t}{dx^2}=\frac{h_S}{\tilde{\lambda}}s_v(t-t_T), \tag{1}$$

where h_s is the coefficient of heat exchange between the material of the structure and the coolant. In view of the lack of data in the literature on heat exchange of liquid metals in a porous layer, we will use known data on heat exchange of liquid metal coolants in bundles of triangular arrays of fuel elements in nuclear reactors as the lower estimate of the coefficient of heat exchange in a porous structure. According to Ref. 3, the following relations will be used to calculate heat exchange of liquid metals in regular arrays of fuel elements:

in the cells of close-packed bundles (s/d = 1)

$$\mathrm{Nu}=\mathrm{Nu}_l+0.0408(1-1/\sqrt{1.24\varepsilon+1.15})\mathrm{Pe}^{0.65}; \tag{2}$$

in cells of separated bundles with $1.0<s/d<1.2$

$$\mathrm{Nu}=\mathrm{Nu}_l+\frac{3.67}{90(s/d)^2}1-\left\{\frac{1}{[(s/d)^{30}-1]/6+\sqrt{1.24\varepsilon+1.15}}\right\}\mathrm{Pe}^{m_1}; \tag{3}$$

in cells of separated bundles with $1.2<s/d<2$

$$\mathrm{Nu}=\mathrm{Nu}_l+3.67\mathrm{Pe}^{m_2}/90(s/d)^2, \tag{4}$$

where $m_1=0.56+0.19\ s/d-0.1/(s/d)^{80}$, $m_2=0.56+0.19s/d$, Nu, Pe are the Nusselt and Péclet numbers,

$$\mathrm{Nu}_l=\left[7.55\left(s/d-\frac{6.3}{(s/d)^{1.7}(s/d)(s/d-0.81)}\right)\right]\left[1-\frac{3.6}{(s/d)^{20}(1+2.5\varepsilon^{0.86})+3.2}\right]$$

is the Nusselt number for laminar flow, s/d is the relative spacing of the fuel elements in the array, $\varepsilon=\lambda_{st}/\lambda_c$ is the ratio of heat conduction of the fuel element cladding material to the heat conduction of the coolant. Relations (2)-(4) are valid for $\varepsilon>0.01$, $1\leqslant\mathrm{Pe}\leqslant4000$. Assuming correspondence between the hydraulic diameter of the array of fuel element bundles and the hydraulic diameter of the porous structure of the reflectors ($d_a=d_p$) and between the diameter of the bundle of rods and the diameter of the wire (for a metal fiber structure), we can get the following relation for felt structures: $d_a=d_s\Pi_v/(1-\Pi_v)$.

Formulas (2)-(4) apply to the region of stabilized flow of liquid metal coolant in cells of rod bundles where there are practically no overflows of the stream between cells. Therefore, using these relations to calculate the heat exchange of liquid metals in a porous structure where there is actually additional turbulizing of the flow by the matrix of the porous material will give an understated value of the coefficient of heat exchange.

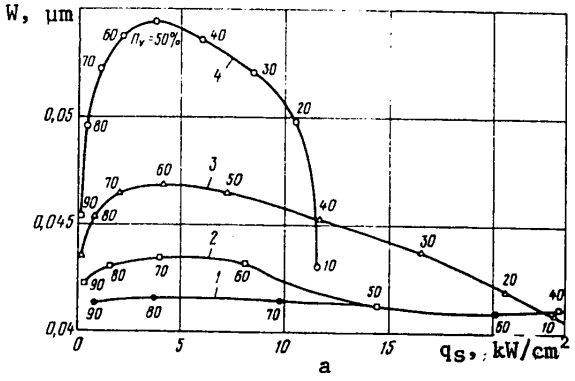

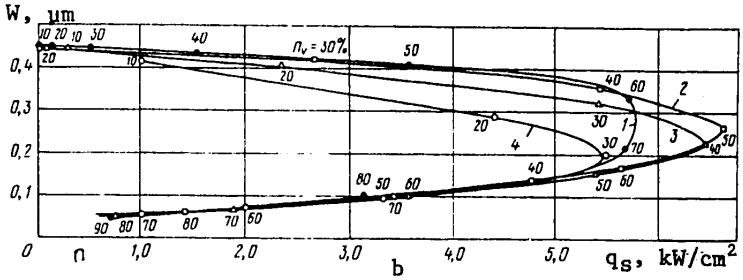

Fig. 1. Nomograms of thermodeformational characteristics of families of reflectors based on metal fiber porous structures of molybdenum cooled by Na-K heat-transfer agent in the zone of injection (a) and runoff (b) of the coolant at d_s = 20 (1), 50 (2), 100 (3) and 200 μm (4)

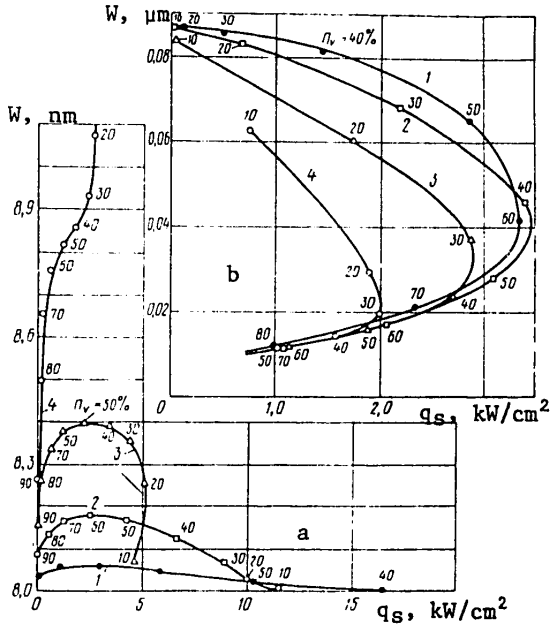

Fig. 2. Nomograms of thermodeformational characteristics of families of reflectors based on metal fiber porous structures of Invar cooled by Na-K heat-transfer agent in the zone of injection (a) and runoff (b) of the coolant at d_s = 20 (1), 50 (2), (100 (3) and 200 μm (4)

Based on the method of Ref. 2, equations (2)-(4) were used to calculate the heat and deformational characteristics of laser mirrors made on the basis of metal fiber porous structures of various materials with cooling by Na-K alloy. It was assumed that the coolant inlet and outlet system was made in the form of uniformly alternating holes. The distribution of the heat load over the mirror surface was taken as uniform. The hydrodynamic characteristics of the flow in the porous layer were calculated from generalized relations given in Ref. 2.

As an example, Fig. 1, 2 show the results of numerical calculations of the thermodeformational characteristics of a family of reflectors cooled by eutectic heat-transfer agent Na-K. It was assumed that the porous structures of the reflectors were made of molybdenum and Invar felt structures. The mean diameter of a fiber and the volumetric porosity of the structure were varied over ranges of $20 \leqslant d_s \leqslant 200$ μm and $0.1 \leqslant \Pi_V \leqslant 0.9$. The curves of Fig. 1, 2 are envelopes of the working thermodeformational characteristics of a family of reflectors and are plotted under condition of constant coolant pressure differential in the reflector at a maximum temperature of the cooled surface equal to 100°C as in Ref. 2. Let us note that in the case of liquid-metal cooling, this limitation is not decisive (as for example in the case of water cooling). The range of working temperatures for liquid metals can be considerably expanded, resulting in a corresponding increase in the heat loads that can be removed.

Fig. 1 shows that deformation of the optical surface in the zone of coolant runoff as calculated with consideration of heating of the coolant in the porous layer considerably exceeds the deformation in the injection zone, $W_2 > W_1$. The limiting heat flux densities for the investigated family of reflectors were: in the zone of coolant injection $q_1 > 20$ kW/cm^2, in the outlet zone $q_1 = 6.6$ kW/cm^2, with $W_2 = 0.3$ μm. The minimum level of deformation in the zone of coolant outflow for a flux drain of 4.2 kW/cm^2 is $W_2 = 0.12$ μm, which is considerably below the threshold of optical breakdown of the reflectors of CO_2 lasers.

The thermodeformational characteristics shown in Fig. 1a for a family of reflectors show the potential capabilities of liquid-metal cooling. The considerable difference in the curves is due to the influence of warming of the heat-transfer agent in the porous layer as a consequence of the relatively low heat capacity of the alloy Na-K, and therefore the degree of perfection of the flow part of the cooling system is decisive in developing reflectors of this class.

Analysis of the theoretical results of Fig. 2 shows that the use of a porous structure made of materials with a low coefficient of thermal expansion (Invar fibers) considerably reduces the thermal deformation of the mirror surface in both the inlet and outlet zones (by a factor of 3-4) when liquid-metal cooling is used. The maximum heat loads that can be removed from the mirror surface to keep the temperature at a level of 100°C in this case are: $q_1 > 20$ kW/cm^2, $q_2 = 3.5$ kW/cm^2 [see Ref. 2]. The thermodeformational characteristics of a reflector based on Invar fibers in the region of minimum deformation of the optical surface (Fig. 2b) and the point W_{min} are characterized by deformation $W_2 \approx 0.02$ μm with heat flux drain of 2.4 kW/cm^2.

The behavior of the curves of Fig. 1, 2 reflects the particulars of heat and mass exchange with convective liquid-metal cooling of reflectors. The family of envelopes

of thermodeformational characteristics enables determination of the optimum parameters of a metal fiber porous structure that ensure drainage of the necessary heat fluxes from the reflector at admissible values of distortion of the mirror surface which can be used to develop requirements for designing the cooling system.

In conclusion, let us note that because of the lack of reliable data on convective heat exchange of liquid metals in a porous layer, the heat and deformational characteristics of mirror surfaces given as an example in Fig. 1, 2 should be treated as estimates only. However, these results do show the good outlook for using liquid metals to cool optical elements based on metal fiber structures. The use of liquid-metal cooling in combination with porous structures made of materials with relatively low coefficient of thermal expansion opens up fundamentally new capabilities in the development of high-precision reflectors with a high threshold of optical destruction.

REFERENCES

1. Apollonov, V. V., Barchukov, A. I., Borodin, V. I., Bystrov, P. I., Goncharov V. F. et al., PIS'MA V ZHURNAL TEKHNICHESKOY FIZIKI, Vol 4, 1978, p 1193.

2. Apollonov, V. V., Bystrov, P. I., Goncharov, A. M., Prokhorov, A. M., Khomich, V. Yu., KVANTOVAYA ELEKTRONIKA, Vol 6, 1979, p 2533.

3. Subbotin, V. I., Ibragimov, M. Kh., Ushakov, P. A. et al., "Gidrodinamika i teploobmen v atomnykh energeticheskikh ustanovkakh (osnovy rascheta)" [Hydrodynamics and Heat Exchange in Nuclear Power Facilities (Fundamentals of Calculation)], Moscow, Atomizdat, 1975.

6610
CSO: 1862/242

UDC 621.375.82

CO_2 LASER WITH RADIATION ENERGY OF 3 kJ EXCITED UNDER MATCHED CONDITIONS

Moscow KVANTOVAYA ELEKTRONIKA in Russian Vol 8, No 6(108), Jun 81 pp 1331-1334

[Article by V. V. Apollonov, F. V. Bunkin, Yu. I. Bychkov, I. N. Konovalov, V. F. Losev, G. A. Mesyats, A. M. Prokhorov, V. F. Tarasenko and K. N. Firsov, Physics Institute imeni P. N. Lebedev, USSR Academy of Sciences, Moscow]

[Text] The article gives the results of investigation of a CO_2 laser with pulsed feed to the gas vessel under matched conditions. A total radiation energy of 3 kJ is obtained at a mixture pressure of 2 atm and active volume of 50 liters. With excitation of an active volume of 12 liters, the energy input to a mixture of $CO_2:N_2:He = 1:2:2$ was 0.6 kJ/(l·atm), and the radiation energy was ~80 J/(l·atm).

In the most powerful laser systems known in the literature that are excited by an electron-beam-stabilized discharge, the discharge is supplied from a capacitive accumulator connected to the laser gap [Ref. 1, 2] or from a pulse voltage generator [Ref. 3, 4]. In the former case, the energy stored in the accumulator is much greater than that fed to the discharge, and as a result a high voltage remains across the electrodes after completion of the excitation pulse for an extended time (as compared with the duration of the excitation pulse). The advantage of this unmatched mode of operation is that the voltage across the electrodes of the gas gap does not change appreciably during pumping. However, the residual voltage across the electrodes of the laser cell restricts the attainment of high field strength in the gas gap due to discharge contraction, and precludes high energy inputs, particularly in mixtures with low helium content. When a pulse voltage generator is used for gap supply in known facilities [Ref. 3, 4], only a part of the stored energy is input to the gas during the action of the electron beam, which limits the overall efficiency, and results in residual voltage across the electrodes.

The use of unmatched conditions for pumping a CO_2 amplifier with characteristic excitation time of ~1 μs was first reported in Ref. 5; however, the specific energy inputs in that research did not exceed 200 J/liter, and no data were given on the output energy characteristics.

The purpose of our research is to study the feasibility of high specific energy inputs and large energy outputs in pulses of ~1 μs duration in the matched mode of excitation of a CO_2 laser.

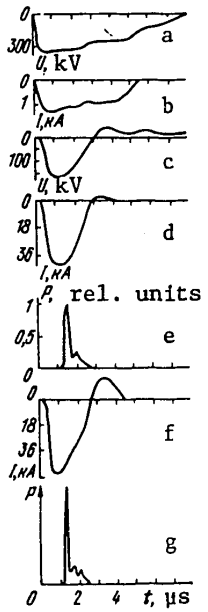

Fig. 1. Oscillograms of accelerator voltage (a) and current (b) pulses, voltage pulse across the gap (c), current pulse in the cell (d, e) and radiation pulses (f, g). Charging voltage of pulse voltage generators supplying the cell 58 kV, mixture $CO_2:N_2:He = 1:2:2$, pressure $p = 2$ atm, active volume 50 (c-e) and 12 liters (f, g)

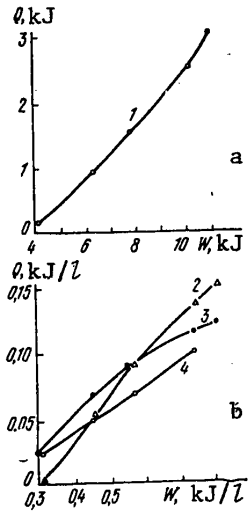

Fig. 2. Dependence of overall radiation energy on input energy with active volume of 50 liters (a) and dependence of specific radiation energy on specific input energy in an active volume of 12 liters (b). Mixture $CO_2:N_2:He = 1:2:2$, pressure $p = 2$ (1-3) and 1.2 atm (4); windows of KRS (1, 3, 4) and NaCl (2)

The laser system was made up of a gas cell, power supply and electron accelerator. The active medium was excited by a non-self-maintained discharge. The maximum active volume of the chamber was 50 liters (20 x 20 x 125 cm). The laser chamber permitted operation at a pressure of up to 2.5 atm. Experiments were done in an active volume of 50 liters, and also with a reduction in active volume to 12 liters (8 x 12 x 125 cm). The electron accelerator provided a current density of the electron beam in the gas chamber of about 0.5 A/cm^2, and accelerating voltage in the vacuum diode of about 300 kV. Oscillograms of the accelerating voltage across the vacuum diode and the current of the electron beam in the gas chamber are shown on Fig. 1a, b. A distinguishing feature of the selected mode of laser operation was that the electron beam pulse duration was double the duration of the current discharge. The discharge in the chamber was delayed relative to the beam current by ~0.3 μs. Thus the discharge took place at constant beam current density and electron energy, which is important for improving discharge stability as it gets rid of the low-energy electrons formed on the rising and falling segments of the accelerating voltage.

We used LC correction in the pulse voltage generator feeding the vacuum diode, giving a near rectangular pulse shape (see Fig. 1b).

The supply to the gas chamber was from a pulse voltage generator in the Marx system consisting of three parallel branches of five stages each. The pulse voltage generator used IK-100/0.4 capacitors, and the LC correction circuit used IMN-100/0.1 capacitors. The equivalent capacitance of the pulse voltage generator was 0.24 μF, characteristic impedance $\rho = 3.3\ \Omega$; at a charging voltage of U = 58 kV, the energy stored in the pulse voltage generator reached 10 kJ. Dry air-blasting of the discharge gaps in the pulse voltage generator ensured stable operation (±20 ns), and enabled pulse synchronization of the discharge current in the gas chamber and the beam current.

The following equation can be written for the discharge current of the given electric circuit:

$$I(t) = (U_0/\omega L) \exp(-Rt/2L) \sin \omega t, \qquad (1)$$

where $\omega = (L/C - R^2/4L^2)^{1/2}$ is the frequency of oscillations of the tank circuit; R is the resistance connected in the tank. In the given case, R is the resistance of the discharge plasma which can be considered linear and constant in time to a good approximation since the electron beam does not vary during discharge. The matched-load condition is $R = (LC)^{-1/2} = \rho$, and (1) implies that the discharge current pulse has the following parameters:

$$t_p = 2\pi(LC/3)^{1/2};\ t_m = 2\pi(LC/27)^{1/2};\ I_m = [U_0/(LC)^{1/2}] \exp(\pi/3\sqrt{3}), \qquad (2)$$

where U_0 is the open-circuit voltage of the pulse voltage generator, t_p is current pulse duration at the base, t_m is the time to attainment of maximum current, I_m is maximum discharge current.

There is practically no need for exact satisfaction of the equality $R = \rho$ since when $0.75\rho \leqslant R \leqslant 2\rho$ the reduction in peak power is only 10%. Let us call attention to the fact that as R varies from 0.75ρ to 2ρ, the voltage across the plasma varies from $0.47U_0$ to $0.74U_0$. This circumstance must be taken into consideration to maximize laser efficiency. In the described laser with maximum active volume of 50 liters for mixture $CO_2:N_2:He = 1:2:2$ at pressure of 2 atm the plasma resistance was $R = 3.8\ \Omega$. For charging voltage U = 58 kV, oscillograms of the voltage across the plasma, the discharge current and the radiation pulse are as shown in Fig. 1c-e. The dependence of the overall radiation energy on the energy stored in the pulse voltage generator is shown in Fig. 2a. The distribution of radiation energy in the cross section of the output beam was uniform, the energy density reached 15 J/cm^2. Damage to the output window was observed. The overall radiation energy reached 3 kJ, and efficiency reached ~27%. The radiation energy was measured by scanning an IKT-1M calorimeter with the sapphire window taken out of the sensor head over the cross section of the laser beam.

To determine the feasibility of attaining high energy inputs in matched operation, the active volume was reduced to 12 liters (8 x 12 x 125 cm). With the 50-liter volume, this could not be done because of the limited energy reserve of the pulse voltage generator supplying the gap. In this operation, the plasma resistance fell

to 2.5 Ω. Oscillograms of the discharge current and radiation pulse for this case are shown in Fig. 1f, g. The energy input in the second half-period does not exceed 10%, and therefore the operation can be considered practically matched. The amplitude value of the voltage across the plasma was 136 kV (E/p = 8.5 kV/(cm·atm)), and the maximum energy inputs exceeded 0.6 kJ/(l·atm). Fig. 2b shows the dependence of radiation energy on energy input at mixture pressures of 2 and 1.2 atm, and also for different resonators using NaCl and KRS output windows. The maximum radiation energy obtained in a volume of 12 liters was 1.8 kJ. We point out that lasing efficiency decreases with an increase in energy inputs, which is in agreement with the results of Ref. 3.

Thus our research has experimentally proved the feasibility of attaining high specific energy inputs in a large volume in matched operation.

REFERENCES

1. Yu. I. Bychkov, Ye. K. Karlova, N. V. Karlov, B. M. Koval'chuk, G. P. Kuz'min, Yu. A. Kurbatov, V. I. Manylov, G. A. Mesyats, V. M. Orlovskiy, A. M. Prokhorov, A. M. Rybalov, PIS'MA V ZHURNAL TEKHNICHESKOY FIZIKI, Vol 2, 1976, p 212.

2. V. A. Adamovich, V. Yu. Baranov, R. K. Bevov, Yu. V. Smakovskiy, A. P. Strel'tsov, PIS'MA V ZHURNAL TEKHNICHESKOY FIZIKI, Vol 4, 1978, p 988.

3. C. Cason, G. J. Dezenberg, R. J. Huff, APPL. PHYS. LETTS, Vol 23, 1973, p 110.

4. A. M. Orishich, A. G. Ponomarenko, V. G. Posukh, R. I. Soloukhin, S. P. Shalamov, PIS'MA V ZHURNAL TEKHNICHESKOY FIZIKI, Vol 3, 1977, p 39.

5. Status Report on Laser Program at LASL (u) LA-5251-PR, July-December, 1972.

6610
CSO: 1862/242

UDC 621.378.4

CONVERSION OF CO_2 LASER EMISSION TO 0.5 μm REGION IN NONLINEAR CRYSTALS

Moscow KVANTOVAYA ELEKTRONIKA in Russian Vol 8, No 6(108), Jun 81 pp 1361-1363

[Article by S. A. Andreyev, N. P. Andreyeva, I. N. Matveyev and S. M. Pshenichnikov]

[Text] An investigation is made of conversion of CO_2 laser radiation to the 0.5 μm region in a two-stage arrangement: first the emission of the CO_2 laser was converted to the near infrared region in crystals of the intermediate infrared range, and then to the visible range in a lithium iodate crystal; the same YAG laser radiation was used in both stages. With different crystals, conversion coefficients of 8-14% were obtained, enabling reliable registration of radiation in the intermediate infrared range with sensitivity equivalent to that of a photomultiplier with quantum yield of 1-2%.

One way to make CO_2 laser emission visible is conversion to the optical band in nonlinear crystals pumped by a pulsed ruby laser [Ref. 1]. In this technique, the converted emission falls in the 0.65 μm region, where the most sensitive photosensors (photomultipliers) have a quantum yield of 1-3%. However, this method of registration has a number of disadvantages: in the first place the resistance of current nonlinear crystals such as proustite and silver thiogallate to ruby laser radiation [Ref. 2] limits the coefficient of conversion of the converter to the 8-10% level; at a higher coefficient of conversion, and hence greater pumping power, the operation of the converter becomes unstable and unreliable. In the second place, the converted emission falls on the slope of the spectral curve of the most efficient multislit photocathode, which limits the equivalent quantum yield of the converter-photosensor system on the 0.2-0.3% level. In the third place, the proximity of the frequencies of the converted and pumping radiation does not permit effective spectral separation. In the fourth place, the frequency of arrival of information received by such a sensor is limited by the pulse recurrence rate of the ruby laser, and in practice does not exceed 10 Hz.

More promising is a double conversion circuit where the radiation of the CO_2 laser is first converted to the 0.97 μm region in crystals of the intermediate infrared range, and then to the 0.5 μm region in crystals of the near-infrared band, the radiation of the same YAG laser being used to pump these crystals. The two-stage conversion arrangement with focusing of pumping proposed in Ref. 3 gives a high conversion coefficient, and is quite effective for reception of one-dimensional signals.

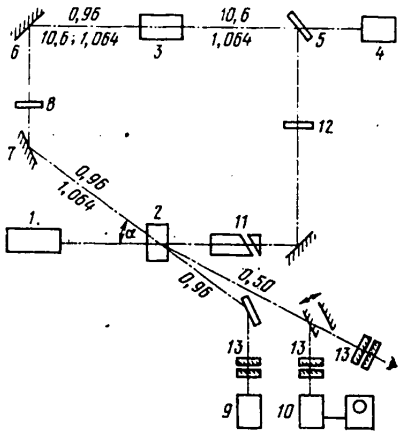

Fig. 1. Diagram of the experimental facility

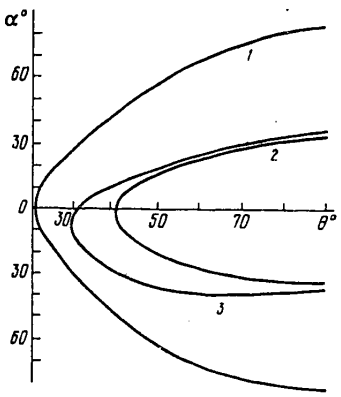

Fig. 2. Curves of vector synchronism (dependence of angle α on θ) for crystals of Ag_3AsS_3 (1), $AgGaS_2$ at $\lambda_s = 10.6$ μm, $\lambda_p = 1.064$ μm (2), and $LiIO_3$ at $\lambda_s = 0.967$ μm, $\lambda_p = 1.064$ μm (3)

In this paper we examine a two-stage conversion scheme without focusing of pumping, which enables its use for image conversion. A diagram of the experimental facility is shown in Fig. 1. A distinguishing feature of the arrangement is that the radiation of pumping laser 1 arrives first at crystal 2 of the near infrared band, which is more resistant to the pumping radiation, and then goes to crystal 3 of the intermediate infrared band. The crystals used in the intermediate infrared band were Ag_3AsS_3, $AgGaS_2$, $ZnGeP_2$ and $HgGa_2S_4$ in which close to collinear interaction of type oee or eoo was realized, while tangential interaction of type ooe was realized in the crystal of the near infrared band ($LiIO_3$). To accomplish this, the planes of synchronism of crystals 2 and 3 were made mutually perpendicular, and the polarization vector of the pumping radiation after crystal 2 was rotated through 90° by polarization direction rotator 11. When the $ZnGeP_2$ crystal was used, near-90° interaction of type eoo was realized, and the plane of synchronism of the crystal coincided with the plane of synchronism of $LiIO_3$. The optical delay around the ring from the near-infrared crystal to the intermediate-infrared crystal and back to the near-infrared crystal was less than 1 ns, i. e. considerably shorter than the duration of the pumping pulse (by a factor of 30).

The signal radiation source was a stabilized single-mode single-frequency LG-76 CO_2 laser 4. The signal radiation together with the pumping radiation went to crystal 3 via the mixing mirror (plane-parallel plate 5 of barius fluoride with a reflective interference coating applied to one of the faces for a wavelength of 1.06 μm). The pumping laser was Q-switched with pulse recurrence rate of 12.5 Hz. The converted radiation ($\lambda = 0.967$ μm) went via reflective mirrors 6, 7 and BS-12 filter 8 for eliminating 10.6 μm radiation to crystal 2, which was lithium niobate (the most effective crystal). The recording system enabled registration of both the signal after the first conversion ($\lambda = 0.967$ μm) by image-converter tube 9,

and the signal after the second conversion, either visually or by photomultiplier 10. Polarization direction rotator 11 was a quartz plate 1.3 cm thick with a wedge-shaped plate for exact control of the angle of rotation of the direction of polarization. The optical axis of the quartz plate coincided with the axis of the pumping radiation.

The geometry of the nonlinear crystals was determined by a computer as follows: for $AgGaS_2$--$\theta = 40°$, $\phi = 0°$, $\alpha = 0°$; for Ag_3AsS_3--$\alpha = 0°$, $\theta = 20°$, $\phi = 0°$; for $LiIO_3$--$\theta = 29°10'$, $\phi = 0°$, $\alpha = 18°$ (in air); for $ZnGeP_2$--$\theta = 82°56'$, $\phi = 45°$, $\alpha = 0°$; for $HgGa_2S_4$--$\theta = 41°34'$, $\phi = 0°$, $\alpha = 0°$. Here θ is the angle between the optical axis of the crystal and the direction of pumping radiation, α is the angle between pumping and signal wave vectors as read out toward the optical axis; ϕ is the azimuthal angle in the XY-plane. Computer calculations for the interaction of 10.6 and 1.06 μm in $ZnGeP_2$ and $HgGa_2S_4$ are given in Ref. 4, 5. Fig. 2 shows vector synchronism curves for crystals of $AgGaS_2$, Ag_3AsS_3 and $LiIO_3$ calculated by an analogous method.

The power coefficient of conversion of the two-stage arrangement $\eta_+ = P_{con}/P_s$ was determined by a direct method through measurement of the emission power P_s of the CO_2 laser by an IMO-2 power meter, and converted radiation power P_{con} ($\lambda = 0.5$ μm) by a calibrated photomultiplier. The measurements gave the following results: for $HgGa_2S_4$ $\eta_+ = 20\%$; for Ag_3AsS_3 $\eta_+ = 8\%$; for $AgGaS_2$ $\eta_+ = 14\%$; for $ZnGeP_2$ $\eta_+ = 6\%$. The pumping power density lay in a range of 0.5-1.2 MW/cm (depending on type of crystal), was far from the admissible limit, and ensured stable operation of the converter throughout the experiment (a few cycles in 0.5-1 hour). No deterioration of the optical characteristics of the crystals was observed. The completed experiments showed that the double conversion arrangement gives a sensitivity in the intermediate infrared range equivalent to that of a photomultiplier with quantum yield of 1-2%.

REFERENCES

1. Voronin, E. S., Divlikeyev, M. I., Il'inskiy, Yu. A., Solomatin, V. S., Badikov, V. V., Godovikov, A. A., KVANTOVAYA ELEKTRONIKA, No 1, 1971, p 151.

2. Andreyev, S. A., Barashkov, M. S., Matveyev, I. N., Pshenichnikov, S. M., Umnov, A. F., "Tezisy dokladov devyatoy Vsesoyuznoy konferentsii po kogerentnoy i nelineynoy optike" [Abstracts of Reports to the Ninth All-Union Conference on Coherent and Nonlinear Optics], Moscow, 1978, Part 1, p 194.

3. Voronin, E. S., Solomatin, V. S., Shuvalov, V. V., "Tezisy dokladov vos'moy Vsesoyuznoy konferentsii po kogerentnoy i nelineynoy optike" [Abstracts of Reports to the Eighth All-Union Conference on Nonlinear Optics], Tbilisi, Metsniyereba, 1976, Vol 1, p 184.

4. Andreyev, S. A., Andreyeva, N. P., Matveyev, I. N., Pshenichnikov, S. M., Ustinov, N. D., KVANTOVAYA ELEKTRONIKA, Vol 6, 1979, p 357.

5. Andreyev, S. A., Andreyeva, N. P., Badikov, V. V., Matveyev, I. N., Pshenichnikov, S. M., KVANTOVAYA ELEKTRONIKA, Vol 7, 1980, p 2003.

6610
CSO: 1862/242

UDC 621.373.826.038.823

INFLUENCE THAT HEATING OF ACTIVE MEDIUM DURING EXCITATION HAS ON CHARACTERISTICS OF PULSED ELECTROIONIZATION CO LASER USING PURE CARBON MONOXIDE

Moscow KVANTOVAYA ELEKTRONIKA in Russian Vol 8, No 6(108), Jun 81 pp 1366-1368

[Article by N. A. Bulavin, A. A. Ionin, I. B. Kovsh, I. V. Kochetov, V. G. Pevgov and B. M. Urin, Physics Institute imeni P. N. Lebedev, USSR Academy of Sciences, Moscow]

[Text] A theoretical investigation is made of the way that the lasing characteristics of a pulsed electroionization CO laser using pure carbon monoxide depend on the fraction η of pumping energy that is expended directly on heating the gas. A comparison is made with the results of theoretical research. It is shown that an increase in η over the theoretical value previously predicted gives good qualitative and quantitative agreement between theoretical and experimental data with respect to laser efficiency, lasing delay time and radiation spectrum.

In Ref. 1, experimental research was done on stimulated emission in a pulsed electroionization CO laser using pure carbon monoxide, showing that its efficiency (~3%) in contrast to that of electroionization lasers based on mixtures of $CO-N_2$ and $CO-N_2-He$, is almost an order of magnitude lower than the calculated values [Ref. 2]. The discrepancy, as noted in Ref. 1, may be due to the fact that the numerical calculation of Ref. 2 (with which the experimental data were compared) used an overstated value of the efficiency γ of vibrational excitation of CO molecules by electron impact (γ is the fraction of pumping energy expended on excitation of vibrational levels of CO molecules). Such an overstatement leads to underestimation of the heating of the working gas mixture during the pumping pulse as a consequence of direct transfer to heat of the fraction $\eta = 1 - \gamma$ of the excitation energy, and accordingly to an overstatement of the lasing efficiency.

In this article, a quantitative evaluation is made of the way that the energy, time and spectral characteristics of radiation of a pulsed electroionization CO laser using pure carbon monoxide depend on the quantity η, and calculated data are also compared with experiments. To get the theoretical values of the laser parameters, the system of equations of vibrational kinetics was solved simultaneously with equations for intensities of stimulated radiation and gas temperature. The calculations were done by a method developed in Ref. 2, 3 for the conditions of Ref. 1: particle density $N = 0.5$ Amagat unit, initial gas temperature $T = 100$ K,

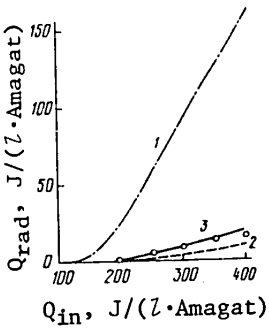

Fig. 1. Radiation energy Q_{rad} as a function of specific energy input Q_{in}: 1, 2--calculation at $\eta \cong 6$ (1) and 20% (2); 3--experiment [Ref. 1, 5]

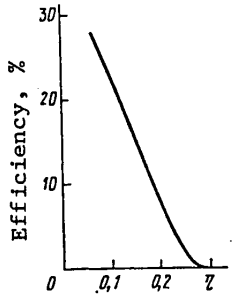

Fig. 2. Theoretical dependence of efficiency of pulsed electroionization CO laser on η

gun current density $i_g \sim 15$ mA/cm^2, pumping pulse duration $\tau_p = 30$ μs, threshold gain $\Gamma = 0.4$ m^{-1}. The energy input level changed in accordance with the initial value of the normalized field strength in the discharge E/N, which was varied over a range of $(0.9\text{-}1.5)\cdot10^{-16}$ V·cm^2; during pumping the quantity E/N decreased by a factor of approximately 1.5. The dependence of the radiation energy on the energy contributed to the discharge was calculated in two variants. In the first, the fraction η of pumping energy expended directly on heat was assigned as a function of E/N calculated in Ref. 4 on the assumption that the gas is heated due to rotational excitation and elastic losses of electron energy. According to Ref. 4 in the given range of E/N, η = 5-7%. In the second variant, the calculations were done for a set of fixed values of η in the range of 5-30%.

Fig. 1 shows theoretical and experimental [Ref. 5] curves for radiation energy as a function of specific energy input. It can be seen that an increase in the amount of energy going to heat leads to a considerable reduction of efficiency and improves agreement with the experiment. This is also implied by Fig. 2, which gives the theoretical dependence of efficiency on η ($Q_{in} = 300$ J/(l·Amagat), $\tau_p = 20$ μs, $\Gamma = 0.05$ m^{-1} and other conditions the same). The theoretical data show that lasing should not arise at all at $\eta > 0.3$ even at a very high value of reflectivity of the output mirror (~90% for an active region 1 m long).

Since lasing was observed on pure CO in the experiment, it can be concluded that $\eta < 0.3$ in the investigated range of E/N. However, this conclusion contradicts the results of Ref. 6, where E/N ≈ 10^{-16} V·cm^2 for pure CO gave $\eta \approx 0.5$. Therefore, we feel that the question of the value of η for carbon monoxide remains open; additional experiments must be done on determining the efficiency of vibrational excitation of CO in an electric discharge.

An increase in the fraction of energy expended on heat leads to an increase in the time of the delay τ_{del} of the lasing pulse relative to the pumping pulse (Fig. 3) since in our temperature range the rate of VV-exchange decreases with heating, and

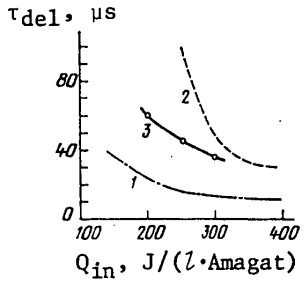

Fig. 3. Delay time τ_{del} as a function of Q_{in}. Notation as in Fig. 1

consequently so does the rate of formation of inverse population. The departure of the experimental curve [Ref. 1, 5] from calculated behavior at $\eta \approx 6\%$ also confirms the fact that $\eta > 6\%$.

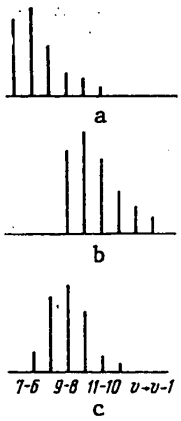

Fig. 4. Emission spectrum of the pulsed electroionization CO laser at $Q_{in} = 400$ J/(l·Amagat): a, b--calculation for $\eta \cong 6$ (a) and 20% (b); c--experiment [Ref. 1, 5]

Comparison of the emission spectra of the pulsed electroionization CO laser using pure carbon monoxide as calculated for different values of η at fixed specific energy input (Fig. 4) shows that an increase in the fraction of energy going directly to heat noticeably shifts the spectrum into the long-wave region, better agreement with the experiment being observed for the spectrum calculated for high values of η (in the experiments of Ref. 1, 5, the rotational structure of the vibrational bands was not resolved, and therefore in the calculation the energies of the radiation on separate rotational transitions were summed for each vibrational band).

Thus the assumption of a greater degree of heating of the active medium of the pulsed electroionization CO laser than previously predicted theoretically in the excitation process leads to better agreement of theoretical and experimental curves for efficiency of stimulated emission, delay time and radiation spectrum for pulsed electroionization CO lasers using pure carbon monoxide. Comparative analysis of the calculated and measured characteristics of the pulsed electroionization CO laser shows that for $E/N \cong 10^{-16}$ V·cm^2 the efficiency of vibrational excitation of CO molecules by electron impact $\eta \cong 85\%$ (in any case no less than 70-80%).

REFERENCES

1. Basov, N. G., Danilychev, V. A., Ionin, A. A., Kazakevich, V. S., Kovsh, I. B., Poletayev, N. L., KVANTOVAYA ELEKTRONIKA, Vol 6, 1979, p 1208.

2. Basov, N. G., Dolinina, V. I., Suchkov, A. F., Urin, B. M., Preprint of Lebedev Physics Institute, USSR Academy of Sciences, Moscow, 1976, No 1.

3. Konev, Yu. B., Kochetov, I. V., Pevgov, V. G., ZHURNAL TEKHNICHESKOY FIZIKI, Vol 49, 1979, p 1266.

4. Konev, Yu. B., Kochetov, I. V., Marchenko, V. S., Pevgov, V. G., Sharkov, V. F., Preprint of the Institute of Atomic Energy, Moscow, 1977, IAE-2810.

5. Ionin, A. A., Candidate's Dissertation, Lebedev Physics Institute, USSR Academy of Sciences, Moscow, 1977.

6. Londer, Ya. I., Menakhin, L. P., Ul'yanov, K. N., TEPLOFIZIKA VYSOKIKH TEMPERATUR, Vol 18, 1980.

6610
CSO: 1862/242

OPTICS AND SPECTROSCOPY

WAVE FRONT SENSOR BASED ON TALBOT EFFECT

Leningrad ZHURNAL TEKHNICHESKOY FIZIKI in Russian Vol 51, No 7, Jul 81 (manuscript received 25 Apr 80, after revision 24 Feb 81) pp 1432-1438

[Article by A. S. Koryakovskiy and V. M. Marchenko, Physics Institute imeni P. N. Lebedev, USSR Academy of Sciences, Moscow]

[Text] A wave front sensor based on the method of multibeam interferometry is considered that has a number of advantages over conventional wave front sensors. A simple algorithm is developed for processing the resultant interference patterns. Phase distortions are measured with precision of $\sim 5 \cdot 10^{-3} \lambda$.

1. A necessary component of active optical systems [Ref. 1, 2] is the wave front sensor. The requirements for wave front sensors are formulated in the survey of Ref. 2.

This paper analyzes the feasibility of developing a wave front sensor using the method of interferometry worked out in Ref. 3, 4 and based on the Talbot effect [Ref. 5, 6]. From the standpoint of spatial resolution and admissible range of measurement of phase distortions, such a wave front sensor has several advantages over those described in Ref. 2. An algorithm is developed for calculating the shape of the wave front.

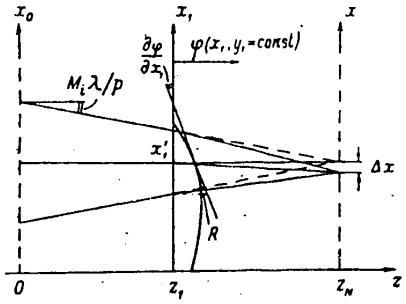

Fig. 1. Optical diagram of an interferometric wave front sensor based on the Talbot effect

An optical diagram of an interferometric wave front sensor is shown in Fig. 1. A wave with a planar or parabolic front is directed toward a two-dimensional periodic grating (with geometry satisfying the conditions of Ref. 6) located in plane $z = 0$. It is further assumed that the lattice periods along the X and Y axes are identical and equal to p. Then the radiation passes thorugh a medium characterized by the function of phase distortions $\phi(x_1, y_1) = \phi_r(x_1, y_1) - \phi_i(x_1, y_1)$ in plane $z = z_1$, where $\phi_r(x_1, y_1)$ and $\phi_i(x_1, y_1)$ are the phase advances in the investigated medium and in the reference medium (of given form) respectively; y_1 is the coordinate along the Y_1 axis perpendicular to plane (X_1, Z). Intensity distribution is recorded in plane $z = z_N$ that

coincident with the plane of reproduction of the field. In the case of an initial planar wave and $\phi(x_1,y_1) = 0$, $z_N = 2p^2N/\lambda$, where λ is wavelength, N = 1, 2,... is the number of the plane of reproduction, and radiation to each point of the plane of reproduction is from region $4M_iNp$ of the grating; $2M_i + 1$ is the number of spatial harmonics (diffraction orders) that take part in image formation; M_i is determined primarily by the geometric parameters of the grating. For example, for a sine-wave amplitude grating $M_i = 1$, and for a rectangular grating with transmission factor rect (x/q) comb (x/p) [Ref. 7], where q is the size of an opening, M_i is very large and is limited by wavelength $M_i < p/\lambda$. Actually, M_i is limited by introducing a spatial filter or by the sensitivity level of the reception equipment, since the intensity of the harmonics I_m falls with increasing m. For example for the above-mentioned rectangular grating

$$\frac{I_m}{I_0} = \operatorname{sinc}^2 \frac{m\sigma}{1+\sigma}, \qquad (1)$$

where $\sigma = q/p$, $m = \pm 1, \pm 2, \ldots$, and I_0 is the intensity of the zeroth harmonic. Since in practice we are dealing with gratings of finite dimensions $2a$, reproduction will take place in region $|x|, |y| \leqslant a - 2M_iNp$, disregarding diffraction by the aperture.

2. If an optically inhomogeneous medium is placed between the grating and the plane of reproduction, the reproduction pattern is distorted as a consequence of the fact that the spatial harmonics acquire different phase advances upon passage through different regions of the medium. The optical quality of the medium can be judged from the distortion of intensity distribution.

In the general case $\phi(x_1,y_1)$ can be found from solution of the inverse problem of reconstructing the phase distribution from the known intensity distribution [Ref. 8].

Let $u(x_1, y_1)$ be the distribution of the field in plane $z = z_1$ of the object. Then immediately behind the object the distribution will be $u(x_1, y_1)e^{i\varphi(x_1, y_1)}$. From measurement of the intensity distribution in the plane of observation, we find $|u_e(x, y)|$; a method of successive approximations is used to get $\phi(x_1, y_1)$. According to Ref. 7, the field $u(x, y)$ can be represented as a Fourier transform of the function $u(x_1, y_1)e^{i\varphi(x_1, y_1)}e^{i\frac{k}{2(z_N - z_1)}(x_1^2+y_1^2)}$, where $k = 2\pi/\lambda$. Let $\phi_0(x_1, y_1)$ be an arbitrary zeroth approximation of the unknown function, then

$$u_0(x, y) = \frac{e^{ik(z_N - z_1)}}{i\lambda(z_N - z_1)} e^{i\frac{k}{z_N - z_1}(x^2+y^2)} \iint_{-\infty}^{\infty} u(x_1, y_1) \times$$
$$\times e^{i\varphi_0(x_1, y_1)} e^{i\frac{k}{2(z_N - z_1)}(x_1^2+y_1^2)} e^{-i\frac{2\pi}{\lambda(z_N - z_1)}(x_1 x + y_1 y)} dx_1 dy_1.$$

Leaving the phase factor in $u_0(x, y)$, we replace the amplitude part by $|u_e(x, y)|$, and find by inverse Fourier transformation $u_1(x_1, y_1)e^{i\varphi_1(x_1, y_1)}$. This cycle is repeated until we get the steady-state solution $\phi_n(x_1, y_1) \cong \phi_{n+1}(x_1, y_1)$, where n is the number of the iteration. The number of steps n depends on how close the $\phi_0(x_1,y_1)$ is to the actual value of $\phi(x_1, y_1)$.

In the given interference technique the number of measurement points is determined by the parameter $(4aM_1/p)^2 \cong 10^4-10^6$ ($p/2M_1$ is the dimension of a minimum structure of the image), and the problem of finding $\phi(x_1, y_1)$ is laborious and time-consuming.

3. It was shown in Ref. 3, 4 that the reproduction effect takes place also in cases of simple optical inhomogeneities such as a plane-parallel plate and a wedge, and in the case of a parabolic lens is accompanied by a change of scale, i. e. the intensity distribution remains discrete and contrasty. Slight disruption of optical homogeneity of such media leads to displacement of contrasing cells in the plane of reproduction. In this connection, it makes sense to use the displacement of images of individual cells in the plane of registration as measured parameters, and to develop a simplified but precise algorithm for quantitative processing of the resultant interference patterns. This automatically does away with the difficulties involved in photometric measurement of resultant intensity distributions since in this case the phase distortions are converted to displacement of the contrasting images of points with respect to X and Y. To make the distorted reproduction pattern sharp enough for measurement, certain conditions must be met with regard to the parameters of the grating and $\phi(x_1, y_1)$. To find these conditions, let us expand $\phi(x_1, y_1)$ in a series with respect to derivatives in the vicinity of the point (x_1', y_1'):

$$\varphi(x_1, y_1) = \varphi(x_1', y_1') + \frac{\partial\varphi(x_1', y_1')}{\partial x_1}(x_1 - x_1') + \\ + \frac{\partial\varphi(x_1', y_1')}{\partial y_1}(y_1 - y_1') + R(x_1, y_1), \qquad (2)$$

where

$$R(x_1, y_1) = \sum_{n=2}^{\infty} \frac{1}{n!}\left[\frac{\partial^n\varphi(x_1', y_1')}{\partial x_1^n}(x_1 - x_1')^n + \frac{\partial^{n-1}\varphi(x_1', y_1')}{\partial x_1^{n-1}}\frac{\partial\varphi(x_1', y_1')}{\partial y_1} \times \right. \\ \left. \times (x_1 - x_1')^{n-1}(y_1 - y_1') + \cdots + \frac{\partial^n\varphi(x_1', y_1')}{\partial y_1^n}(y_1 - y_1')^n\right].$$

Here the first term of the second member describes the constant phase shift in the vicinity of (x_1', y_1') that displaces the plane of reproduction along the Z axis by $l = \phi(x_1', y_1')/k$, and the second term is the slope of the wave front that shows up in displacement of images of the cells in the vicinity of point (x_1', y_1') by an amount

$$\Delta x = \frac{\partial\varphi(x_1', y_1')}{\partial x_1}\frac{z_N - z_1}{k}; \quad \Delta y = \frac{\partial\varphi(x_1', y_1')}{\partial y_1}\frac{z_N - z_1}{k}. \qquad (3)$$

These two types of distortions are distinguished by the fact that they introduce phase shifts that are the same for all spatial harmonics, and hence do not affect the contrast of the reproduction pattern. Therefore in the given case the condition of image contrast will be met if the displacement l of the reproduction out of the plane of registration is less than the depth of field of the reproduction, which is found as the distance from the position of reproduction where the advance of the M_1-th harmonic changes by π relative to the zeroth harmonic. From this condition, using the results of Ref. 3, 4, we get

$$\varphi \leqslant 2\pi(p/M_1\lambda)^2. \qquad (4)$$

If we take into consideration that usually $(p/M_i\lambda)^2 \sim 10^3$–$10^4$, condition (4) is met over a wide range.

The quadratic term of expansion (2) and the terms of higher order describe distortions that introduce phase shifts in the vicinity of the point (x', y') of the expansion that depend on the number of the harmonic, blurring the pattern of reproduction in plane z_N. Since radiation arrives at point (x', y') in the plane of observation from the section of the investigated object $|x_1 - x_1'|$, $|y_1 - y_1'| \leqslant 2M_i Np(1 - z_1/z_N)$, the contrast will be preserved if in this region

$$R(x_1, y_1) \leqslant \pi. \tag{5}$$

We note that distortion of the wave front due to the quadratic term of (2) shifts the reproduction pattern without blurring it, and changes the scale [Ref. 3, 4]

$$\frac{1}{z_N - z_1} = \frac{1}{\frac{2p^2}{\lambda} - z_1} + \frac{1}{f}; \quad p' = p\frac{f - z + z_1}{f}, \tag{6}$$

where f is focal length. This enables the method to be used for studying the optical quality of lenses and parabolic mirrors. In this case $\phi(x_1, y_1)$ is the deviation $\phi_r(x_1, y_1)$ that characterizes the actual object away from the quantity assigned by the object with focal length $\phi_i = (x_1^2 + y_1^2)/2f$.

Thus by selecting the type of grating (p, M_i) and the position z_1 of the investigated medium, we can get a contrasting distribution of intensity in registration plane z_N by satisfying inequality (5).

From the dependence of the position of the plane of reproduction on p we get the condition for precision (periodicity) and alignment of the grating. Assuming that the pattern in the plane of registration is not blurred if displacement of the plane of reproduction due to imprecision of the period Δp is less than the depth of field defined above, we get

$$\Delta p \leqslant p/4M_i^2 N. \tag{7}$$

Inclination of the grating at angle β leads to a change in the effective period $p' = p\cos\beta \cong p(1 - \beta^2/2)$. Then from (6) we get the condition for alignment $\beta \lesssim 1/M_i\sqrt{2N}$.

4. The initial material for getting quantitative information on phase distortions of the investigated medium is an interference pattern that is a set of contrasting images of the grating cells shifted relative to the undisturbed initial positions.

The algorithm for processing the interference pattern is as follows: 1) the position of points of measurement of the function of phase distortions of the investigated object $\phi(x_1, y_1)$ is given by projections of transmitting cells of the grating on the object (x_l^l, y_1^s), where l, $s = 0, 1, 2, \ldots 2a/p$; 2) at each point (x_l^l, y_1^s), $\phi(x_1, y_1)$ is represented as a series (2), and since the interference patterns are obtained under condition (5), we can limit ourselves to constant and linear terms of the expansion; 3) from the displacement of images of the grating cells in the plane of registration $z_N\Delta x_l$, Δy_s (Fig. 1), in accordance with (3), we

determine $\partial\phi(x_1^7, y_1^8)/\partial x_1$, $\partial\phi(x_1^7, y_1^8)/\partial y_1$; 4) beginning with an arbitrary point $(x_1^{7\circ}, y_1^{8\circ})$, we find over the entire aperture $2a$

$$\varphi(x_1^{l+1}, y_1^s) = \varphi(x_1^l, y_1^s) + \frac{p}{2}\left[\frac{\partial\varphi(x_1^l, y_1^s)}{\partial x_1} + \frac{\partial\varphi(x_1^{l+1}, y_1^s)}{\partial x_1}\right],$$

$$\varphi(x_1^l, y_1^{s+1}) = \varphi(x_1^l, y_1^s) + \frac{p}{2}\left[\frac{\partial\varphi(x_1^l, y_1^s)}{\partial y_1} + \frac{\partial\varphi(x_1^l, y_1^{s+1})}{\partial y_1}\right],$$

$$\varphi(x_1^{l+1}, y_1^{s+1}) = \frac{1}{2}\left\{\varphi(x_1^{l+1}, y_1^s) + \frac{p}{2}\left[\frac{\partial\varphi(x_1^{l+1}, y_1^s)}{\partial y_1} + \right.\right.$$

$$\left.\left. + \frac{\partial\varphi(x_1^{l+1}, y_1^{l+1})}{\partial y_1}\right] + \varphi(x_1^l, y_1^{s+1}) + \frac{p}{2}\left[\frac{\partial\varphi(x_1^l, y_1^{s+1})}{\partial x_1} + \frac{\partial\varphi(x_1^{l+1}, y_1^{s+1})}{\partial x_1}\right]\right\}. \quad (8)$$

In most cases errors by a constant phase shift due to arbitrary selection of $\phi(x_1^{7\circ}, y_1^{8\circ})$ play no part since we are usually interested in the behavior of $\phi(x_1, y_1)$ rather than in its absolute value.

The error on one step will be $2R(p/2, 0)$. If it is assumed that the unknown $\phi(x_1, y_1)$ is a sufficiently smooth function, the main contribution to the error will be from the quadratic term of expansion (2), and in accordance with (5) $2R(p/2, 0) \leq \pi/16M_1^2N^2$. It may happen in practice that it is impossible or unnecessary to meet condition (5). Then error 2R can be estimated from the modulation of the image in the plane of registration due to phase mismatch of harmonics. If the intensity distribution in the cells of the plane of registration z_N is modulated with period τ, this means that the $m = p/\tau$-th harmonic is out of phase, i. e. $R[(2p/\tau)Np(1 - z_1/z_N), 0] \sim \pi$, and consequently the error on one step is $2R(p/2, 0) \sim (\pi/16N^2)(\tau/p)^2$. Thus the sharpness of the interference pattern is an index of accuracy of determination of $\phi(x_1, y_1)$.

The accuracy of determining $\phi(x_1, y_1)$ can be improved if it is averaged at each computational point (x_1^7, y_1^8), i. e. if we take the average value between those obtained in calculation by different routes, e. g. as is done in (8) $\varphi(x_1^{l+1}, y_1^{s+1}) = (\varphi_1 + \varphi_2)/2$, where ϕ_1 is obtained from $\varphi(x_1^l, y_1^s)$ by route $\varphi(x_1^l, y_1^s) \to \varphi(x_1^{l+1}, y_1^s) \to \varphi_1(x_1^{l+1}, y_1^{s+1})$, and ϕ_2 is obtained by route $\varphi(x_1^l, y_1^s) \to \varphi(x_1^l, y_1^{s+1}) \to \varphi_2(x_1^{l+1}, y_1^{s+1})$. Averaging can be done with respect to three, four or more values of $\varphi(x_1^{l+1}, y_1^{s+1})$, obtained from different trajectories of computation, or for example around a ring $\varphi(x_1^l, y_1^s) \to \varphi(x_1^{l+1}, y_1^s) \to \varphi(x_1^{l+1}, y_1^{s+1}) \to \varphi(x_1^l, y_1^{s+1}) \to \varphi(x_1^l, y_1^s)$.

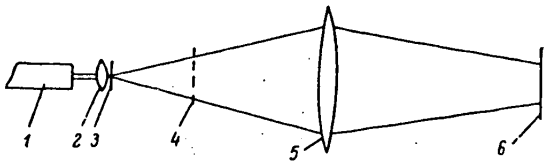

Fig. 2. Diagram of facility for measuring wave front distortions

5. The facility for measuring wave front distortions shown in the diagram of Fig. 2 is an example of realization of the described method. Radiation of He-Ne laser 1 is expanded by eyepiece 2 with spatial filter 3 placed at the focus. Objective lens 5 is set so that its central part received the incident beam so as

to reduce the intensity differential over the cross section. Two-dimensional periodic grating 4 is placed in the divergent beam, enabling variation of the period of distribution in the plane of registration by longitudinal displacement of the grating. The spacing σ can be varied by relative displacement of two identical gratings superimposed on each other. The intensity distribution is registered by photographic plate 6 in the plane of reproduceion, the position of this plane being defined by formula (6). Objects to be studied can be placed anywhere between grating 4 and registration plane 6.

As an illustration of the possibilities of the method, measurements were made of the distortions of a wave front by inhomogeneities modeled by a glass plate. On the interference patterns of Fig. 3 [photo not reproduced] the unperturbed distribution is shown on the left, and the distribution distorted by optical inhomogeneities of the plate is shown on the right. The photographs were obtained for the same region of the plate (the period of distribution on the object was 1.3 mm, N = 1) with grating spacings $\sigma_1 = 0.15$, $\sigma_2 = 0.5$. In the former case, the number of harmonics of comparable intensities is greater than in the latter case [for example for σ_1, according to (1), $I_3/I_0 \cong 0.5$, and for σ_2, $I_1/I_0 \cong 0.41$], and more blurring of the image is observed as a consequence of violation of condition (5). The one-dimensional nature of inhomogeneities introduced by the plate simplifies processing of the interference pattern, reducing this procedure to a one-dimensional problem. The interference pattern of the second photograph can be interpreted as follows.

In the center of the photograph (in the vicinity of the 17-th line from the bottom) the images of the squares are blurred, i. e. in this area $R(x_1)$ is large, and the period of distribution is smaller than in the undistorted left part, indicating a focusing convexity in the relief of the plate. In the region of the 8-14-th lines, the images of the squares are fairly sharp, $R(x_1)$ is small, and displacement of the lines in case of the period of the image equal to the undistorted value indicates an optical wedge in this region. In the upper and lower parts of the photograph the image is blurred, and the period of the distribution is greater than the undistorted period, which is an indication of a defocusing concavity. For numerical processing of the interference pattern in this photograph, the displacements Δx_l of the squares, where l is the number of the line, were measured relative to the left part that had not been subjected to the action of the investigated plate, which to some extent eliminated the influence of nonideality of optical components of the system. Derivatives were found by the formula $\partial\phi(x_1)/\partial x_l = 2\pi(\Delta x_l)/\lambda z^*$, where $z^* = z_{05} + z_{56} - (z_{05}z_{56}/f)$, z_{05} is the distance from the object to the objective lens, z_{56} is the distance from the objective lens to the plane of registration, f is the focal length of the objective lens. Considering that $\phi(x_1) = \Delta L(x_1)(n-1)\cdot 2\pi/\lambda$, where n is the index of refraction of glass, $\Delta L(x_1)$ is the change in thickness of the plate along X_1, we find $\Delta L(x_1)(n-1)$ (Fig. 4). It can be seen that the resultant relation coincides with the qualitative study of the interference pattern outlined above. The accuracy of measurement of Δx_l was 0.1 mm, which in the given measurement system corresponded to $8\cdot 10^{-2}$ λ.

The third photograph of Fig. 3 [photo not reproduced] is the interference pattern of a fairly smooth section of the plate, the region $|x_1 - x_1'|$ [see (5)] being reduced by a factor of 1.7 as compared with the preceding case. The change in the phase front of the plate is shown in Fig. 4. In the given case, the initial

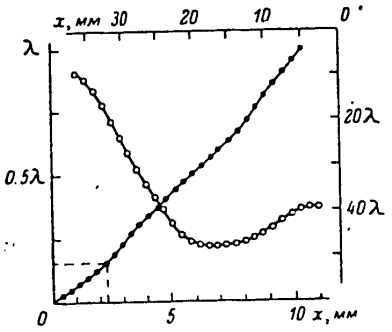

Fig. 4. Change of phase front in glass plate as a function of x_1, obtained from processing interference patterns 2 (upper scale) and 3 (lower scale) of Fig. 3 [not reproduced]

interference pattern is fairly contrasty, which enabled measurement of Δx with accuracy of 20 μm, and accordingly the accuracy of determining $\Delta L(x_1)(n-1)$ was $4 \cdot 10^{-3}$ λ.

If only the curvature of the wave front is of interest, the measurements can be done with respect to the distorted right-hand part of the interference pattern. In this case Δx_i is measured to within an unknown constant that corresponds to a fixed optical wedge over the aperture.

6. This wave front sensor based on the method of multibeam interferometry has certain advantages over conventional sensors. The optical system of the wave front sensor is analogous to that of the Hartmann sensor [Ref. 2], is simple, and is easily realizable. However, the sensitivity of the wave front sensor to phase distortions is considerably higher [Ref. 4], and the accuracy of measurements increases with their reduction. A wave front sensor with grating of small size enables investigation of a medium with large apertures. The spatial resolution defined by the parameter $4M_1Np(1 - z/z_N$ may be considerably higher due to the capability of reducing the lattice period. The range of phase distortions that the wave front sensor registers is determined by the condition of contrast of the intensity distribution in the plane of registration (5), and may amount to many wavelengths. Studies have shown that the wave front sensor is not very sensitive to nonuniformities in illumination of the aperture.

The wave front sensor is especially convenient in use as an indicator of wave front distortions, for example in systems of aperture probing or sharpness enhancement [Ref. 2]. It is less sensitive to perturbations of equipment by vibrations than other interference wave front sensors.

The capability of real-time use of the wave front sensor is determined by the rate of computer input of information on intensity distribution in the plane of registration, which depends on the reception device, and by computing time. The data processing algorithm developed in this paper is simple and permits rapid computation of the shape of a wave front.

In conclusion the authors thank A. M. Prokhorov for useful discussion.

REFERENCES

1. Bakut, P. A., Ustinov, N. D., Troitskiy, I. N., Sviridov, K. N., ZARUBEZHNAYA ELEKCTONIKA, No 3, 1977, p 55.

2. Hardy, J. W., PROC. IEEE, Vol 66, 1978, p 651; TRUDY IIER, Vol 6, 1978, p 31.

3. Koryakovskiy, A. S., Marchenko, V. M., FIAN Preprint No 89, Moscow, 1979.

4. Koryakovskiy, A. S., Marchenko, V. M., KVANTOVAYA ELEKTRONIKA, Vol 7, 1980, p 1048.

5. Deckers, Ch. NOUV. REV. OPTIQUE, Vol 7, 1976, p 113.

6. Montgomery, W. D., JOSA, Vol 57, 1967, p 772.

7. Goodman, J. W., "Vvedeniye v Fur'ye optiku" [Introduction to Fourier Optics], "Mir", Moscow, 1970 [New York, McGraw-Hill Book Co., 1968].

8. Bakut, P. A., Troitskiy, I. N., Demin, A. A., Safronov, A. N., ZARUBEZHNAYA RADIOELEKTRONIKA, No 11, 1978, p 3.

6610
CSO: 8144/1798-A

UDC 621.3.038.8

FEASIBILITY OF MAKING AN ABSORBING CELL FOR $\lambda = 1315$ nm

Moscow KVANTOVAYA ELEKTRONIKA in Russian Vol 8, No 6(108), Jun 81 pp 1315-1319

[Article by O. B. Danilov, A. P. Zhevlakov and I. L. Yachnev]

[Text] It is experimentally shown that a concentration of unexcited iodine atoms of $(2-5)\cdot10^{17}$ cm^{-3} can be obtained on the pyrolysis phase of photolysis of perfluoroalkyl iodides. The velocities of pyrolysis and compressional waves are measured in a thick layer of perfluoroalkyl iodide. It is found that the velocity of the pyrolysis wave is much greater than that of the compressional wave. The authors discuss the feasibility of constructing a pulse absorption cell for $\lambda = 1315$ nm in which the absorbing medium is produced by a pyrolysis wave.

At the present time the amplification stages of a photodissociation iodine laser are decoupled by using an absorbing cell [Ref. 1, 2] that works on the transition $I(5^2P_{3/2} - 5_2P_{1/2})$. Unexcited iodine atoms are produced by thermodissociation of iodine molecules I_2. The cell is placed in a thermostat with temperature of ~800°C. The working temperature of the iodine atoms was ~10^{17} cm^{-3}. Since the absorbing transition is the inverse of the stimulated transition $I(5^2P_{1/2} - 5^2P_{3/2})$ and the widths of the lines of both are made equal, the iodine absorbing cell should work with reduction of the cross section of the luminous flux of the preceding amplification stage. A weak point of the thermal absorbing cell is the windows that are always in contact with iodine, which reduces their radiation strength. An absorbing cell in which unexcited iodine atoms are formed upon flash photolysis of perfluoroalkyl iodides is free of this disadvantage. The photolysis region in the absorbing cell can be localized at any distance from its windows, and therefore the dimensions can be selected in accordance with the admissible requirements for radiation loading. A pulse absorbing cell has been used for decoupling the master laser and amplifier [Ref. 3]. However, Ref. 3 contains no data on the transmission factors and operating conditions of the absorbing cell that would help us to understand whether such a cell can be used for decoupling powerful amplification stages.

In photolysis of perfluoroalkyl iodides, a concentration of iodine atoms of 10^{17} per cc or more is difficult to achieve on the pre-pyrolysis stage of photolysis even when a strong quenchant of excited iodine atoms I* is used because of rapid recombination of iodine atoms with radicals CF_3, C_3F_7 [Ref. 4]. But such a concentration of iodine atoms is easily realized on the post-pyrolysis stage of

photolysis. This has been established in experiments on transillumination of a medium being photolyzed on $\lambda = 1315$ nm that were done on the facility described in Ref. 5. The source of transillumination was a photodissociation laser operating on one transition F = 3 - F = 4. According to Ref. 6 the half-width of the emission line of such a photodissociation laser is 0.0015 cm^{-1}. The half-width of the absorption line was calculated from the data of Ref. 7. Conformity to Bouguer law was verified by varying the length of the absorbing medium. The experiments were done on mixtures of CF_3I, n-C_3F_7I with air and Xe. The oxygen of the air, a strong quenchant of I*, prevented amplification of the transilluminating signal on the pre-pyrolysis stage of photolysis.

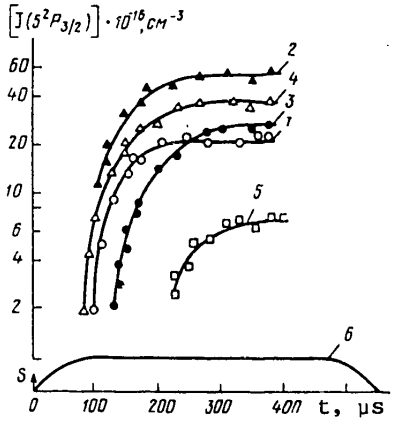

Fig. 1. Time dependences of the concentration of unexcited iodine atoms in the following mixtures: CF_3I:air = 15:75 (1), 30:75 (2), C_3F_7I:air = 15:50 (3), 30:50 (4) and C_3F_7I:air:Xe = 15:75:300 mm Hg (5); 6--pumping pulse; standard error of measurements of concentration of iodine atoms for curves 1-4 is ±20%, and for curve 5--40%

The time dependences of concentration of iodine atoms for different mixtures (curves 1-5) are given on Fig. 1. This figure shows that with photolysis of mixtures of CF_3I, n-C_3F_7I with air we can get concentrations of iodine atoms of about $(2-5)\cdot10^{17}$ cm^{-3}. The region of fast formation of iodine atoms corresponds in time to the region of intense photolysis [Ref. 8]. The concentration of iodine atoms is $6\cdot10^{16}$ cm^{-3} on the pre-pyrolysis stage of photolysis, which lasts for the entire pumping pulse in a mixture of n-C_3F_7I:air:Xe = 1:5:20 ($p_{n\text{-}C_3F_7I}$ = 20 mm Hg).

Passage of a nanosecond pulse through the amplifier is accompanied by the appearance of a pedestal (pre-pulse) that is longer than the part of the pulse in which the main energy is concentrated [Ref. 2]. The transilluminated absorbing cell should maximally attenuate the radiation of the pre-pulse, superluminescence and luminescence of the preceding amplifier (weak signal) and should pass the radiation of the main pulse (strong signal) with minimum losses. For effective decoupling of amplification stages by an absorbing cell, the absorption linewidth should be no narrower than the amplification line of the preceding stage. It is known [Ref. 3] that the amplification line is intentionally broadened by adding large concentrations (~10^{19} cm^{-3}) of buffer gas to suppress self-excitation of the amplifier. It is not advantageous to use such a method of line broadening in the absorbing cell as it leads to a reduction in the concentration of iodine atoms. It is suggested that the widths of the absorption and amplification lines be matched by applying an inhomogeneous longitudinal magnetic field on the absorbing cell. Broadening of the absorption line of the absorbing cell by the magnetic field enables us to use a relatively low concentration of the working mixture. This is important since a reduction in the pressure of the medium increases its resistance to optical breakdown.

A possible design of an absorbing cell is shown in Fig. 2. Thin magnet coils 8 are placed at the ends of quartz vessel 1 to set up an inhomogeneous longitudinal

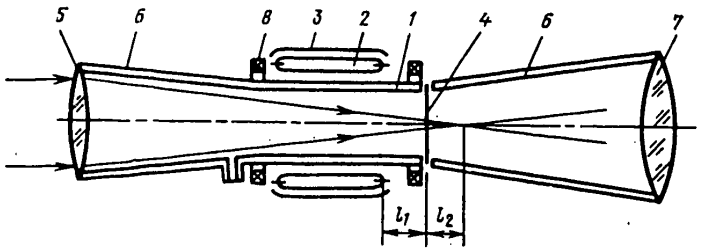

Fig. 2. Construction of an absorbing cell

magnetic field. The working mixture is admitted to the chamber with bell mouths 6 as far as vacuum gate 4, and the rest of the absorbing cell is evacuated. Opening the gate gives rise to a rarefaction wave at the gas-vacuum interface, this wave moves through the gas at the speed of sound c, and the gas begins to escape into the vacuum. The velocity of the gas boundary is $u = [2/(\gamma - 1)]c$, where γ is the adiabatic exponent [Ref. 9]. To eliminate the influence of both processes on the operation of the cell, it is necessary to locate the gate at certain distances both from the pumped region of the gas (l_1, see Fig. 2) and from the focal plane of the input lens of the absorbing cell 5 (l_2). Let us estimate the lower limit of the values of l_1, l_2, after assigning the shutter opening time t_3. At $t_3 = 1$ ms [Ref. 10], $c = 160$ m/s, $u = 2.2$ km/s, we get $l_1 = 16$ cm, $l_2 = 220$ cm. Firing of pumping lamps 2 located in illuminator 3, establishment of the magnetic field and transmission of the monopulse through the absorbing cell up to input lens 7 of the following stage all take place before arrival of the gas in the region near the focus of lens 5 to preclude optical breakdown there. In determining the parameters of the absorbing cell, we begin with the premise that the pressure of the working mixture must ensure the necessary concentration of iodine atoms on the one hand, and must ensure resistance of the medium to optical breakdown on the other hand. A concentration of iodine atoms of $\sim 4 \cdot 10^{17}$ cm^{-3} can be obtained from a mixture of $CF_3I:O_2 = 1:1$ ($p_{CF_3I} = 20$ mm Hg). Assuming that the breakdown threshold for this mixture is the same as for air (~250 GW/cm^2) [Ref. 11], we find that at a pulse duration of 1 ns a beam can be sent through the absorption region with energy density $\varepsilon = 250$ J/cm^2. On the gas-vacuum interface, the admissible energy density is certainly greater than 250 J/cm^2. For subsequent estimates, let us take the energy density of the signal incident on the absorbing cell as $\varepsilon = 50$ J/cm^2. An absorbing medium in a magnetic field that is inhomogeneous lengthwise of the medium has a nonuniformly broadened absorption line. The problem of calculating the saturated coefficient of absorption of such a medium transilluminated by a nanosecond radiation pulse has not yet been solved [Ref. 12]. For estimates of the weak-signal and strong-signal transmission coefficients of the absorbing cell, let us assign the length of the pumped region (120 cm), and assume that its central region with length of 20 cm is in a magnetic field $H \approx 0$. In the absence of a magnetic field, the absorption line is uniformly broadened. According to Ref. 13, for the main pulse ($\tau_1 \sim 1$ ns), the pre-pulse ($\tau_2 \geqslant \tau_1$) and the superluminescence signal at a gas pressure in the absorbing cell of 40 mm Hg we have the relation $\Delta\nu_2 \leqslant \Delta\nu_1 \approx \Delta\nu_{sl} < \Delta\nu_{Lor}$ ($\Delta\nu_{1,2,sl,Lor}$ are the half-widths of the main pulse, pre-pulse, superluminescence signal and Lorentz absorption line respectively). The strong-signal

transmission coefficient of the given segment of the medium is

$$T_1 = 1 - h\nu N l/[(1 + g_1/g_2)\varepsilon],$$

where $h\nu$ is the energy of a quantum of incident radiation, N is the concentration of unexcited iodine atoms, l is the length of the absorbing medium, g_1, g_2 are the statistical weights of the ground and excited states of the iodine atom. We will assume that the rate of intermixing of sublevels of the hyperfine structure of the ground state $\nu_m > \tau^{-1}$. At $N = 4 \cdot 10^{17}$ cm^{-3}, $l = 30$ cm, $g_1 = \sum_{i=1}^{i=4} g_{F'=i} = 24$, $g_2 = g_{F=3} = 7$ and $\varepsilon = 50$ J/cm^2, $T_1 \geqslant 0.99$. Considering that the weak-signal transmission T_2 is determined by Bouguer law, and taking the absorption cross section σ_{ab} equal to $5.8 \cdot 10^{-19}$ cm^2 [Ref. 14], we get $T_2 \approx 10^{-3}$. Let us note that in the phototropic filters used in photodissociation lasers for these same purposes [Ref. 15] at the present time, values of T_1 and T_2 that are close to those obtained above are not simultaneously realized.

The region of the absorbing cell medium that is located in the magnetic field is necessary only for suppressing the luminescence of the preceding amplification stage. Assuming that over the entire length of the absorbing cell the minimum cross section of absorption of iodine atoms is realized in a magnetic field of 0-8000 oersteds ($\sigma_{ab} \approx 9 \cdot 10^{-20}$ cm^2 [Ref. 14]), ensuring the equality $\Delta\nu_{abs} = \Delta\nu_{lum}$, we get an upper limit for the coefficient of absorption of the luminescence signal of $\sim 10^{-2}$. When the entire length of the working medium is taken into consideration, T_1 decreases to 0.97. It should be noted that in a pulse absorbing cell, the values of the coefficients T_1, T_2 may vary over rather broad limits due to the capability of changing the length and concentration of the absorbing medium.

Simultaneous pyrolysis of the working gas throughout the active volume of a pulse absorbing cell for a vessel diameter of 30-100 mm and working gas pressure of 30 mm Hg is impossible because of the large cross section of absorption of the pumping light by the perfluoroalkyl iodide molecules. Sufficiently intense pumping in the medium of such an absorbing cell should give rise to a pyrolysis wave [Ref. 16] with velocity determined by the time of readiness of the vessel for operation, and a gasdynamic perturbation wave [Ref. 17] that leads to disruption of the optical homogeneity of the medium. The velocities of both waves were measured in a cylindrical chamber 175 mm in diameter with flashlamp on the axis. This lamp had an outside diameter of 70 mm, and the length of the interelectrode gap was 1 m. The lamp input energy was about 48 kJ. Duration of the half-period of the discharge current was 40 μs. The chamber was placed in a planar optical cavity. Time-scan photography of the radiation field in the near zone showed a lasing cutoff wave on the field pattern, propagating from the surface of the lamp to the wall of the vessel. This wave arose only in the pure perfluoroalkyl iodide, and was not present in a mixture of the iodide with buffer gas (SF_6) during the pumping pulse. On this basis, the effect was identified with the pyrolysis wave. The gasdynamic perturbation wave (compressional wave) in a mixture of C_3F_7I-SF_6 showed up well on the field pattern of radiation in the near zone, and had the form of a pronounced narrow zone of absence of lasing, but with lasing retained in the region between the compressional wave and the lamp surface. Fig. 3 shows Rt plots

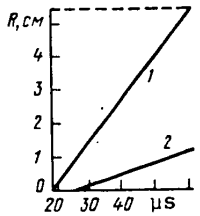

Fig. 3. Rt-diagram of pyrolysis and compressional waves: 1--$p_{C_3F_7I}$ = 23 mm Hg; 2--mixture of $C_3F_7I:SF_6$ = 23:92 mm Hg; R = 0 corresponds to the lamp surface; the broken line denotes the wall of the chamber

of pyrolysis and compressional waves. It can be seen that the pyrolysis wave (curve 1) arises prior to the compression wave (curve 2) and works through the entire active space of the chamber. The velocities of the pyrolysis and compressional waves under the conditions of the experiments were 1.2 and 0.3 km/s respectively.

The resultant data demonstrate the feasibility of an absorbing cell with working vessel 100 mm in diameter. In such an absorbing cell the diameter of the region of the absorbing medium undisturbed by the compression wave will be 70 mm when the pumping that is used is external with respect to the vessel of the absorging cell. A cell with such an aperture can be used to decouple the target unit from the last amplification stage of a powerful monopulse photodissociation laser [Ref. 2].

The authors thank S. A. Tul'skiy for assistance with the experiments on observation of the pyrolysis wave.

REFERENCES

1. Gaydash, V. V., Yeroshenko, V. A., Lapin, S. G., Shemyakin, V. I., Shurygin, V. K., KVANTOVAYA ELEKTRONIKA, Vol 3, 1976, p 1701.

2. Hohla, K., "High Power Lasers and Applications", Ver. Springer, 1978.

3. Brederlov, G., Fil, Ye., Fuss, V., Khola, K., Fol'k, R., KVANTOVAYA ELEKTRONIKA, Vol 3, 1976, p 906.

4. Yershov, L. S., Zalesskiy, V. Yu., Sokolov, V. N., KVANTOVAYA ELEKTRONIKA, Vol 5, 1978, p 865.

5. Belousova, I. M., Gorshkov, N. G., Danilov, O. B., Yachnev, I. L., ZHURNAL TEKHNICHESKOY FIZIKI, Vol 40, 1970, p 1562; Belousova, I. M., Danilov, O. B., Gorshkov, N. G., Zalesskiy, V. Yu., Yachnev, I. L., ZHURNAL EKSPERIMENTAL'NOY I TEORETICHESKOY FIZIKI, Vol 65, 1973, p 517.

6. Belousova, I. M., Kiselev, V. M., Kurzenkov, V. N., OPTIKA I SPEKTROSKOPIYA, Vol 33, 1972, p 210.

7. Borovich, B. L., Zuyev, V. S., Katulin, V. A., Mikheyev, L. D., Nikolayev, F. A., Nosach, O. Yu., Rozanov, V. B., "Intense Radiating Discharges and Optically Pumped Gas Lasers", Moscow VINITI, 1978; Babkin, V. I., Kuznetsova, S. V., Maslov, A. I., KVANTOVAYA ELEKTRONIKA, Vol 5, 1978, p 495.

8. Zalesskiy, V. Yu., Kokushkin, A. M., Yachnev, I. L., ZHURNAL TEKHNICHESKOY FIZIKI, Vol 47, 1977, p 2123.

9. Zel'dovich, Ya. B., Rayzer, Yu. P., "Fizika udarnykh voln i vysokotemperaturnykh gidrodinamicheskikh yavleniy" [Physics of Shock Waves and High-Temperature Hydrodynamic Phenomena], Moscow, Nauka, 1966.

10. Isakov, S. N., USSR Patent No 496405, BYULLETEN' IZOBRETENIY, No 47, 1976.

11. Rayzer, Yu. P., "Lazernaya iskra i rasprostraneniye razryadov" [Laser Spark and Propagation of Discharges], Moscow, Nauka, 1974.

12. Pilipovich, V. A., Kovalev, A. A., "OKG s prosvetlyayushchimisya fil'trami" [Lasers With Phototropic Filters], Minsk, Nauka i tekhnika, 1975.

13. Kharkevich, A. A., "Spektry i analiz" [Spectra and Analysis], Moscow-Leningrad, GITTL, 1952.

14. Hohla, K., "Photochemischer Jodlaser", Max-Planck Inst. Plasmaphys., Garching, Munich, 1971; Bobrov, B. D., Kiselev, V. M., Grenishin, A. S., KVANTOVAYA ELEKTRONIKA, Vol 4, 1977, p 619.

15. Batashev, S. P., Gal'pern, M. G., Katulin, V. A., Lebedev, O. L., Luk'yanets, Ye. A., Mekhryakova, N. G., Mizin, V. M., Nosach, V. Yu., Petrov, A. P., Petukhov, V. A., KVANTOVAYA ELEKTRONIKA, Vol 6, 1979, p 2652.

16. Zalesskiy, V. Yu., ZHURNAL EKSPERIMENTAL'NOY I TEORETICHESKOY FIZIKI, Vol 69, 1975, p 513.

17. Belousova, I. M., Danilov, O. B., Sinitsyna, I. A., Spiridonov, V. V., ZHURNAL EKSPERIMENTAL'NOY I TEORETICHESKOY FIZIKI, Vol 58, 1970, p 1481.

6610
CSO: 1862/242

- END -